TAMPEREEN TEKNILLINEN YLIOPISTO
TAMPERE UNIVERSITY OF TECHNOLOGY

Timo Vuorela

Computational Modeling of Lipoprotein Particles

Julkaisu 1538 • Publication 1538

Tampere 2018

Tampereen teknillinen yliopisto. Julkaisu 1538
Tampere University of Technology. Publication 1538

Timo Vuorela

Computational Modeling of Lipoprotein Particles

Thesis for the degree of Doctor of Science in Technology to be presented with due permission for public examination and criticism in Tietotalo Building, Auditorium TB104, at Tampere University of Technology, on the 4th of April 2018, at 12 noon.

Tampereen teknillinen yliopisto - Tampere University of Technology
Tampere 2018

Doctoral candidate:	Timo Vuorela, M.Sc. Biological Physics and Soft Matter Group Laboratory of Physics Tampere University of Technology Finland
Supervisor:	Ilpo Vattulainen, Prof. Biological Physics and Soft Matter Group Laboratory of Physics Tampere University of Technology Finland
Pre-examiners:	Jesus Perez-Gil, Prof Department of Biochemistry Faculty of Biology Complutense University of Madrid Spain
	Kari Laasonen, Prof Department of Chemistry Aalto University Finland
Opponent:	Matthias Weiss, Prof Chair for Experimental Physics I University of Bayreuth Germany

ISBN 978-952-15-4115-5 (printed)
ISBN 978-952-15-4123-0 (PDF)
ISSN 1459-2045

Abstract

Ischemic heart disease and stroke are the leading causes of death in the industrialized countries. The driving mechanism behind these diseases is the atherosclerotic process leading to narrowing of the arteries and eventually a reduction of blood supply to the target organs. Lipoproteins known as carriers of cholesterol play an essential role in that process. However, despite intensive research over more than 100 years, the molecular level structure and function of lipoproteins are not fully understood. This largely stems from the fact that due to the small size and the dynamic nature of lipoproteins, experimental techniques are not able to gauge lipoprotein structure and dynamics in sufficient detail. Meanwhile, molecular dynamics (MD) simulation has proved to be a powerful and simple method to explore the properties of various biological systems and to overcome many limitations of experimental techniques. In this thesis, the MD method was used to study lipoproteins at the molecular level. To this end, coarse-grained molecular models for high- and low-density lipoprotein (HDL and LDL, respectively) particles were constructed to study their structure and dynamics. Further, atomic-scale models were used to study the interaction between HDL and CETP, a lipid transfer protein. Finally, atomic simulations were also employed in a lipoprotein-like environment to assess the validity of using BODIPY, a common molecular probe, to explore lipoprotein properties.

The first key result of this thesis is the detailed structural model found for both HDL and LDL, showing that the previously proposed 2- and 3-layer models are inadequate for describing lipoprotein structure to a sufficient degree. It was found that the structural and dynamic properties of lipids hosted by lipoproteins depend significantly on their location and distance from the center of the particle. Second, this thesis work revealed the mechanism and the residues involved in anchoring CETP to the surface of lipoprotein particles. Also, the critical role of helix X as a door to the hydrophobic tunnel carrying the cargo lipids was clarified. Third, based on BODIPY-simulations reported in this thesis one can conclude that BODIPY-labeled cholesteryl oleate is not a suitable probe for experimental cholesteryl oleate tracking

studies in lipoprotein environments. It appears that a successful probe in a lipoprotein environment should have no significant affinity for the hydrophilic surface region.

The findings give a solid grounds for further studies to explore the key initial steps associated with atherosclerosis and also the molecular-level events in the lipid exchange processes. For future purposes, this work demonstrates that the used simulation methods are particularly useful for studies of, e.g., the coupling between the lipid composition of lipoprotein particles and their structure and function.

Preface

Here lies the thesis "Computational Modeling of Lipoprotein Particles", which is written to fulfill the requirements for the degree of Doctor of Science (D.Sc.) at Tampere University of Technology. Its mission is to explore lipoproteins on a molecular level, to seek out structure and dynamics, to boldly go where experimental studies have not gone before.

Almost ten years ago I started this Ph.D. project, which at that time seemed to be over rather quickly. My M.Sc. thesis was a success, and many results, tools, and methods developed in that work were supposed to be applied in many promising projects. At the same time I was accepted to medical school, to my surprise, and doing research got sidetracked. During all these years there have been moments when I was pretty sure of never finishing this project. However, life is full of surprises, and here I find myself writing the last few words of this thesis.

First I wish to thank professor Ilpo Vattulainen for supervising my work and being patient with this project and reaching out to me during the years of intensive medical studies. Seldom one finds a person as positive, motivating and encouraging as Ilpo. Many group members have come and gone during these years, but the atmosphere in the group was always great, and we had many valuable, inspiring and also funny moments. For these moments, special thanks go to Sanja Pöyry, Anette Hall, Eero Hytönen, Matti Javanainen, Andrea Catte, and Samuli Ollila, just to name a few. I greatly appreciate the work and effort of all co-authors not yet mentioned.

My parents Tuula and Seppo and my brother Tero have always placed a high value on education and encouraged me to pursue a D.Sc., even after completing medical school. I cannot express enough appreciation to my wife, Tea, for sharing the life with me and being my best friend. Our children, Alma, Reima and Hertta, remind me everyday about what is essential in the midst of everyday hustle and bustle.

Tampere, February 2018
Timo Vuorela

Contents

List of Abbreviations

CE	Cholesteryl Ester
CETP	Cholesteryl Ester Transfer Protein
CG	Coarse-Grained
CHOL	Cholesterol
CO	Cholesteryl Oleate
dHDL	Discoidal High-Density Lipoprotein
HDL	High-Density Lipoprotein
HL	Hepatic Lipase
LCAT	Lecithin-Cholesterol Acyl Transferase
LD	Lipid Droplet
LDL	Low-Density Lipoprotein
LJ	Lennard-Jones
lysoPC	Lysophosphatidylcholine
MD	Molecular Dynamics
PBCs	Periodic Boundary Conditions
PLTP	Phospholipid Transfer Protein
PME	Particle Mesh Ewald
POPC	Palmitoyl-oleoyl-phosphatidylcholine
PPC	Palmitoyl-phosphatidylcholine
REUS	Replica Exchange Umbrella Sampling
sHDL	Spheroidal High-Density Lipoprotein
SMC	Smooth Muscle Cell
TG	Triacylglycerol
VLDL	Very Low-Density Lipoprotein

List of Publications

This thesis consists of the following publications:

I Vuorela, T., Catte, A., Niemelä, P., Hall, A., Hyvönen, M., Karttunen, M., Vattulainen, I. Role of Lipids in Spheroidal High Density Lipoproteins. PLoS Computational Biology **6**, e1000964 (2010).

II Murtola, T., Vuorela, T., Hyvönen M., Marrink S-J., Karttunen M., Vattulainen I. Low density lipoprotein: structure, dynamics, and interactions of apoB-100 with lipids. Soft Matter **7**, 8135-8141 (2011).

III Koivuniemi A, Vuorela T, Kovanen PT, Vattulainen I, Hyvönen MT. Lipid Exchange Mechanism of the Cholesteryl Ester Transfer Protein Clarified by Atomistic and Coarse-grained Simulations. PLoS Computational Biology **8**, e1002299 (2012).

IV Karilainen T, Vuorela T, Vattulainen I. How Well Does BODIPY-Cholesteryl Ester Mimic Unlabeled Cholesteryl Esters in High Density Lipoprotein Particles? Journal of Physical Chemistry B **119**, 15848-15856 (2015).

In Paper I, the simulations, a significant part of the analysis, and the writing of the paper were carried out by the author. The only part of the project where the author did not play the substantial role was the construction of the protein model that was prepared by Andrea Catte, who also contributed, in part, to the writing process. In Paper II, the protein part of the simulation model was constructed by Teemu Murtola, who also carried out the simulations. Meanwhile, the lipid droplet of the lipoprotein system was prepared and researched by the author. The analysis, interpretation of the research data, and the writing of the article were also jointly done by the author and Teemu Murtola. In this manner, the distribution of the work was shared equally. Given this, Teemu Murtola and the author share the leading authorship with equal contributions (though this is not explicitly stated in the paper). In Paper III, the author contributed significantly to the design of the project, and he prepared,

simulated, and analysed the coarse-grained models, while Artturi Koivuniemi was responsible for carrying out the simulations of the atomistic models and the analysis of the simulation data. The writing process was led by Artturi Koivuniemi with a significant contribution given by the author. In Paper IV, the author constructed the simulation models, did the analysis (the exception being the analysis of free energy calculations), and contributed significantly to the writing of the article. Topi Karilainen took care of the free energy calculations and the analysis of the free energy computations. Given this distribution of work, the author and Topi Karilainen in practice share the leading authorship (although this is not explicitly mentioned in the article in this case either). Finally, Paper III is also included in the Ph.D. thesis of Artturi Koivuniemi (Ph.D. granted by TUT in 2013). Paper IV may further appear in the Ph.D. thesis of Topi Karilainen (currently a Ph.D. student at TUT).

1 Introduction

Cholesterol was found more than 100 years ago, and the research in this field has been very active ever since [1]. Cholesterol plays many roles in biological processes, for instance as an important structural component of cell membranes, as a building block of different hormones, and as a key player in cardiovascular diseases caused by atherosclerosis [2]. Meanwhile, lipoproteins are macromolecular complexes consisting of lipids and carrier proteins transporting cholesterol to every part of the body via the bloodstream [2]. Lipoproteins are very heterogeneous, differing in size, density, and molecular composition. There are different classes of lipoproteins with different roles in the cholesterol metabolism. For example, low-density lipoprotein's (LDL) main task is to carry cholesterol to the periphery, while high-density lipoprotein (HDL) transports cholesterol to the opposite direction [2].

In certain conditions, LDL and very low-density lipoprotein (VLDL) start to accumulate inside the arteries [3]. Under normal circumstances, the endothelium lining, i.e. the interior surface of blood vessels, maintains vascular tone, hemostasis, and permeability [4]. However, a range of different factors can cause endothelial dysfunction, where endothelial barrier integrity is compromised, initiating the accumulation process [4, 5]. This is the initial phase of the process called atherosclerosis, which leads to lesion development, narrowing the blood vessel and limiting the blood flow [6]. The endpoint of this atherosclerotic process is plaque rupture resulting in a rapid stop in blood flow, i.e. a heart infarct or stroke depending on the location of the plaque. Atherosclerosis is a key mechanism behind a considerable fraction of cardiovascular diseases [7]. Given this, understanding the causes of atherosclerosis is essential, and indeed cardiovascular diseases are the primary cause of death in the industrialized countries [8, 9].

Pushing further in lipoprotein research is essential for understanding the biophysical and pathophysiological processes related to cholesterol, lipoproteins, and the development of atherosclerosis. This information can be used to develop methods to prevent or hinder atherosclerotic processes. Lipoproteins, as well as many other

biological systems, are small in size, complex in structure, and highly dynamic by nature. These are challenges for experimental research. To overcome these challenges, computer simulations, e.g. molecular dynamics (MD) simulation, can be used to study the systems on a molecular and even atomic level. MD simulation has been proven to be a robust method to explore a variety of different biological systems.

Despite extensive studies, the structures and dynamics of HDL and LDL are not well understood. The objective of this thesis is to obtain more detailed insights into the lipoprotein particles. The primary focus is on the molecular structures, dynamics, and interactions between the lipid and the protein part of lipoproteins. The secondary objective is to study the interaction between HDL and one of the lipid transfer proteins. Finally, the last goal is to assess the validity of a molecular probe often used in a lipoprotein-like environment.

The structures and dynamics of both HDL and LDL were studied using a coarse-grained model over time and length scales not accessible by atomistic simulation models [10–12]. The first detailed models for HDL and LDL were clarified. It was found out that the structural and dynamic properties of lipids inside the lipoproteins depend significantly on the location and the distance from the center of the particle, and that the lipid and the protein part interact strongly instead of being largely independent of one another. Next, the initial steps in the lipid exchange mechanism of cholesterol ester transfer protein (CETP) were studied [13], and the results provided information as to how CETP anchors to the lipoprotein particle through charged residues. The new knowledge gained in this work helps to understand the initial steps of the CETP-mediated lipid exchange process. Finally, the feasibility of BODIPY-labeled cholesteryl oleate in a lipoprotein-like environment was examined, and the result revealed that the BODIPY-labeled cholesteryl oleate is quite unsuitable for studies in a lipoprotein-like environment [14]. The accumulated information is interesting and relevant as such, but more importantly it provides a solid platform for further studies.

The thesis is structured as follows. The necessary biological background information related to lipoproteins and the current knowledge about their structure and function is covered in Chapter 2. The used research methods, including the molecular dynamics method, the concept of coarse-graining, and analysis methods are described in Chapter 3. Chapter 4 gives an overview of the studied systems. In Chapter 5 the primary findings of this thesis are introduced and discussed. Chapter 5.1, based on Paper I, focuses on HDL and its structure and dynamics through coarse-grained MD simulations. In the same fashion, the properties of LDL studied

in Paper II are covered in Chapter 5.2. Chapter 5.3, based on Paper III, gives insight into the function of CETP anchored on the surface of an HDL lipid droplet. The feasibility of the BODIPY molecular probe in a lipoprotein environment to track cholesteryl oleate molecules is discussed in Chapter 5.4, based on Paper IV. Finally, concluding remarks are given in Chapter 6.

2 | History and Background

The early history of cholesterol dates back to the 18th century when Poulletier de la Salle discovered the molecule we know as cholesterol in gallstones in 1769 [1]. Chevreul introduced the name 'cholesterine', later changed to 'cholesterol', in 1816. Some twenty years later cholesterol was found in human blood, brain, and liver. Gradually it was recognized as a normal component of all animal cells and also as a component of specific pathological collections, i.e. atheromatous arteries and cholesteatomas [1]. The structure of cholesterol was determined by Heinrich O. Wieland and Adolf Windaus in the 1930s, who were awarded the Nobel Prize in chemistry in 1927 and 1928, respectively. In 1964 Konrad Bloch was awarded the Nobel Prize for resolving the steps of cholesterol synthesis.

Cholesterol serves as a constituent of cellular membranes and a precursor for bile acids, sex hormones, and cortisol. Further, already in 1901 is was observed that lipids in the blood were bound to proteins, but still, the discovery of lipoproteins was delayed for many years [15]. In 1924 chylomicrons were identified by Cage and Fish [16]. Finally, HDL was discovered in 1924, and later LDL and VLDL in the 1940s [16].

The structure and function of cholesterol and lipoproteins and their role in cardiovascular diseases have been under extensive studies for over 100 years, and multiple Nobel prizes have indeed been awarded to this field. However, the research is still active, and the structure and function of lipoproteins are not fully understood, and the role of the lipoproteins in cardiovascular diseases is debated.

In this chapter the biological roles of cholesterol and lipoproteins are discussed, after which their role in cardiovascular morbidity is explored in more detail. Finally, the current knowledge of the molecular level structure and function of lipoproteins is reviewed together with the limitations of experimental methods in lipoprotein research to justify the use of computer simulations in this work.

2.1 Biological Roles of Cholesterol

Cholesterol plays essential roles in different biological processes. Next, a short overview of these functions is discussed to give an idea about the importance of cholesterol in human body.

Structural Component

Cellular membranes are composed of a lipid bilayer hosting proteins that interact with lipids [17]. Cellular membranes are characterized by an impressive complexity to perform all the functions required by cells. Cholesterol is an essential component of cellular membranes. Eukaryotic cell membranes contain a significant amount of cholesterol, as much as up to one cholesterol for each phospholipid [17].

The cellular membrane can segregate its constituents laterally to perform and coordinate its functions. This property of subcompartmentalization is described by the lipid raft concept [18]. Lipid rafts are considered as functional, fluctuating nanoscale structures composed of sphingolipids, cholesterol, and proteins. According to the current view, cholesterol is a fundamental component of rafts that form a platform for membrane signaling and trafficking [18].

The axons of some nerve cells are surrounded by a myelin sheath [19]. The purpose of the myelin sheath is to form an electrically insulating layer that increases the impulse conduction velocity that is essential for the proper functioning of the nervous system [19]. Cholesterol is one of the components forming the myelin sheath, and it has been shown that it is an indispensable component [20].

Hormones

Steroid hormones, including cortisol, the steroid sex hormones, and vitamin D utilize cholesterol as a necessary building block [2]. Cortisol is produced in the cortex of the adrenal glands and affects many biological functions, such as regulating the metabolism of sugar, fat, and protein; it also suppresses the immune system and reduces the formation of bone and collagen synthesis, and many other processes [2, 17]. The steroid sex hormones define the secondary sex characteristics distinguishing males from females, and the testes and the ovaries are responsible for their production [2, 17]. Vitamin D is synthesized in the skin in response to sunlight, and the activation happens in the liver and the kidneys [2, 17]. Vitamin D has an essential role in the bone synthesis as well as in many other health benefits that however are still under further research [2, 21].

Biosynthesis

Most of the cholesterol is produced in the liver, but since all cells can synthesize cholesterol, it is not indispensable in the diet [2]. The structure of cholesterol suggests a complex biosynthetic pathway, but the building blocks are the same as for long-chain fatty acids, i.e. acetyl-CoA [2]. The actual synthesis requires several complex reactions that are not of major interest here, but it is interesting that the intermediates in the synthesis process serve as precursors for many important biological molecules, such as many vitamins. After synthesis cholesterol is exported in three forms: biliary cholesterol, bile acids, and cholesteryl esters. Bile acids and biliary cholesterol are formed in the liver and excreted into the gut aiding in lipid digestion and serving as a means to eliminate excess cholesterol from the body [2]. Cholesteryl ester molecules are transported in blood inside lipoproteins to the tissues or cells in which they are stored or consumed. The basis of the transportation system is covered in the next section, and the structures and the dynamics of lipoproteins are discussed in more detail in Section 2.4.

2.2 Lipoproteins - the Cholesterol Carriers

Lipids are virtually insoluble in water, and thus a unique system is required for the transportation of these molecules in the blood that is virtually a water-like environment. Many lipids are carried by lipoproteins that are macromolecular complexes consisting of carrier proteins, called apolipoproteins, and a lipid part, consisting of a mixture of phospholipids, cholesterol, cholesteryl esters, and triacylglycerols [2].

Lipoproteins are very heterogeneous and classified based on their density, size, and molecular composition (Table 2.1). The different classes have different roles in the lipoprotein metabolism [2].

Chylomicrons

Chylomicrons are the largest and the least dense of the lipoproteins, functioning in the transportation of dietary fats from the intestine to other tissues [22]. Epithelial cells that line the small intestine synthesize chylomicrons that enter the bloodstream through the lymphatic system. The apolipoproteins associated with chylomicrons are apoB-48, apoE, and apoC-II [2, 22]. From these apoC-II activates lipoprotein lipase (LPL) in the capillaries of adipose, heart, and muscle tissues, releasing free fatty acids to these target tissues, where fatty acids are either stored or utilized [22]. After almost depleting triacylglycerols, the remnants containing cholesterol are

Lipoprotein	Density (g/ml)	Size (nm)	Apolipoproteins	Function
Chylomicrons	<1.006	50-200	apoB-48, apoE, apoC-II	Transport of dietary fatty acids from the intestine to other tissues
VLDL	0.95-1.006	28-70	apoB-100, apoC-I, apoC-II, apoC-III, apoE	Transport of triacylglycerols from liver to other tissues
LDL	1.006-1.063	20-25	apoB-100	Carries cholesterol to extrahepatic tissues
HDL	1.063-1.210	8-11	apoA-I, apoA-II, apoC-II, apoC-III, apoD, apoE	Reverse cholesterol transport

Table 2.1: Major classes of human lipoproteins: Density, size, composition, and function. Data adapted from [2].

conveyed to the liver where their uptake is mediated by endocytosis, and cholesterol content is released, and the rest of chylomicrons are degraded [22].

Very Low-Density Lipoproteins

The excess fatty acid that is not used immediately is converted to triacylglycerols in the liver and combined with specific apolipoproteins to form a very low-density lipoprotein (VLDL) [22]. Also, surplus carbohydrate can be converted to triacylglycerols in the liver and exported in VLDLs. Also, some cholesterol and cholesteryl esters and apolipoproteins apoB-100, apoC-I, apoC-II, apoC-III, and apoE are included in VLDLs [2, 22]. The blood carries these lipoproteins from the liver to the muscle and adipose tissues, where apoC-II causes the activation of lipoprotein lipase, and fatty acids are released into the target tissues [22]. Muscle cells use the fatty acids as fuel while adipocytes, i.e. fat cells, reconvert them to triacylglycerols for storage [22]. Most VLDLs depleted of triacylglycerols are removed from the blood circulation by the apoE dependant uptake in the liver [22].

Low-Density Lipoproteins

Further decrease in the triacylglyceride content of VLDL and exchange of apolipoproteins between other lipoproteins leads to the formation of low-density lipoprotein (LDL) [22]. The cholesterol and cholesteryl ester content in LDL is considerable. The main apolipoprotein is apoB-100 [22]. The main function of LDL is to carry cholesterol and cholesteryl esters to extrahepatic tissues. LDL receptors on the surface of the cells, taking up cholesterol, recognize apoB-100, and the binding of LDL to the LDL receptor initiates endocytosis [22]. LDL is contained inside an endosome that fuses with a lysosome which contains enzymes that hydrolyze the cholesteryl esters. Cholesterol and fatty acids are released inside the cell, and apoB-100 is broken down into amino acids. The LDL receptor escapes the degradation and is recycled to the cell surface. Experimental studies suggest that the liver removes over 70% of circulating LDL, and the rest is taken up by other tissues [22]. ApoB-100 is also found on the surface of VLDL, but the receptor-binding domain is not exposed on VLDL [23]. The cell can then use the cholesterol immediately or re-esterify and store it in cytosolic lipid droplets. The uptake of cholesterol inhibits cholesterol synthesis in the cell and thus prevents accumulation of excess intracellular cholesterol [22].

High-Density Lipoproteins

All of the previously described lipoproteins carry their load to the periphery, but the fourth primary lipoprotein type, high-density lipoprotein (HDL), works oppositely [22]. HDL is synthesized in the liver and initially contains just a little of cholesterol and apolipoproteins apoA-I, apoC-I, apoC-II, as well as other apolipoproteins, see Table 2.1. After synthesis, HDL is secreted into the blood where HDL is subject to a continuous and extensive remodeling by a range of different factors.

On the surface of HDL resides the enzyme lecithin-cholesterol acyltransferase (LCAT) that aids in the formation of cholesteryl esters from lecithin (phosphatidylcholine) and cholesterol. LCAT takes phosphatidylcholine and cholesterol from chylomicrons and VLDL remnants and stores the resultant cholesteryl esters in HDL, which gradually transforms the HDL from a disc-like to a spherical particle where cholesteryl ester is stored in the core [2, 22]. Phospholipid transfer protein (PLTP) is another glycoprotein contributing to the transfer of phospholipids between HDL and other lipoproteins [22]. PLTP also transfers unesterified cholesterol between lipoproteins [22]. Both LCAT and PLTP increase the size of HDL [2, 22].

Cholesteryl ester transfer protein (CETP) is a hydrophobic glycoprotein in plasma,

facilitating the redistribution of cholesteryl esters and triglycerides between different lipoproteins. The net effect is the transportation of cholesteryl esters from HDL to VLDL and LDL, while triglycerides are transferred in the reverse direction [22]. Also, hepatic lipase (HL) on the luminal surface of endothelial cells in the liver is involved in the HDL metabolism by selective uptake of HDL cholesteryl esters. The activity of both CETP and HL reduces the size of HDL [22].

Experimental studies are suggesting that the conversion of small HDL particles to larger ones occurs in proximity to the cells and not while HDL circulates in the blood [24]. Picking up cholesterol from extrahepatic tissues back to the liver is called reverse cholesterol transport, which takes place by two alternative pathways [25]. HDL interacts with the specific receptors on the surface of cholesterol-rich cells and that in turn triggers passive movement of cholesterol from the surface of a cell into HDL. The second pathway involves endocytosis of HDL by an active transporter protein, after which HDL is resecreted with a load of cholesterol. HDL then returns to the liver where the cholesteryl esters are unloaded. Lipid-free or lipid-poor Apo A-I is removed partly by the kidneys, and the remainder is catabolized by the liver [25].

2.3 Role of Lipoproteins in Atherosclerosis and Cardiovascular Morbidity

Cardiovascular diseases, e.g. heart attack, stroke, and peripheral vascular diseases, are the primary cause of deaths in the industrial world [8, 9]. Atherosclerosis, i.e., accumulation of lipids and plaque formation on arterial walls, is the underlying cause of these diseases [7]. The goal of this section is to focus on the role of lipids and lipoproteins in the pathogenesis of atherosclerosis. The cellular and molecular level of the process is covered in more detail, since the work conducted in this thesis deals with the molecular level structure and function.

2.3.1 Short History of Atherosclerosis

Atherosclerosis is a disease mankind has been suffering for thousands of years, demonstrated by the findings in the aorta, coronary and peripheral arteries of ancient Egyptian mummies [26–28]. The findings show that the lesions found in the ancient mummies are similar to those of lesions in patients who have atherosclerosis today.

At the beginning of the 19th century, medical research started showing interest in vascular alterations in the search for the reason of angina pectoris, i.e. precordial

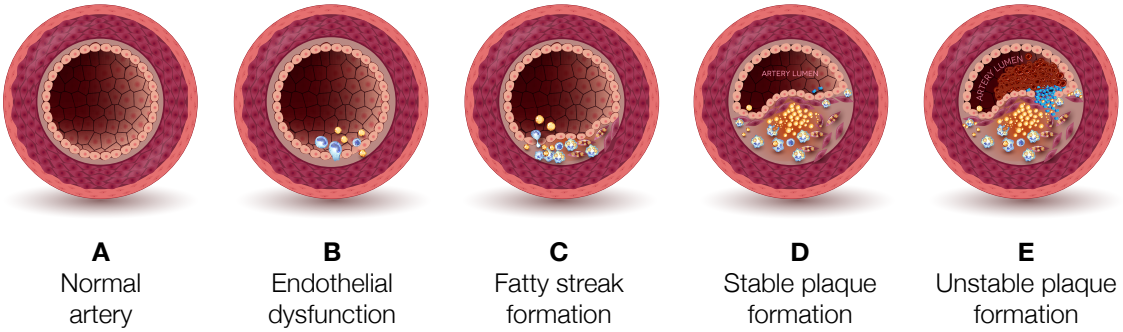

Figure 2.1: Atherosclerotic process. A) Normal artery. B) Endothelial dysfunction. The permeability of the endothelium increases and macrophages (blues cells) and low-density lipoproteins (yellow spheres) migrate to the tunica intima under the endothelium. C) Fatty streak formation. Macrophages uptake LDL and transform into foam cells. Also smooth muscle cells migrate and transform into foam cells. D) Stable plaque formation. Foam cells die and release lipid debris from the core of the plaque. Smooth muscle cells form a fibrous cap to cover the plaque to prevent exposure to the artery lumen. E) Unstable plaque formation. If the plaque is exposed, platelets (bright blue) start to cover the exposure and the release of procoagulation factors leads to formation of thrombus.

pain. The term arteriosclerosis (later became atherosclerosis) was introduced in 1829 by J. Lobstein [29]. Virchow discovered in the 19th century that the lesions in the arteries contain a yellow fatty substance, and later Windaus identified that the lesions consisted of calcified connective tissue and cholesterol [30]. Anitschkow and Chaltow managed to induce atherosclerosis in rabbits by feeding them with a cholesterol-rich diet [31]. These findings suggested that lipids and lipoproteins have a significant role in the pathogenesis of atherosclerosis. Virchow was first to recognize atherosclerosis as an inflammatory disease, and this recognition has led to massive progress in the understanding of the pathogenesis of atherosclerosis. Next, a description of the current understanding of the molecular level events of atherosclerosis is discussed.

2.3.2 Initiation of Atherosclerotic Lesions

The endothelium lining, i.e. a thin layer of squamous cells lining the interior surface of blood vessels, plays a crucial role in the initiation of atherosclerotic lesions [4, 5]. The normal function of the endothelium lining is to maintain vascular tone, hemostasis, and inflammation [4]. Laminar flow and the resultant laminar shear stress activate signaling pathways that maintain the normal function of the endothelium. Atherosclerotic lesions likely occur at arterial curves and branches, where the laminar blood flow is disturbed, and the endothelium is subjected to a low shear stress [25]. The mechanical stimuli in addition to traditional cardiovascular risk factors includ-

ing smoking, aging, hypercholesterolemia, hypertension, hyperglycemia, and family history are associated with alteration in endothelial function, resulting in endothelial dysfunction [4].

Endothelial dysfunction is a systemic pathological state of the endothelium in which an imbalance between vasodilatation and vasoconstriction is present due to the substances produced by the endothelium. In endothelial dysfunction, the endothelial barrier integrity is compromised leading to increased accumulation and retention of subendothelial atherogenic LDL and remnant of VLDL [25]. Also, the production of reactive oxygen compounds is increased, causing oxidative modifications of apoB-containing lipoproteins [25]. The increased expression of monocyte adherence proteins, proinflammatory receptors, and different cytokines lead to monocyte recruitment and migration of monocytes into the subendothelial space [25].

Monocytes are converted into macrophages that start to take up apoB-containing lipoproteins, degrading and storing resultant cholesterol in cytoplasmic lipid droplets as cholesteryl ester through a regulated pathway [25]. Lipoproteins modified by oxidation or glycosylation are taken up by macrophages through a non-regulated receptor pathway including CD36, scavenger receptor A, and lectin-like receptor family [25]. Aggregation of apoB-containing lipoproteins enhances the uptake via phagocytosis contributing to the influx of cholesterol into macrophages and forming of the so-called foam cells [25]. ApoB containing lipoproteins that also contain apoE (apoE remnants, VLDL) can cause cholesterol accumulation via interaction of apoE with apoE receptors, which are not regulated by cellular cholesterol [25]. This phase of the pathogenesis is usually called *fatty streak formation*.

2.3.3 Progression of Lesions and Rupture

Fatty streaks do not cause any symptoms and can undergo even regression [25, 32]. However, once the process progresses the regression is less likely to occur because of the more irreversible changes that take place [25]. Macrophages infiltrated to the subendothelial space produce cytokines and growth factors that promote smooth muscle cells (SMC) infiltration. These SMCs originate from the SMCs already present in the intima and also from tunica media. Accumulated SMCs produce a complex extracellular matrix composed of collagen, proteoglycans, and elastin to form a fibrous cap covering the foam cells [32]. The role of the fibrous cap is to prevent occlusion and exposure of prothrombotic factors that might lead to thrombus formation causing heart infarct or stroke.

Some SMCs can take up cholesteryl oleate and transform into foam cells [25].

Compared to macrophages SMCs are more inefficient in processing and transporting cholesterol, resulting in impaired cholesterol efflux. Also, the ability of macrophages to process cholesterol is reduced in more advanced lesions. Due to the accumulation of cells, the volume of the lesion grows. However, there is vascular remodeling of the lesion to reduce the protrusion into the lumen [33].

Within a lesion, changes in different signaling pathways accelerate macrophage death, and decreased phagocytosis of dead macrophages lead to the necrotic death of macrophages [25]. Necrotic death causes a release of intracellular oxidative and inflammatory components that in turn contribute to a vicious circle of forming a necrotic core of the lesion. Components of the necrotic core lead to increased SMC death, accelerated degradation of extracellular matrix, and decreased extracellular matrix production [25]. This, in turn, causes thinning of the fibrous cap, which makes the cap prone to rupture that might expose prothrombotic components and procoagulation factors, leading to the formation of thrombus and clinical ischemic cardiovascular events [25].

2.3.4 Role of HDL

Reverse Cholesterol Transport

HDL in both forms, lipid-poor apoA-I, and mature HDL, contribute to removing cholesterol from macrophages, and thus preventing the formation of foam cells [25]. The efflux of cholesterol from macrophages to HDL reduces inflammation, being the first step in reverse cholesterol transport [25]. HDL collects cholesterol via different transporter proteins on the surface of the macrophages and also via passive diffusion. The more lipid-poor HDL is, the more it stimulates HDL efflux, and it loses the ability to bind different transporters as it grows and transforms into spherical mature HDL, at the same time promoting free cholesterol efflux from the plasma membrane [25]. HDL then transports cholesterol to peripheral tissues and back to the liver. HDL also interacts with other plasma lipoproteins, as discussed in Section 2.2. See Figure 2.2 for illustration of reverse cholesterol transport.

Other Functions of HDL

Reverse cholesterol transport has historically been assumed to be the reason for HDL's anti-atherogenic properties given that HDL removes excess cholesterol from the atherogenic lesions and other peripheral tissues. However, other alternative HDL functions probably contribute to protective cardiovascular properties, perhaps even

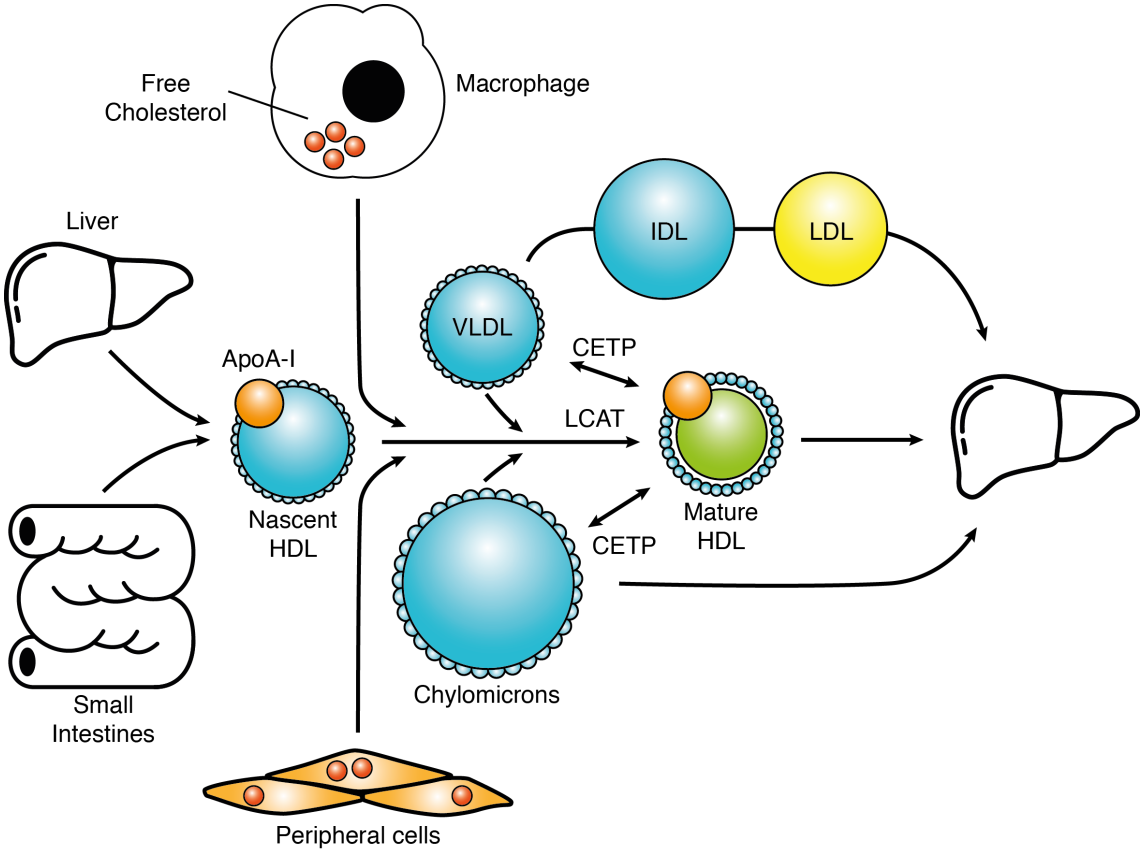

Figure 2.2: Reverse cholesterol transport. Nascent HDL is secreted from the liver and the small intestine. After secretion HDL picks up cholesterol from macrophages and peripheral cells, where it also interacts with other lipoprotein particles. As a result, a mature HDL particle is formed carrying cholesterol back to the liver. IDL stands for intermediate density lipoprotein. (the "Liver" symbol is by Laymik, the "Intestine" symbol is by Nook Fulloption, and the "Fried Egg" symbol by Curve represents a macrophage. All symbols are from thenounproject.com.)

more than reverse cholesterol transport.

HDL's apoA-I has been found to decrease expression of adhesion molecules in the endothelial cell through multiple mechanisms [25]. HDL has effects also on monocytes and macrophages, in which it inhibits monocyte adhesion and migration and activation of macrophages. Through removal of excess cholesterol and induction of signaling pathways, HDL can promote migration of macrophages from the lesions [34]. In addition to HDL's effect on macrophages and monocytes, also neutrophile activation is suppressed. All these contribute to HDL's anti-inflammatory properties and thus limit atherosclerosis [25].

HDL also has anti-thrombotic properties that inhibit thrombus formation, which forms after a plaque is ruptured, and thus contributes to HDL's anti-atherogenic properties [35]. For normal function of platelets, the removal of surplus cholesterol

from the platelet plasma membrane by HDL is required [25]. HDL also affects signaling pathways that reduce platelet activation [36]. Further, inhibition of thrombus promoting coagulation factors by HDL has been observed [37].

Oxidized LDL deposited in the subendothelial space is a major factor inducing monocyte migration and activation. Oxidized LDL is more pro-inflammatory and thus more atherogenic than normal unmodified LDL [25]. HDL can reduce and prevent oxidation of LDL [38, 39]. HDL can uptake oxidized lipids and other oxidizing factors from cells, preventing LDL oxidation, and HDL is also capable of removing lipid peroxides, i.e., oxidized lipids, directly from LDL [39]. On the surface of HDL, there are also other proteins in addition to apoA-I, and these HDL-associated proteins seem to have anti-oxidative functions [25].

As described earlier, the loss of endothelial barrier function is the initial step in the process of lesion development. In addition to affecting adhesion properties of endothelial lining, HDL also affects the barrier integrity. HDL improves vascular integrity by inducing vasodilatation, tightening of cell-to-cell junctions [40]. HDL has also been found to have anti-apoptosis properties [25]. Apoptosis of macrophages and endothelial cells contributes to the development of the necrotic core of a plaque.

2.4 Current Knowledge of the Lipoprotein Structure and Function

The current knowledge and understanding of the molecular composition of different lipoprotein particles are quite extensive. Meanwhile, the structures of lipoproteins are rather poorly understood. This is primarily due to experimental difficulties to deal with dynamic nano-sized particles. The limitations are discussed in Section 2.5, while this section covers the current state of the knowledge about lipoprotein structure and function. First, the molecular composition is briefly covered, and secondly, the molecular structure is discussed in more detail.

2.4.1 Molecular Composition

The lipoproteins are macromolecular complexes composed of proteins and lipids, as discussed in Section 2.2, and the lipoproteins can be classified into different subclasses based on their size, density, protein content, and function. The following discussion covers only the lipoproteins studied in this thesis, namely HDL and LDL. The molecular composition expressed in weight percent are shown in Table 2.2.

The lipid part of LDL consists on average of about 3000 lipids: 1600 cholesteryl esters, 700 phospholipids, 600 unesterified cholesterol molecules, and 170 triacylglyc-

Lipoprotein	Composition (wt %)				
	Protein	Phospholipids	Cholesterol	CE	TG
HDL	55	24	2	15	4
LDL	23	20	8	37	10

Table 2.2: Molecular composition of high density lipoprotein (HDL) and low density lipoprotein (LDL) expressed in weigh percent. CE stands for cholesteryl ester, TG triacylglycerol. Data adapted from [2].

erides [41, 42]. The main phospholipid components are phosphatidylcholine (POPC, about 450 molecules), sphingomyelin (about 185 molecules), and lysophosphatidylcholine (about 80 molecules). In addition to these phospholipids, smaller amounts of other molecules are usually present in LDL [43–46].

On the surface of LDL lies a single copy of the apoB-100 apolipoprotein that wraps around the lipid part of the lipoprotein. ApoB-100 is one the largest monomeric proteins known and consists of 4536 amino acids [41].

HDL is a very heterogenous subclass of lipoproteins. Its molecular composition varies markedly according to the stage in the HDL life cycle. The most abundant protein in HDL is apoA-I, though also some other proteins are found, see Table 2.1. The lipid-poor, disc-like HDL particles contain two copies of apoA-I in a double belt conformation on its surface [47–52]. A recent study proposed that spherical HDL contains three apoA-I molecules in a cage-like formation and even five copies on a single particle seem possible [53].

Compared to LDL the lipid composition of HDL is considerably different and varies greatly depending on the size of HDL. In the HDL studied in this work, there is relatively speaking twice as many phospholipids in HDL than in LDL. The same also applies to triacylglycerides. At the same time, the number of unesterified cholesterol and cholesteryl esters is half of the amount compared to LDL.

2.4.2 Molecular Structure

High-Density Lipoprotein

Like all lipoproteins, also HDL constitutes a heterogeneous class of lipoproteins, and different subclasses can be isolated by particle size, density, shape, and apolipoprotein content [54–57]. During assembly and early remodeling, HDL is in discoidal form (dHDL). However, it is converted to spheroidal HDL (sHDL) during maturation.

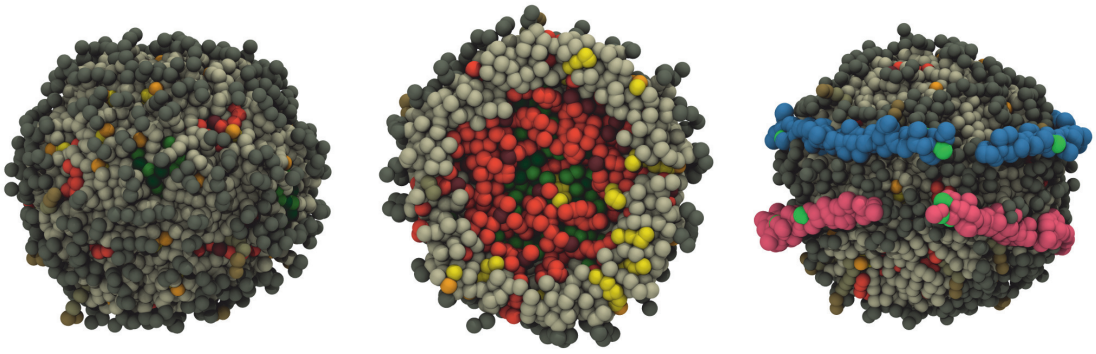

Figure 2.3: Example of a protein-free lipid droplet (left), its molecular distribution shown through a slice across the particle (middle), and HDL including two apoA-I proteins (right). Dark gray stands for POPC headgroup and dark brown for PPC headgroups, light gray for POPC hydrocarbon chains, light brown for PPC chains, light orange for CHOL OH-groups, bright yellow for cholesterol body, dark orange for CE ester bond, orange for CE ester body and chain, dark green for TG ester bonds, and bright green for TG chain. In HDL, proline residues in apoA-I sequences are in green. Reproduced from [10].

dHDL contains a core of apolar cholesteryl esters and triglycerides as a disordered lipid melt. On the surface are located amphipathic phospholipids and the proteins. Figure 2.3 illustrates the structure of spheroidal HDL.

A number of experimental studies have focused on the structure and dynamics of apoA-I in a lipid-free form [58], in lipid-bound dHDL [59, 60], and also in sHDL [53, 55]. Earlier computational attempts have focused on dHDL composed of phospholipids and two apoA-I [61–64]. Catte et al. performed the first computational approach towards understanding the structure of sHDL [65]. Shih et al. modeled the maturation process from dHDL to sHDL [66]. Regardless of the previous studies, the role of lipids is still only vaguely understood. Lipid organization and interplay with apoA-I are still yet to be grasped. Considering findings that lipids are essential components of protein structure, e.g. proteins embedded in cellular membranes are in constant interplay with lipids [67], it is clear that one cannot overemphasize the importance of clarifying the role of lipids in HDL properties. In Paper I [10], sHDL with a realistic lipid composition together with two apoA-I was simulated and provided the first detailed structural model for HDL and its dynamics with and without apoA-I.

Circulating sHDL contains 2-4 apoA-I molecules, which represent about 70-80% of HDL protein content by weight, apoA-II about 20%, the rest is due to other proteins in rather minimal quantities associated with sHDL [55]. Apo-I and apoA-II interact with lipids just like some other proteins associated with HDL, but certain

HDL associated proteins also interact through protein-protein interactions with apoA-I [55].

Studies applying immunoaffinity chromatography methods have isolated two subsets of sHDL. One subset contains both apoA-I and apoA-II, and the other contains only apoA-I [55]. A recent study combining immunoaffinity chromatography with volumetric analysis discovered that sHDL contains 3-4 apoA-I molecules usually, while a small HDL particle contains two copies of apoA-I [55]. In the case of two apoA-I molecules, the double-belt organization is observed, while in the case of three copies a modification of the double-belt model called the trefoil model was found to result in a cage-like structure [53].

Low-Density Lipoprotein

The current understanding of the structure of LDL describes LDL as a spherical particle consisting of an apolar core and an amphipathic surface [2, 17, 41]. The core is comprised mostly of cholesteryl esters, a small amount of triacylglyceride, and also some free, i.e. unesterified cholesterol. The surface is formed by a phospholipid monolayer incorporating free cholesterol and a single copy of apoB-100 apolipoprotein. An average diameter of an LDL particle is 22 nm. However, LDL particles are very heterogeneous, and their size varies from 18 to 25 nm [68].

The core of LDL has been shown to have a phase transition at almost physiological temperatures [69]. Below the transition temperature, the core-located lipids are arranged in an ordered liquid-crystalline phase. Above the transition temperature, however, the neutral core lipids are organized in a fluid, randomly distributed state [70]. The importance of this phase transition is unknown.

The surface layer surrounding the apolar core has been shown to separate into local molecular environments rich in phosphatidylcholine and/or sphingomyelin and cholesterol [43]. These microenvironments are most likely highly dynamic and in relation to the dynamics and the structure of apoB-100. It has been estimated that about 20% of the polar headgroups are immobile and probably interacting closely with apoB-100 [71]. Cholesterol modulates surface layer fluidity, which influences the availability of molecules in chemical reactions directly. A correlation between fluidity, enzyme activity, oxidisability, and LDL metabolism has been seen in different studies [68]. According to Hevonoja et al. [41], the two-layer model for the LDL lipid droplet is not sufficient, and a more advanced model is needed. They have proposed a new three-layer model to explain the details of the LDL structure. This model includes an interfacial layer between the core and the surface and contains molecules

of interpenetrating core and surface lipids.

The protein component of LDL, apoB-100, is one of the largest monomeric proteins known with its 4536 amino acid residues. ApoB-100 is moderately hydrophobic and thus insoluble in water, remaining bound to LDL during circulation in the bloodstream [72]. Results from experimental studies suggest that apoB-100 consists of globular domains connected by flexible chains that surround the LDL particle in a belt-like configuration [68]. Experimental studies have been able to identify a varying number of domains [73, 74], but the knowledge of the detailed configuration has remained a mystery. The locations of different domains have been studied using electron microscopy methods [75]. Computational modeling based on the secondary structure analysis has yielded a model consisting of five separate domains with amphipathic α-helixes and β-sheets representing the major secondary units, and this model currently serves as a basis for further research [76, 77]. The first 1000 residues have been found to be similar to lipovitellin, and using this information a homology model for the first 1000 residues has been constructed [78]. The most recent effort using sequence homology modeling and fold recognition has lead to a theoretical model consisting of eight connected domains [79], however, the validity of the model has not yet been confirmed experimentally.

Somewhat surprisingly, LDL has been studied only a little using molecular dynamics (MD) simulations. The structure of the LDL core has been studied earlier, but these studies completely ignored the surface layer and other lipids present in the core [80]. According to these results, cholesteryl ester molecules close to each other seem to have some orientational ordering, which gradually vanishes at longer distances. The hydrocarbon chains were found to be highly mobile, but the diffusion of the molecules was found to be slow and of the order of 2×10^{-9} cm^2/s. The slow diffusion supports the assumption that cholesteryl ester tails are strongly entangled above the phase transition temperature [70, 81]. Also, properties of a pure triglyceride melt have been studied using MD simulations [82]. In Paper II [11], we conducted the first MD simulations using a molecular-scale model for LDL structure and dynamics based on near-atomistic models.

2.5 Limitations of Experimental Methods In Lipoprotein Research

In science experiments play a central role. The abundance of experimental results has laid down the basis for the understanding of the chemical machinery of life. Despite great advances in experimental methods, in some cases, experiments can

be impossible, dangerous, expensive, or blind. In the case of biological systems, experimental methods often face the challenge of dealing with short time and length scales, and many events are therefore invisible to experiments, i.e., they take place over time and length scales that are inaccessible to experiments.

Lipoproteins, as many biologically relevant systems, are not static objects but highly dynamic. Conformational changes of proteins and lipids play a key role in their functionality. Thus knowing the molecular structure and dynamical behavior is essential for understanding how they function. High-resolution structural information can often be obtained by X-ray crystallography or nuclear magnetic resonance (NMR) spectroscopy. The results are however like snapshots, as they describe the transient structure of the target at a specific time, thus usually these methods are unable to provide sufficiently detailed information about the dynamics, especially on a single-molecule level.

Progress in experimental techniques, e.g. pump-probe spectroscopy, neutron scattering, cryo-electron microscopy, and advanced NMR experiments, provide information about the dynamics. However, it is not straightforward to translate the results into a detailed atomic picture because the results represent data averaged over quite long periods of time, and therefore, interpretation requires additional tools, such as molecular simulations.

In the MD method, each particle in the system is followed: its position and velocity in space relative to all other particles are known at all times. MD methods make it possible to observe atomic motion over broad time scales spanning from femtoseconds to milliseconds. Spatiotemporal domains challenging to probe by experimental techniques are therefore accessible to MD simulations.

3 | Methods

3.1 Classical Molecular Dynamics

The molecular dynamics (MD) method can be divided into two main categories [83]. In classical MD, atoms, and molecules are modeled as classical objects, such as the ball-and-stick models. Balls describe the atoms, and elastic pegs describe the bonds. The dynamics of the system is defined by the laws of classical mechanics. Meanwhile, the quantum mechanical approach takes the quantum nature of the chemical bond into account when describing the behavior of the system. The electron density functions for the valence electrons are computed using quantum mechanical equations, however, the dynamics of atoms is often managed using classical equations of motion [83].

There is a reason to stress that here we used the concept of "quantum mechanical approach" in a quite loose sense. There are rigorous theoretical descriptions to deal with quantum mechanical degrees of freedom, without any classical component. Such first-principles (ab initio) techniques are the method of choice to consider, e.g., reactions or protons. Yet, due to their computational complexity, fully quantum mechanical techniques are often not used in cases when the impressive accuracy given by quantum mechanics is not needed. For discussion on these methods, see for example [83–85].

Quantum MD simulations are indeed superior to classical MD when the accuracy is considered. However, as mentioned above, they require enormous computational capacity compared to the classical approach. In many cases, classical MD can provide as accurate answers as quantum MD in a fraction of the computer time [86]. In this work, classical MD is used because the time and length scales of the studied lipoprotein systems are out of scope of quantum MD methods. In the remainder of this work, the classical MD will simply be referred to as MD. The following sections give an overview of the MD method. The overview is based mostly on the GROMACS manual [87] and the book by Tamar Schlick [83], which give a solid description of

MD.

3.1.1 Force Field

The term "force field" is used to refer to the collection of mathematical equations describing the chemical interactions, parameters used in these equations, and also the algorithms used [88]. The force field describes the potential energy of the system as a function of the coordinates of its particles. The forces acting on each particle can be derived from the potential energies.

The potential $V(\vec{r_1}, \vec{r_2}, ..., \vec{r_N})$ represents the potential energy of N interacting atoms as a function of their position $\vec{r_i} = (x_i, y_i, zi)$. The force $\vec{F_i}$ acting on a given particle i can be calculated from the potential function in terms of

$$\vec{F_i} = -\frac{dV}{d\vec{r_i}}. \tag{3.1}$$

The interactions between particles are divided into bonded and non-bonded interactions. Bonded interactions describe the interactions between particles connected by chemical bonds. In addition to bonded and non-bonded interactions, different types of restraints can be imposed on the motion of the system. This is done by adding special potentials to achieve the wanted effects. The reason for adding these restraints is to include knowledge from experimental results, and to avoid unwanted deviations that might even crash the simulation.

Bonded Interactions

Covalent bonds between atoms are modeled by introducing a bonded potential between two atoms involved in the covalent bond in question. This potential allows small-scale deviations around the reference bond length value. The reference values for different bonds can be obtained either from X-ray crystal structures or quantum mechanical calculations. Values are presented in many textbooks, e.g. CRC Press Handbook of Chemistry and Physics [89]. The most straightforward formulation for bond length vibration is the harmonic potential given as:

$$V_b(r_{ij}) = \frac{1}{2} k_{ij}^b (r_{ij} - b_{ij})^2, \tag{3.2}$$

where b_{ij} is the reference bond length, k_{ij} is the force constant, and r_{ij} is the distance between the particles i and j in question. The harmonic potential is suitable for modeling only small deviations from the reference values. To model deformations that

exceed these small fluctuations, a more advanced and computationally demanding formulation can be used, e.g. Morse potential [90].

The hybridization of the orbitals around the atom determine the bond angles of each atom. As for the bond stretching, the harmonic potential is also used for modeling the bond angle vibration, see Equation 3.3.:

$$V_a(\theta_{ijk}) = \frac{1}{2}k^a_{ijk}(\theta_{ijk} - \theta^0_{ijk})^2, \tag{3.3}$$

where i, j, and k are used for a sequence of bonded particles. Particle j is in the middle and i and k in the ends. k^a_{ijk} is the force constant, θ_{ijk} is the bond angle, and θ^0_{ijk} the reference angle. The force constants for angle bending are obtained from vibrational frequency measurements [83].

The previously presented potentials (stretching and bending) do not prevent internal rotations. To prevent this, a torsional dihedral angle potential is included. The general function for the torsion potential τ can be written as

$$V_t(\tau) = \sum_n \frac{V_n}{2}[1 + \cos(n\tau - \tau_0)], \tag{3.4}$$

where τ is the torsional angle, defined as the angle between the planes of atoms (i, j, k) and (j, k, l), whereas τ_0 is the reference angle, n is an integer denoting the periodicity of the rotational barrier, and V_n is the associated barrier height. The value used for n depends on the atoms sequence and the force field parametrization (typical values of n are 1, 2, and 3). Experimental data from spectroscopic studies can be used to estimate the values for n and V_n [83].

To keep the planar groups (e.g., aromatic ring structures) planar and to prevent molecules from flipping over to their mirror-image enantiomer, improper dihedral potentials are introduced. The most straightforward potential for the improper dihedral is the harmonic potential:

$$V_{id}(\xi_{ijkl}) = \frac{1}{2}k_\xi(\xi_{ijkl} - \xi_0)^2, \tag{3.5}$$

where the improper dihedral angle ξ is defined as the angle between the planes of atoms (i, j, k) and (j, k, l), k_ξ is the force constant for the potential, and ξ_0 is the reference angle.

Non-Bonded Interactions

Non-bonded interactions typically contain three different terms: a repulsion term, a dispersion term, and a Coulombic term. The repulsion and dispersion terms are combined in terms of the van der Waals force using the Lennard-Jones (LJ) potential, while charged particles interact via the Coulombic potential:

$$V_{LJ}(r_{ij}) = \left(\frac{C_{ij}^{(12)}}{r_{ij}^{12}}\right) - \left(\frac{C_{ij}^{(6)}}{r_{ij}^{6}}\right), \tag{3.6}$$

$$V_C(r_{ij}) = \frac{q_i q_j}{4\pi\epsilon_0 r_{ij}}, \tag{3.7}$$

where q_i and q_j are the charges of atoms i and j, r_{ij} is the distance between atoms, and $C_{ij}^{(12)}$ and $C_{ij}^{(6)}$ are parameters depending on the pair of atom types.

Since the LJ potential decays rapidly, it is possible to cut off the interaction beyond a distance between the atoms that is greater than the preset cut-off value (typically 2 nm). This decreases the computational load by reducing the number of pairs for the LJ potential calculation without causing significant errors in results [87].

Contrary to the LJ potential, Coulombic potential's decay rate is slow, and ignoring it after some cut-off distance would produce undesired artifacts [91]. A method to overcome the problems arising from cutting off the Coulombic interactions after some specific distance is the reaction field method [92]. It also features a cut-off, but instead of just ignoring everything beyond the cut-off, a correction is introduced by assuming a uniform dielectric constant. Another popular method is the Ewald or the Particle Mesh Ewald (PME) method [93]. By utilizing periodic boundary conditions (see section 3.1.4) and Fourier transformations, some of the calculations can be efficiently done in reciprocal space and transferred back into real space. PME is considered more reliable, but RF scales up better and makes simulations of multimillion atoms more feasible [91, 94].

3.1.2 Atoms in Motion

From the force field, the force acting on each atom in the system can be derived, and the resulting movement of each atom can be solved by Newton's equations of motion:

$$\frac{d^2\vec{r}_i}{dt^2} = \frac{\vec{F}_i}{m_i}, \tag{3.8}$$

where m_i is the mass, $\vec{r_i}$ is the position of the atom i, and $\vec{F_i}$ is the total force calculated from the potential.

The equations of motion are numerically integrated over a discrete time step Δt. A trajectory describes the positions and velocities of each atom at each time step. There are several different algorithms to do the job, from which the most commonly used one, the leap-frog algorithm, is also used in this work [95]. The algorithm can be written as

$$\vec{v}\left(t+\frac{\Delta t}{2}\right) = \vec{v}\left(t-\frac{\Delta t}{2}\right) + \frac{\vec{F}(t)}{m}\Delta t, \tag{3.9}$$

$$\vec{r}(t+\Delta t) = \vec{r}(t) + \vec{v}\left(t+\frac{\Delta t}{2}\right)\Delta t, \tag{3.10}$$

where Δt is the length of a time step, $\vec{r}$ is the position, and $\vec{v}$ the velocity.

3.1.3 Temperature and Pressure

Direct use of MD leads to an ensemble, where the particle number, volume, and energy are constant. The simulations included in this work were conducted in the NpT ensemble, where particle number (N), pressure (p), and temperature (T) were kept constant. To achieve this, special algorithms for *a thermostat*, and *a barostat* were used.

In the early parts of the simulations included in this work, the Berendsen temperature coupling [96] was used to equilibrate the systems. In this approach, the idea is to mimic weak coupling to an external reservoir. The Berendsen algorithm slowly corrects the deviation of the system temperature from the reference temperature T_0:

$$\frac{dT}{dt} = \frac{T_0 - T}{\tau}, \tag{3.11}$$

meaning that the temperature deviation decays exponentially with a time constant τ. The advantage of the Berendsen method is that the strength of the coupling can be easily adjusted. By using the Berendsen method fluctuations of kinetic energy are suppressed, however, the fluctuations of energy and temperature are not correctly captured. Because of that, this method does not generate a proper canonical ensemble.

To overcome this significant limitation of the Berendsen method, a different approach by Nosé and Hoover [97, 98] was also exploited. The Nosé-Hoover thermostat produces the correct canonical ensemble. A thermal reservoir and a friction term are

introduced into the equations of motions:

$$\frac{d^2\vec{r}_i}{dt^2} = \frac{\vec{F}_i}{m_i} - \xi\frac{d\vec{r}_i}{dt}, \tag{3.12}$$

where the heat reservoir parameter ξ follows the equation

$$\frac{d\xi}{dt} = \frac{T - T_0}{Q}. \tag{3.13}$$

The reference temperature is T_0, the instantaneous temperature T, and Q is the parameter defining the strength of the coupling.

Similar to temperature coupling, there are different methods for controlling the pressure. The Berendsen method [96] for pressure coupling functions basically the same way as in the temperature coupling. It scales the atom coordinates and the simulation box vectors leading to exponential relaxation towards the reference pressure. As with the temperature coupling, the Berendsen method does not yield a correct NpT ensemble. It is mainly used in equilibrating the system. After equilibration, a more sophisticated and complex method by Parrinello and Rahman is often used [99, 100]. This method introduces changes in the equations of motions similar to the Nosé-Hoover method for thermal coupling. The Parrinello-Rahman method produces the true NpT ensemble. For more details of this method, see [87, 99].

3.1.4 Simulation Boundaries

There are several ways to treat the boundaries of the simulated system in MD simulations. The most common method is to use periodic boundary conditions (PBCs). In PBCs, the particles to be simulated are put in a space-filling box, which is surrounded by translated copies of itself. With PBCs a particle crossing one side of the simulation box re-enters the box immediately from the opposite side of the box. The particles in the box always interact with their nearest neighbors and it does not matter if the neighbor is in the original box or one of its copies.

3.1.5 Limitations of Molecular Dynamics Method

MD is a method that makes a study of biological phenomena on the molecular level possible. However, the phenomena on the molecular level are very complex, and some simplifications and assumptions have to be made to make the simulations feasible. This leads to several limitations, and it is important to be aware of those when considering the results.

Quantum Effects

Many biological phenomena involve quantum effects, e.g. chemical bonds, and tunneling of protons and electrons. Classical MD cannot model those kinds of events. There are *ab initio* simulation methods based on full quantum mechanical treatments of the Schrödinger equation for a given many-body system, but these methods are limited to very small systems and short time scales.

Reliability of the Force Field

The force field defines all interactions between particles, and thus the results will be realistic only if the potential energy functions mimic accurately enough the real forces acting on the real atoms. Furthermore, the form of the potential functions should be computationally efficient. In addition to these properties, the force field should be applicable to many different systems in different conditions. Currently, there are many different force fields available, some suitable for simulating proteins, while others being appropriate for lipid simulations. There is a need to develop force fields that could cover a wide range of chemical and biological systems [87].

A general approach is to combine experimental data for structural parameters and *ab initio* calculations for defining partial charges. Experimental methods have limits, however. Sometimes there are limited or no experimental data available. Then one has to use what is available and for example, combine a force field for a large molecule from smaller pieces of knowledge, and sometimes make educated guesses about the molecular structure [11].

Limits in Time and Size

The most severe limitation of MD is the time limitation. Time scales for many relevant biological processes extend over many orders of magnitude. For example, the nitric oxide binding to myoglobin takes tens of picoseconds, while protein folding may take minutes [101]. To access the large time scales, enormous computational power is required. The current state-of-the-art atomic MD simulations can handle the millisecond time scale [102, 103]. Computational capacity of supercomputers is improving all the time, and also novel methods are developed to overcome or at least push back the limitations related to time and size. One of these methods, coarse-graining, is discussed in the next section 3.2.

3.2 Coarse-Graining Method

Conventional atomic scale MD simulations provide valuable and detailed information about the properties of the local structure and dynamics. However, the length and time scales related to phenomena seen in large systems or phenomena taking place in the micro- or millisecond range are out of reach from the conventional atomistic methods because of the enormous computational load. To decrease the computational requirements and thus make longer and larger simulations feasible, it is possible to eliminate some of the details. This process is called *coarse-graining*. Coarse-grained (CG) models do not attempt to describe the shortest atomic length scales, but instead, they focus on features that are relevant on larger scales, describing large-scale behavior such as viscosity or order. To achieve this aim, CG models simplify molecular description by modeling the behavior of a group of atoms using only a single particle or an interaction site. The reduction in computational requirements is achieved through a reduction of the number of degrees of freedom and by simplifying the description of interatomic interactions. Meanwhile, when one simplifies the description of a molecular system, it also has a price that one has to pay. The main disadvantages are obvious, the loss of some details and the question regarding the validity of the coarse-grained model. The loss of details has to be accepted, since it is an inherent feature of this simplification process. Confirming the validity of the coarse-grained model is a more tedious process, but with systematic and careful validation processes using solid experimental and theoretical/simulation data, this challenge can be overcome in a successful manner.

Different ways to employ coarse-graining are briefly introduced in the following section, and the method applied in this work is discussed in more detail in Section 3.2.3. Also, the limitations of coarse-graining are discussed in Section 3.2.2.

3.2.1 Different Approaches to Coarse-Graining

Since the number of non-bonded interactions, and thus the computational load, scales with the square of the number of interaction sites, there are obvious advantages if the number of interacting sites is trimmed. The simplest solution is to group some atoms into a new interaction site, e.g. a methyl group would be represented by a single site. In the *united-atom* approach, nonpolar hydrogen atoms are fused into the adjacent carbon atom [104–106]. In the case of membrane systems, this approach gives up to 60% reduction in particle number, providing a substantial reduction in the computational load.

The previously described method can be taken further by grouping more atoms into a single interaction site. The Martini force field maps on average four heavy atoms and their associated hydrogen atoms into a single interaction center [12, 107, 108], whereas the model by Shelley et al. uses a three-to-one mapping [109]. From these approaches, the Martini model has become more popular and has successfully been used in many studies ranging from lipid membranes and lipoproteins to membrane fusion and nanoparticles and many more, see [110] and references therein. The particle types and interaction parameters of the Martini force field are calibrated against thermodynamic data of oil/water partitioning [12]. The Martini force field is discussed in more detail in Section 3.2.3. Another commonly used approach to derive interaction parameters is *force matching*. In this method, a trajectory from atomistic MD simulation is used to match the force acting on a coarse-grained particle (describing multiple atoms) with the forces acting on the corresponding group of atoms in an atomistic system [111].

Developing even coarser descriptions usually means ignoring of electrostatic interactions and reducing the interaction action site types. Smit et al [112] and Goetz and Lipowski [113] have modeled amphiphiles using only oil- and water-like particles connected via harmonic springs. Despite their simplicity, these models can reproduce many structural, thermodynamic, and mechanical properties of bilayers and vesicles.

A further step in coarse-graining is to eliminate the solvent while taking its effect into account implicitly. The number of solvent particles increases much faster than the number of amphiphiles, and often the role of the solvent is just to stabilize the amphiphiles. Therefore, the removal of the solvent would result in a huge computational speed-up. Several methods utilizing this approach and even coarser ones have been developed, see [114] and references therein.

All the previous methods are so-called *off-lattice* models where the interaction sites are allowed to move freely in space. The next step in coarse-graining is to limit the movement of interaction sites by introducing a lattice. Models taking this approach are called *on-lattice*. Many on-lattice models are based on the idea of Larson's on-lattice model [115–117], where a simple cubic lattice of interaction sites was used. Each interaction site interacts with all 26 interaction sites within one lattice spacing. Interaction sites are either oil-like or water-like, and amphiphiles are formed by connecting water and oil sites together. Interaction strengths are equal between similar sites, but interactions between different types of sites are not favored. The model is characterized by only one parameter, the difference in interaction strength. Monte Carlo simulations using a model similar to Larson's have successfully produced

phase behavior and given insight into the nature of micelles [115].

As shown by this short introduction of different coarse-graining concepts, there is a wide range of alternatives when choosing a suitable research method for the task. One has to know what kind of properties one wants to study and what are the advantages and disadvantages of different methods. The Martini force field was used in Papers [I]-[III]. The method is discussed in more detail in Section 3.2.3.

3.2.2 Limitations of Coarse-Graining

Each different approach to coarse-graining has distinct limitations. The limitation affecting all approaches is the loss of information. Some information is always lost when coarse-graining is carried out, and this applies to all research methods, both experimental and computational. The more important question is how much the loss of information affects the results.

There is no general answer for the effect of the loss of information covering all different coarse-graining approaches. The only reasonable way is to test the used method with different systems under varying conditions to understand how and why the excluded interactions or particles affect the results. Coarse graining can provide unique insights, but without testing the results cannot be trusted.

Coarse graining methods thus cannot be used as a standalone tool from start to finish, but they have to be used in conjunction with other techniques to get a more solid understanding of the system studied. In particular, validation against solid experimental data is essential.

3.2.3 The Martini Coarse-Grained Force Field

The first version of the force field for lipids developed by Marrink et al. was published in 2004 [12]. The name 'Martini' was adapted in 2007 when the version 2.0 for lipids was released [107]. The parameters for peptides and proteins were released in the version 2.1 in 2008 [108]. The most recent version with parameter refinements was published in 2013 [118].

The Martini force field does not focus on reproducing accurate results for a specific system under specific conditions. Instead, it aims to describe a broad range of applications without the need to reparameterize the model each time. Interactions and other simulation parameters were adjusted using a reference oil/water system to reproduce the experimental densities of pure water, and oil, the mutual solubility of oil and water, and the relative diffusion rates [12].

The Martini model is based on a four-to-one mapping, i.e., on average four heavy atoms and adjacent hydrogens are grouped into a single interaction center. Some situations, e.g. ring-like fragments or molecules, require finer description and thus even a two-to-one mapping is used. The mapping ratio was chosen as an optimum between computational efficiency and chemical representability. The Martini model has four main types of particles: polar, non-polar, apolar, and charged. Each category has subtypes based on the hydrogen-bonding capacity and the degree of polarity. Altogether there is a total of 18 particle types.

Non-bonded interactions are described by a Lennard-Jones potential, see Equation 3.6. Different interaction strengths for a given particle pair is assigned based on the types of the particles. The values for different types of pairs can be found in the reference [107]. The electric interaction between charged groups is described by Coulombic potential, see Equation 3.7. A relative dielectric constant is introduced to account for the reduced number of partial charges and dipoles present in atomistic force fields. Both the LJ and Coulombic interactions are cut off at a distance $r_{cut} = 1.2$ nm. The LJ potential is shifted from $r_{shift} = 0.9$ nm to r_{cut}, whereas the Coulombic potential is shifted from $r_{shift} = 0.0$ nm to r_{cut}. The shifting of the electrostatic interactions mimics the effect of distance-dependent screening. The interaction strengths are based on experimental thermodynamic data. The Martini model gives correct trends in free energies of hydration and solvation, but the actual values are systematically too high [107]. Because of that, the use of the Martini model should be restricted to a condensed phase. As mentioned earlier, the Martini model has been parameterized on the basis of solvation free energies, describing the partitioning of molecules to different environments. Thus, the Martini model cannot describe short-scale interactions such as hydrogen bonding in a reliable fashion. Bonded interactions are described by a standard potential shown in Section 3.1.1. The parametrization of the bonded interactions is based on the atomistic geometry or by a comparison with atomistic simulations.

The Martini model currently contains parameters for different lipids, sterols, peptides and proteins, sugars, polymers, nanoparticles, and dendrimers built from the different CG particle types connected together. The model has been well validated, and compared with atomistic simulations as well as experimental data [110]. The parametrization of conformational changes of protein secondary structure is not adequate, thus the secondary structures of proteins simulated in this thesis are fixed [108].

3.3 Analysis Methods

3.3.1 Radial Density Distribution

To characterize the structure of lipoprotein droplets, radial density distributions were coupled using number densities of particles. The distance from the center of mass of the lipids to each particle was calculated at each time step, and a histogram was created. The number of particles in each bin was normalized by the volume of the bin.

3.3.2 Order Parameter Describes Orientational Ordering

The intermolecular ordering induced by cholesterol and cholesteryl oleate ring structures between cholesterol and cholesteryl oleate molecules is studied using an order parameter S_{RR}, defined as

$$S_{RR} = \frac{1}{2}\langle 3\cos^2\theta - 1\rangle, \tag{3.14}$$

where θ is the angle between the directors of two cholesterol (or cholesteryl oleate) molecules. The director of the cholesterol (or cholesteryl oleate) ring structure is defined as a vector from the particle where the short acyl chain is connected to the ring and pointing to the carbon connected to the hydroxyl oxygen. Also, the distance between the centers of the directors was measured and divided into bins, and within each bin, the average order parameter was computed to give a plot of the order parameter as a function of the distance between the directors.

A similar order parameter is used to measure ordering relative to the local normal of the particle. The local normal is the vector pointing from the center of mass of a lipid to the center of the director. The distance from the center of mass of the droplet was measured, and the average order parameter was plotted as a function of radial distance.

3.3.3 Diffusion Characterizes Movement

The mean-squared displacements in the long-time limit are usually used to study the diffusion of molecules [119]. Since in Papers I, II, and IV diffusion takes place in a confined environment, this approach is not useful here.

It is assumed that on the surface of the lipoprotein droplet the diffusion takes place on a two-dimensional surface, whereas in the core all the three dimensions are available. Given this, we use a different approach.

Calculating the displacements of the centers of mass of the molecules over a time scale t gives a histogram, i.e. a jump length distribution. Assuming the movement of the centers of mass to follow a random walk, the obtained jump length distributions can be fitted to the theoretical curves based on two- and three-dimensional random walkers, i.e. to the Gaussian distributions

$$P_{2d}(d;t) = \frac{r}{2Dt} e^{-\frac{r^2}{4Dt}} \tag{3.15}$$

and

$$P_{3d}(d;t) = \frac{4\pi r^2}{(4\pi Dt)^{\frac{3}{2}}} e^{-\frac{r^2}{4Dt}}. \tag{3.16}$$

Different values for the time interval t were used to get the diffusion coefficient D as a function of time. It is expected that the diffusion coefficient levels off at long times, indicating the diffusive behavior to emerge in the hydrodynamic (long-time) limit. At short time scales, the diffusion deviates from the long-time hydrodynamic behavior due to dynamical correlations in the motion of the particles, while at very long time scales the limited size of the confined environment may cause deviations.

3.3.4 Free Energy Calculations

In Paper IV free energy calculations were used to study the difference in free energy profiles between cholesteryl oleate and BODIPY-labeled cholesteryl oleate. The method of choice was replica exchange umbrella sampling (REUS) [120]. In umbrella sampling, a number of initial configurations for the umbrella windows are generated, each having a different value for the chosen reaction coordinate [121, 122]. In this case, the reaction coordinate r was chosen as the distance between the center of mass of HDL and the center of mass of the cholesterol ring structure of the studied molecule. Each umbrella window is then simulated for a sufficiently long time while holding the reaction coordinate by an umbrella potential. The free energy profiles for both molecules were computed using the weighted histogram analysis method [123]. The error was estimated by bootstrap analysis with autocorrelation estimation [124]. REUS combines replica exchange with traditional umbrella sampling. In REUS a replica exchange event means exchanging the umbrella potentials of two neighboring umbrella windows at specified time intervals. The REUS method has been shown to provide a better quality of the resulting free energies than conventional umbrella sampling [125, 126].

4 | Overview of the Simulation Models Studied

Paper I

In Paper I, MD simulations of spheroidal HDL particles were performed using the full lipid compositions of human plasma HDL [127]. The Martini model, described in Section 3.2.3, was employed. Both the protein-free lipid droplet and the full apoA-I containing HDL particles were considered. Cholesteryl oleate was used to model cholesteryl ester, and trioleate to model triglycerides.

The construction of lipoprotein models was implemented in two stages. First, lipid droplets without the apoA-I proteins were constructed. This was accomplished by placing the lipid molecules randomly into a three-dimensional simulation box without any solvent. The mixture of lipids was simulated under NpT conditions to reach the correct density. After that, the lipid melt was solvated and equilibrated for 8 μs. After equilibration, the lipid droplet was simulated for 4 μs.

Next, all-atom apoA-I molecules were generated and coarse-grained. The molecular belt model of apoA-I for discoidal HDL was used as a reference for the conformation of apoA-I [47, 62, 63, 128, 129]. Finally, two apoA-I molecules were added around the equilibrated lipid droplet in a double-belt conformation at a distance of 4 nm from each other. The complete system was shortly equilibrated and simulated over a total period of 19 μs.

The standard components of the Martini model were used for the phospholipids (POPC and PPC), cholesterol, and water. The parameters for cholesteryl oleate and trioleate were constructed using the Martini building blocks, carefully adjusting the key particle types and angle potentials to match the bulk molecular properties found through extensive atomic scale simulations [80, 82]. For the apoA-I molecules, a pre-released version of the Martini model for proteins was used [108].

Paper II

In Paper II, coarse-grained MD simulations of LDL particles were performed, one system containing only the lipid droplet and four others considered with different apoB-100 protein configurations. All the systems had the same lipid composition, corresponding to an average LDL particle [41]. As in Paper I, the construction of the models was implemented in two stages.

First, the lipid droplet was constructed in the manner as in Paper I by creating a lipid melt which was solvated. The lipid melt was allowed to self-organize into a lipid droplet containing phospholipids and some of the free cholesterol on the surface, and cholesteryl oleate, trioleate, and the rest of free cholesterol in the core.

Because the exact structure for the apoB-100 protein is not known, two different secondary structure configurations were constructed. Different sources and methods were combined because none of the suggested models describe the full protein [78, 79, 130]. The first model was mainly based on the theoretical models [79], though some parts of the model were constructed using secondary structure prediction [130]. The second model was similar to the first model, but the first 1000 residues were based on a homology model [78] and the residues 1000-2000 were modeled as a continuous amphipathic β-sheet. For both secondary structures, two different initial placements were constructed.

The force field parameters used for the lipids were the same as in Paper I. The apoB-100 protein was modeled using the Martini model for proteins [108]. For the apoB-100 protein the elastic network model was employed. This approach has a disadvantage in the sense that the secondary structures of proteins will remain fixed. Because of this, it was not possible to study the apoB-100 protein itself in detail. Also since the interaction between the protein and the lipids is defined by the structure of the protein, the behavior of lipids close to apoB-100 was studied on a larger scale.

Paper III

In Paper III, cholesteryl ester transfer protein (CETP) was studied together with HDL-like lipid droplets. Both atomistic and coarse-grained MD simulations were performed.

The structure of CETP was acquired from the RCSB Protein Data Bank. Two cholesteryl esters and two phospholipids were also included in the acquired structure. The lipid droplet consisted of 180 POPC molecules and 35 cholesteryl oleate molecules. CETP was initially placed close to the lipid droplet. Simulations with

different lipid compositions were performed, and the role of helix X was assessed in additional simulations. To study the effect of curvature, a simulation with a planar trilayer system including 512 POPC and 796 CE molecules was carried out.

In the atomistic simulations, Berger parameters [104] were used for the lipids, and the GROMOS53A6 force field was employed for the protein [131]. The Martini force field was applied in the coarse-grained simulations [12, 108]. For CETP, the elastic network model was employed to keep the secondary structure stable.

Paper IV

In Paper IV, the function of BODIPY-labeled cholesteryl ester in HDL particles was studied using atomistic MD simulations. The atomistic model of a pristine HDL particle was taken from a previous study [65] containing 16 cholesteryl ester molecules in the core, 56 POPC molecules, and two apoA-I chains on the surface of the particle. In modified HDL, one or three of the cholesteryl ester molecules were replaced with BODIPY-labeled cholesteryl esters. Free energy calculations were performed using a series of replica exchange umbrella sampling simulations.

The Berger force field was used for the lipids [104], together with the OPLS-AA force field for the apoA-I proteins [132]. The combination of the two force fields has been validated, and the combination rules with the technique described by Neale and Pomes were applied [133, 134]. The parameters for the BODIPY-probe were adapted from an earlier study [135].

5 | Results and Discussion

The results discussed in this Chapter are based on data presented in Papers I - IV. The publishers of these articles have granted permissions to show the articles in this thesis, thus permissions to show the figures depicted in Chapter 5 are in order.

5.1 Role of Lipids in Spheroidal High-Density Lipoproteins

Cardiovascular diseases are the primary cause of death in western countries [8, 9]. Atherosclerosis, accumulation of lipids and plaque formation on arterial walls, is one of the main causes. High levels of high-density lipoprotein (HDL) circulating in the bloodstream is associated with a reduction of risk for atherosclerosis. However, the function and also the structure of HDL are not well understood, partly due to experimental difficulties to deal with soft and nanosized HDL. Computational methods can give insight that is not accessible through experiments. In Paper I, models mimicking high-density lipoprotein were constructed and simulated to study the role of lipids in HDL structure and dynamics. Molecular dynamics (MD) using the coarse-graining approach for both a lipid droplet without apoA-I and the full HDL particle including two apoA-I molecules surrounding the lipid droplet were performed. These simulations were the first computational studies where the size and lipid composition of HDL were realistic, i.e., corresponding to human serum HDL. The main focus was on the assembly of lipids and the influence of lipid-protein interactions on HDL properties.

The simulations revealed the internal structure of the simulated HDL particles. Here we summarise the main findings. The radial densities of different molecule types are shown in Figure 5.1. The hydrophobic cholesteryl oleate and triglyceride are located in the core, and the polar lipids are at the surface region facing the water. Most of the cholesterol is located in the surface region, but a small but significant amount is also found in the core. The apoA-I proteins are embedded on the surface, and the presence of the proteins just slightly disturbs the lipid distribution when compared with the result without the protein part. There is no relevant change in

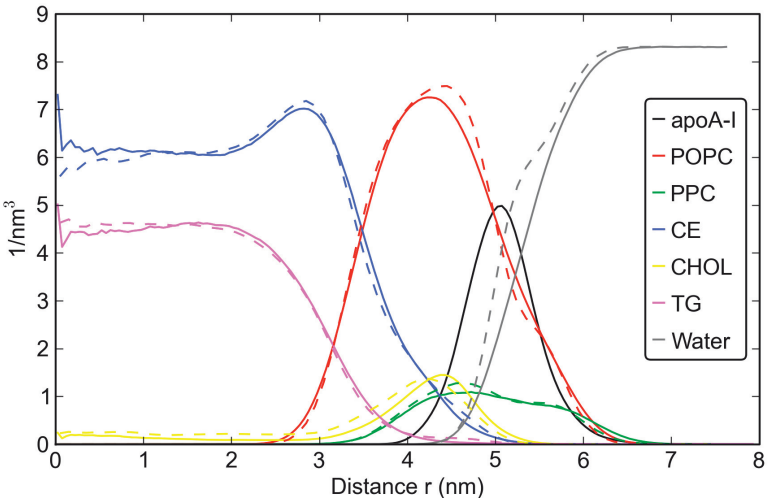

Figure 5.1: Radial densities showing the composition of the studied particles versus distance from the center of mass (COM) of the particle. The solid lines are for the full HDL particle, the dashed lines for the lipid droplet without apoA-I. Reproduced from [10].

the distributions of hydrophobic lipids. The most significant change observed is the shifting of the cholesterol distribution towards the water interface. Cholesterol seems to prefer interactions with the apoA-I proteins.

The density distribution of cholesteryl oleate overlaps significantly with the distributions of the surface lipids, i.e., phospholipids and cholesterol. This finding is in disagreement with the previously suggested two-layer model, i.e., a model consisting of a hydrophobic core and a polar surface suggested for the structure of the lipid droplet. Furthermore, the inspection of the ring structure orientation of cholesterol and cholesteryl oleate reveals that in the center of the particle the orientation is totally random, but as one approaches the surface region, ordering starts to appear, see Figure 5.2. Close to the surface region the cholesteryl oleate ring structure prefers to be aligned along the radial direction of HDL and interdigitating with the phospholipid tails. Also, changes in the preferred conformations of cholesteryl oleate and triglyceride are observed when the behavior in the core and close to the surface is compared. The data show that the two-layer model is not sufficient and the structure is better described by a model consisting of a surface, a core, and a more ordered intermediate transition region between them. This transition region is rather narrow, and rather difficult to define spatially, and it represents a crossover from the hydrophobic to the hydrophilic environment rather than a true layer of its own.

In addition to structural properties, also the dynamics varies significantly in the different regions. The diffusion is found to be about ten times faster on the surface

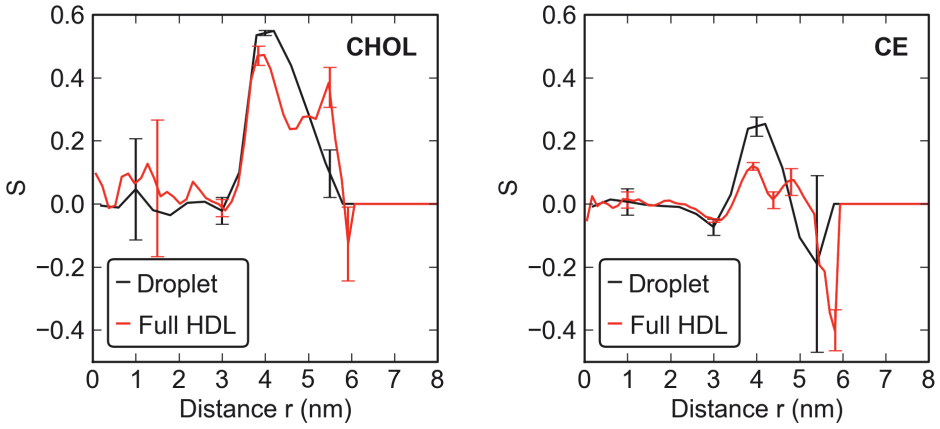

Figure 5.2: Order parameter S for the ring structures of CHOL (left) and CE (right). The black curves describe the lipid droplet and the red curves the full HDL. Reproduced from [10].

than in the core, and the diffusion coefficient in the intermediate region is between the two extremities. Since theoretically the diffusion is inversely proportional to the viscosity of the surrounding medium of the diffusing particle, this result suggests that the viscosity increases as one moves towards the center of a lipoprotein particle. The viscosity in turn could be increased by, e.g., entanglement between lipid chains. However, how the intermolecular orientations affect the viscosity (or diffusion) of lipid systems has not been discussed in the literature to the extent that a comparison would here be possible. The apoA-I proteins may slow down the diffusion of lipids slightly, especially close to the interfacial regions. It seems that the molecular transport between the surface and the intermediate region is relatively fast, but the transport between the surface and the core is relatively slow.

Studying protein-lipid interactions reveals that phospholipids and triglycerides prefer to interact through the acyl chains, and phospholipids also through the glycerol backbone. Cholesterol and cholesteryl oleate, on the other hand, interact mainly through the sterol ring structure. About 80% of cholesterol is annular to apoA-I, while only 10% of cholesteryl oleate is close to the protein part. Cholesterol molecules spend half of their time in contact with apoA-I. The lifetime of cholesterol-protein interaction is relatively long (175 ns) and longer than for cholesteryl oleate (15 ns).

The molecular scale insight of HDL structure and dynamics found and confirmed here derives from the ordering and dynamical phenomena taking place close to the HDL-water interface, in part driven by the interactions between cholesterol and apoA-I. The results pave the way for future studies to gain a deeper understanding of HDL properties and their relation to health.

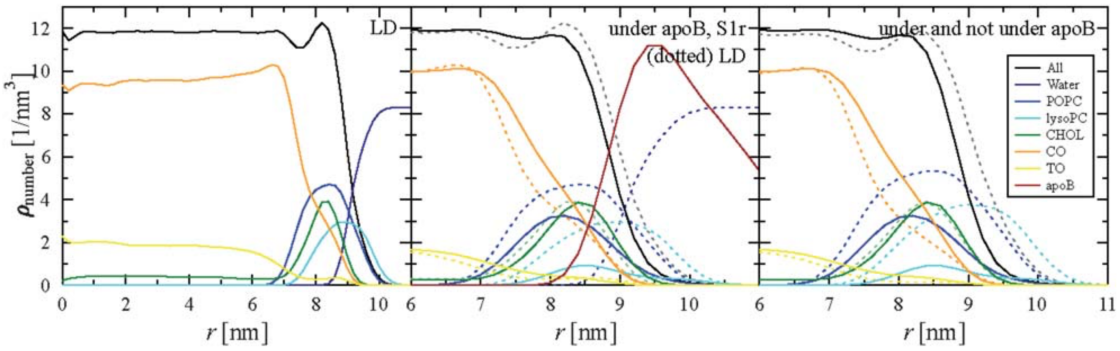

Figure 5.3: Number density of particles vs. distance from the centre of the droplet (r): all lipids (black), POPC (blue), PPC (cyan, scaled by 10), CHOL (green), CO (orange), TO (yellow), water (dark blue, not in right panel), protein (brown, only middle panel). The left panel shows the distribution in the lipid droplet (LD) without apoB-100. The middle panel shows how the distribution changes under apoB-100. The dotted lines are identical to those in the left panel; the solid lines show the distribution in regions where there is protein on the surface. The right panel compares the distribution between the regions covered and not covered by apoB-100 in S1r. S1r refers to system S1 where the structure of LDL was mainly based on theoretical models, for more details, see [11]. The solid line is identical to the middle panel. The dotted line shows the distribution in regions not covered by apoB-100. Reproduced from [11].

5.2 Effects of ApoB-100 Binding on an LDL Lipid Droplet

Low-density lipoprotein (LDL) particles transport cholesterol and its esters in the bloodstream. LDL has a central role in the development of cardiovascular diseases, in particular, atherogenesis, as discussed in Section 2.4. Despite the importance of LDL, its structure is not known in detail, which in turn is rather distressing since the lack of LDL's structural information makes it more difficult to understand its function and develop treatments for cardiovascular diseases.

In Paper II, experimental and theoretical data were combined to construct low-density lipoprotein models for near-atomistic MD simulations. Through multi-microsecond molecular simulations using two different models for apoB-100, structural and dynamical properties of LDL were unraveled with the primary focus on lipids and their interactions with the apoB-100 protein. Doing this was exceptionally challenging due to the size of LDL particle and the lacking knowledge about the precise structure of apoB-100. Here we again summarise the main findings.

Figure 5.3 (left panel) illustrates the structure of the LDL lipid droplet by showing particle densities as a function of distance from the center of the droplet. The LDL particle is partitioned into a surface monolayer consisting mostly of phospho-

lipids (POPC and PPC) and cholesterol (CHOL), and a hydrophobic core containing cholesteryl oleate (CO), triglycerides (TO), as well as about 13% of the cholesterol molecules. It is noteworthy that the distribution of core lipids (CO and TO) extends to the water phase. Given this, it is possible that the proteins on the surface can interact with the neutral lipids in the core of the particle. This possibility is highly relevant for lipid transfer proteins, for example, cholesterol ester transfer protein (CETP), which is studied in Paper III [13]. Figure 5.3 (middle panel) shows the changes on the surface close to apoB-100. It is observed that the densities of POPC and lysoPC are reduced closer to apoB-100, suggesting that apoB-100 prefers to interact directly with core lipids. ApoB-100 pushes POPC and lysoPC away, and this increases the packing of surface lipids, which in turn affects the core lipids, as they are not able to penetrate as often to the surface, as seen in Figure 5.3 (right panel).

The ordering of lipids was studied using the orientation of the ring structures of cholesterol and cholesteryl oleate, see Figure 5.4 for the order parameters. In the core the ordering is random, however within the surface monolayer the ring structures are already mainly aligned along the normal, i.e. ring structures stand upright between the phospholipid chains. Adding apoB-100 displaces the surface monolayer, and the protein prefers to interact directly with the core of the particle. This results in a significantly lower area per lipid in the surface monolayer, which in turn affects the density distribution as the core lipids do not penetrate as often to the surface. The ordering of the ring structures increases in regions not under apoB-100 and decreases under the protein.

It is observed that the diffusion speeds up as one moves from the core towards the surface, the diffusion coefficient increasing by a factor of 10. This observed change in the diffusion rate might be related to changes in viscosity, local density, and entanglement effects between lipid chains. The same behavior is observed in the HDL lipid droplet in Paper I, as discussed in the previous chapter. ApoB-100 does not affect the diffusion of the core lipids, but it slows down the diffusion of lipids on the surface. The effect is more clearly seen close to apoB-100, but it is present also in the other parts of the surface. The factors explaining the slowing down of diffusion are in particular the decreasing area per lipid and possible specific interactions with the protein residues.

Because of the limitations of the model used (uncertainty in the 3D structure of apoB-100 and its fixed secondary structure), it is not possible to study the protein in detail, or the specific interactions between the protein and the lipids that may depend on the protein secondary structure, and are thus disregarded from this discussion.

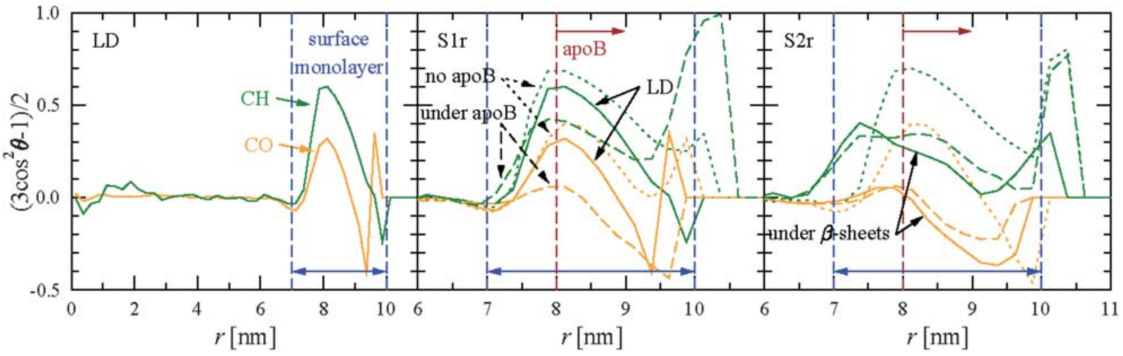

Figure 5.4: Order parameter of the angle between the CHOL plane and the local normal for CHOL (green) and CO (orange) versus distance from the center of the droplet. The left panel shows the situation in the absence of apoB-100. The middle panel shows the effect of apoB-100 in S1r. The solid lines are identical to the left panel, while the dashed and dotted lines show the situation in regions covered and not covered by apoB-100, respectively. The right panel shows the effect of protein secondary structure on the ordering in S2r. The dotted and dashed lines show the order parameter in regions covered and not covered by apoB-100, respectively. The solid line represents regions where apoB-100 has b-strands close to the lipid surface. Reproduced from [11].

However, on a larger scale where the simulation used in the Ph.D. thesis work was expected to be valid, the behavior of apoB-100 in the simulations is in agreement with experimental findings [11].

In conclusion, this study provided the first molecular-scale model for LDL structure and dynamics based on near-atomistic simulations. The results show that LDL structure cannot be described using a simple two- or three-layer model. According to the results, the structure is better described with a hydrophobic core and a polar surface, and a broad transition region between them. The results provide a solid basis for future studies unraveling the role of LDL and its modifications in the development of atherosclerosis.

5.3 Trying to Understand the Function of Cholesteryl Ester Transfer Protein

Cholesteryl ester transfer protein (CETP) facilitates the transport of cholesteryl esters, triglycerides, and phospholipids between different lipoprotein fractions. CETP has a potentially important role in the development of cardiovascular diseases, since lower CETP activity has been associated with a decreased risk for coronary heart disease [136]. The inhibition of CETP has been shown to be a valid strategy to prevent and treat the coronary heart disease [137, 138].

In Paper III, MD simulations were performed to complement experiments and to study mechanisms associated with the CETP-mediated lipid exchange. Both atomistic and coarse-grained approaches were used. The results were consistent with each other. Key findings are summarised here.

CETP anchors to the surface of high-density lipoprotein-like lipid droplets mainly through its charged and tryptophan residues located mainly at the edge of the concave surface. Figure 5.5 shows the locations of the amino acids playing a role in the binding process, also showing the number of salt bridges formed. The structure of CETP is found to be rather elastic, making it possible to adapt to different curvatures of the lipoprotein lipid droplet.

Upon binding, CETP rapidly (in about 10 ns) induces the formation of a small hydrophobic patch to the phospholipid surface of the droplet, opening a route from the core of the droplet to the binding pocket of CETP. The timescale for the complete formation of these hydrophobic patches might be of the order of microseconds. After careful inspection of atomistic simulation data, the effect is also observed in these cases, but the effect is not as profound as in coarse-grained simulations. By removing phospholipids and thus lowering the surface pressure, the number of contacts between cholesteryl oleate molecules and CETP increased. Figure 5.6 shows a snapshot of the attachment and visualizes the formation of the hydrophobic patch, especially in the case of a reduced number of phospholipids. Also, the number of contacts between CETP and core lipids is shown.

Helix X and its hinge region are highly mobile, and it is observed that under favorable conditions helix X becomes buried inside CETP, creating a hydrophobic pathway from the droplet surface to the hydrophobic tunnel. The accessibility of cholesteryl esters to the tunnel opening of CETP is observed to increase when helix X is in an open state.

Removal of helix X leads to diffusion of cholesteryl oleate molecules into CETP. The results hint that helix X might work as a lid, opening the hydrophobic tunnel when bound to a lipoprotein and closing the tunnel when moving between lipoproteins.

This study provided a detailed atomistic picture regarding the first initial steps in the process of the lipid exchange mechanism of CETP. This serves as a solid foundation for further studies aiming for a more detailed understanding of the function of CETP and also for discovering possibilities to design new drugs to be used in the fight against atherosclerosis.

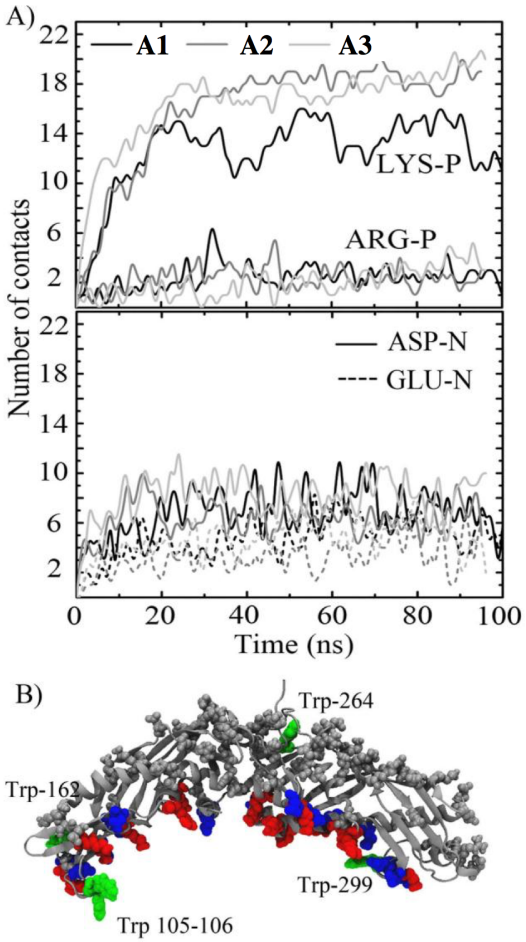

Figure 5.5: Electrostatic interactions between CETP and lipid droplet. A) A number of salt bridges formed between the charged residues of CETP and the head groups of POPCs as a function of time. The upper profile shows the number of contacts between the positively charged residues and P atoms of POPCs, and the lower profile shows the number of contacts between the negatively charged amino acids and N atoms of POPCs. B) Salt bridge-forming positively (red) and negatively (blue) charged amino acids are marked to the structure of CETP. Trp residues are labeled (green). Reproduced from [13].

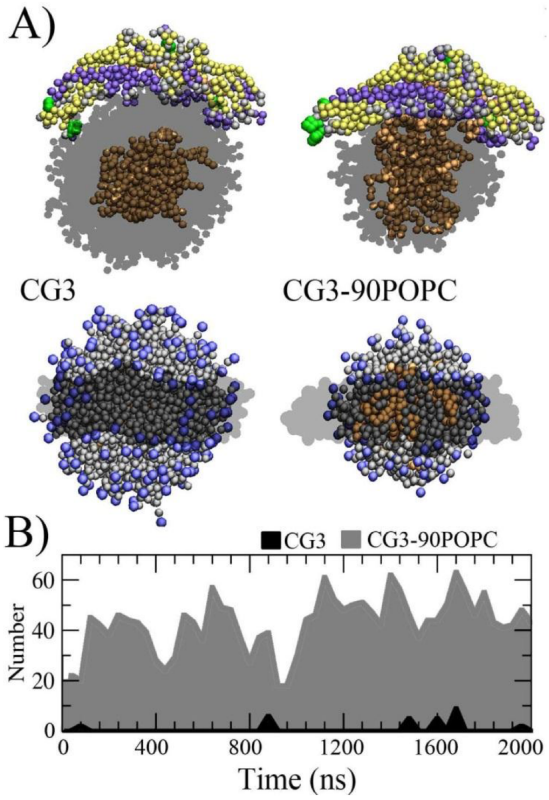

Figure 5.6: Interaction of CETP with core lipids. A) Snapshots from the coarse-grained simulations. CG3 (left) corresponds to coarse-grained atomistic system A3 and CG3-90POPC (right) to the same system but half (90) of POPCs removed, for more details of the systems, see [13]. The upper snapshots show side views and the lower ones show top views of CETP bound to a lipid droplet. In the case of CG3-POPC, the hydrophobic patch under CETP is clearly visible, mainly because the removal of POPCs give CETP better access to core lipids. The structure of CETP has been rendered using secondary structure information in upper snapshots (β-sheets are yellow, α-helices violet, and random coils gray) or as dark transparent phantom in lower snapshots. The green spheres are Trp residues. POPCs are transparent in the upper snapshots, while those in the bottom snapshots are visible as grey (the choline head groups are visible as blue). CEs are rendered with orange spheres. Water molecules were omitted for clarity. B) Number of contacts between core CEs and CETP with different surface-core lipid ratios as a function of time. The results confirm what is visually observed in panel A. Reproduced from [13].

5.4 Is BODIPY a Feasible Molecular Probe in Lipoprotein Environment?

Fluorescent probes are essential tools in experiments to visualize various cellular transport processes and also to help in clarifying physiological and pathophysiological changes in a body. However, labeling of molecules with fluorescent probes always changes the nature of the host molecules. Sometimes the changes in behavior are

so subtle that the properties of the labeled molecule closely match the properties of the original molecule. Problems arise when the changes are substantial enough to alter the behavior completely, thus making the probe unsuitable for a given task. The probe might work in one environment but fail completely in a different situation. It is thus vital to validate the used probes in the studied environment before using them, or at least before interpreting the results.

In Paper IV, the behavior of BODIPY-labeled cholesteryl ester (BODIPY-CE) was studied in a high-density lipoprotein environment and compared with the behavior of unlabeled cholesteryl ester. Below we highlight the main results.

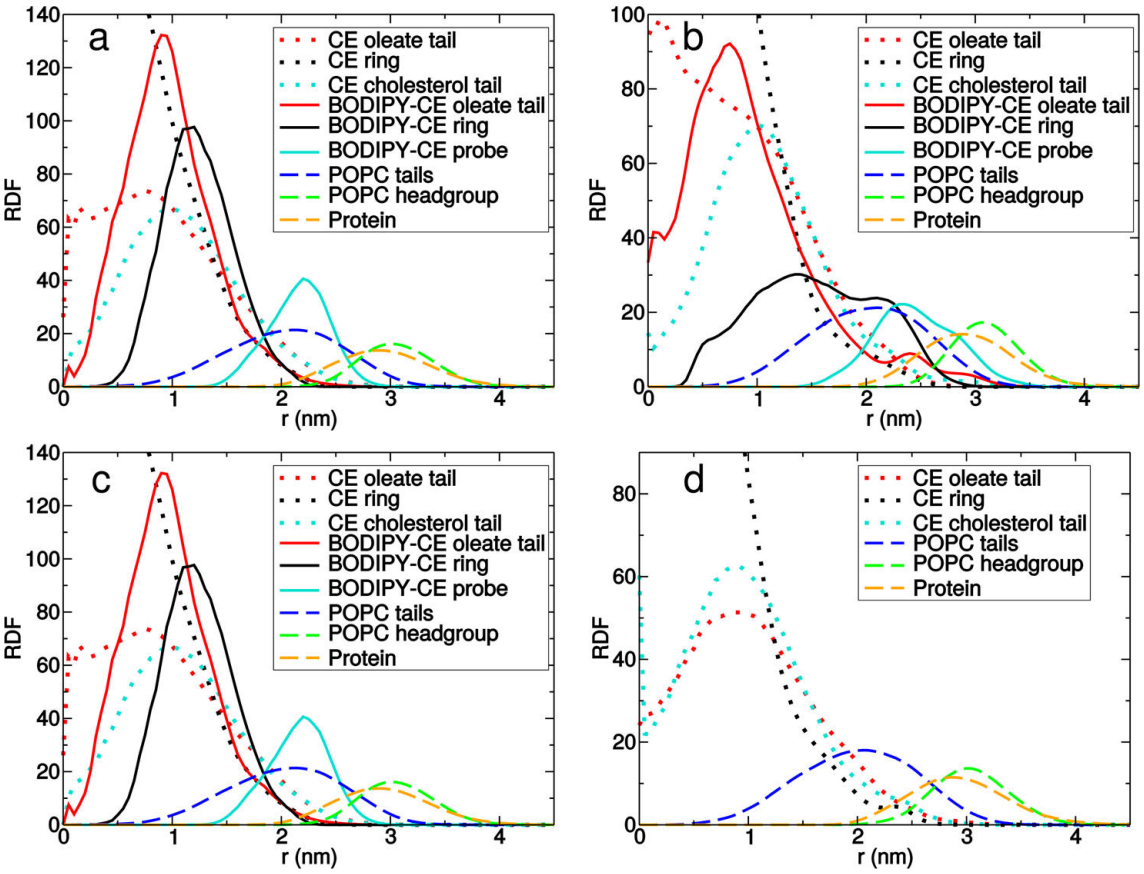

Figure 5.7: Radial distribution functions (RDF) from four independent unbiased simulations of HDL. From a to d, the CE/BODIPY-CE counts are 13/3, 13/3, 15/1, and 16/0, in respective order. At small distances the RDF value of the CE ring extends to 250, but for clarity's sake we draw the plot only up to 140. In panel b, one of the BODIPY-CE molecules is oriented tangentially with respect to HDL, giving rise to a shoulder in the plot of the BODIPY-CE ring at r=2.3 nm. Reproduced from [14].

The radial distribution functions are shown in Figure 5.7. In the unlabeled HDL (Panel d), apoA-I proteins are located at the surface region comprised of POPC molecules. The CE molecules are in the core, and based on their radial distribution

they are randomly oriented as in a melt. Comparing the unlabeled HDL to the systems with labeled BODIPY-CE (Panels a-c) reveals a major difference in the core region. BODIPY-CE does not favor being in the center of the HDL particle, as the oleate tail and the ring part avoid the particle center. This is due to the BODIPY part favoring the region between the acyl chains and the headgroups of the phospholipids. Studying the preferred orientation of both CE and BODIPY-CE shows that the orientation of the ring structures of unlabeled CE is almost random, whereas BODIPY-CE prefers orientations pointing outwards from the center of the HDL particle.

The differences in localization were studied also using replica umbrella sampling. The results show that both BODIPY-CE and unlabeled CE assemble similarly into HDL upon contact. However, BODIPY-CE does not diffuse all the way to the core but remains between the surface and the core, whereas unlabeled CE readily migrates to the HDL core. Also, the diffusion of BODIPY-CE is slower than the diffusion of its counterpart, which can be explained by the preference of keeping the BODIPY probe in the surface region and the CE body away from it.

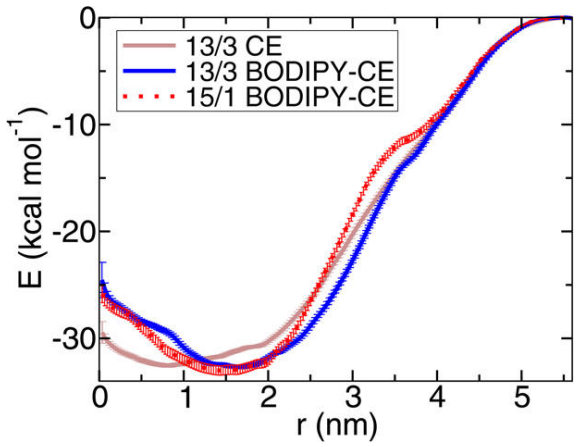

Figure 5.8: Free energy E as a function of distance r shown for CE and BODIPY-CE. The distance r is from the center-of-mass (COM) of HDL to the COM of the cholesterol ring in CE or BODIPY-CE. The free energy is set to zero at r = 5.5 nm. The presented data also show the error bars depicted by varying thickness of the curves. Reproduced from [14].

Based on the results, the labeling of CE with the BODIPY probe alters the properties of BODIPY-CE to the extent that renders it unable to fully mimic the behavior of cholesteryl ester in a lipoprotein environment. It seems that an essential property for a valid probe in a lipoprotein environment is to have little or no affinity for the hydrophilic surface region.

6 | Concluding Remarks

Studying the structure and function of lipoprotein particles using experimental methods is rather challenging due to the small size and dynamic nature of lipoproteins. Often experiments are carried out in unphysiological conditions which might dramatically alter the structure and function of lipoproteins. Through molecular dynamics (MD) simulations, phenomena or properties unreachable by experimental methods can be accessed. MD simulation methods can overcome limitations of experimental methods related to the short time and length scales.

However, many biological processes take place in relatively long time and length scales that for simulations in the atomistic regime are challenging due to the enormous computational load. By removing some details through coarse-graining, one can develop models that are feasible enough to consider sufficiently large system sizes and time scales. In this thesis, MD simulations were employed to explore cholesterol transport, high- and low-density lipoproteins in particular.

Through extensive coarse-grained simulations, the first detailed structural model for both HDL and LDL was provided showing that the previously proposed 2- and 3-layer models are inadequate to describe the properties of the lipid droplets. It was found that the structural and dynamic properties of lipids depend significantly on their location and distance from the center of the particle. The protein components, apoA-I in HDL and apoB-100 in LDL, are not just lying on top of the surface of the lipid droplets but they, e.g., interact also with the hydrophobic lipids located beneath the surface.

The detailed atomistic picture of the initial steps in the lipid exchange mechanism of CETP was provided. The mechanism and the residues involved in the process of anchoring CETP onto the surface of the droplet was revealed. Also, the critical role of helix X as a door to the hydrophobic tunnel carrying the cargo lipids was studied. CETP anchors to the surface of HDL mainly through charged and tryptophan residues. After attachment to HDL, a small hydrophobic patch forms rapidly, opening a route from the binding pocket of CETP to the core of the lipid droplet. Helix

X of CETP seems to work as a lid, opening the hydrophobic tunnel when bound to a lipoprotein and closing it when moving between lipoproteins. These findings help us to understand in a mechanistic way how CETP-mediated lipid exchange takes place between different lipoproteins.

Studying the properties of BODIPY-labeled cholesteryl oleate in a lipoprotein-like environment revealed that the influence of BODIPY is strong enough to render the behavior of the BODIPY-labeled cholesteryl ester qualitatively different from its unlabeled counterpart. Based on these differences BODIPY-labeled cholesteryl oleate is not suitable to be used experimentally in a lipoprotein environment. It appears that a successful probe in a lipoprotein environment should have no significant affinity for a hydrophilic surface region.

Looking back and evaluating the work done, the choice of the Martini model and the idea to apply it to lipoprotein systems is one of the strengths of this work. In the beginning, it was not clear whether it could be applied successfully on lipoprotein systems, as it was earlier mainly used for membrane studies [107]. The selected method made it possible to simulate systems inaccessible at that time by conventional atomic MD simulations. The results of these studies and later also the studies by other groups have shown that this model can be applied to study many different phenomena taking place in lipoproteins [110]. If the same studies were repeated today, longer time scales would probably be used to improve the statistics, and more realistic models for HDL in papers III and IV would be used. In the Martini model, the secondary structure of proteins is fixed, and it limits the possibilities of studying the dynamic nature of lipoprotein-associated proteins [108].

When the results of this thesis are considered overall, one can conclude that there are three key take-home messages that have the most significant impact. First, the research results discussed in this thesis provide compelling evidence that atomistic and molecular-scale computer simulations are an exceptionally competent tool able to complement experiments in the nanoscale. Consideration of the structure and dynamics of soft nanoscale particles such as lipoproteins is an exceptionally tough challenge, but through computer simulations, this insight can be revealed. Second, these simulations provided pioneering atomistic insight into the structure and dynamics of lipoprotein particles and their interactions with carrier particles such as CETP. Third, based on this knowledge, one can conclude that the simulation models developed and the results found in this work provide a solid basis for further investigations of cellular processes dealing with lipoproteins and lipid trafficking, examples including the binding of lipoproteins with their receptors, the fusion of lipoproteins,

and the development of new drugs for modulating the lipid trafficking processes. All these processes contribute to our health in the context of cardiovascular diseases, and thus further studies of these ideas using the models and tools developed in this thesis work would be more than welcome.

Moving on in the same context, the findings pave the way for further studies of HDL and LDL to better understand the key steps in the initial events of atherosclerosis, and the molecular level events in the lipid exchange processes. One interesting research topic would be to apply reverse coarse-graining on the CETP model to get back to atomistic scale [139]. This would give a possibility to study the protein behavior after the initial attachment and to get rid of the limitations of the Martini model as to the protein secondary structure. Further, given that dietary and living habits affect the lipid composition of lipoprotein particles [57, 140], methods used in this work could be extended to study the coupling between the lipid composition of LDL and its structure and function.

Bibliography

1. *Cholesterol. Chemistry, Biochemistry and Pathology* (ed Cook, R. P.) (Academic Press, New York, 1958).
2. Nelson, D. L. & Cox, M. M. *Lehninger Principles of Biochemistry* 4. edition (W. H. Freeman and Company, New York, 2005).
3. Libby, P, Aikawa, M & Schönbeck, U. Cholesterol and Atherosclerosis. *Biochimica et Biophysica Acta* **1529,** 299–309 (2000).
4. De Groot, L. J., Beck-Peccoz, P., Chrousos, G., Dungan, K., Grossman, A., Hershman, J. M., Koch, C., McLachlan, R., New, M., Rebar, R., Singer, F., Vinik, A., Weickert, M. O., Linton, M. F., Yancey, P. G., Davies, S. S., Jerome, W. G. J., Linton, E. F. & Vickers, K. C. in *www.endotext.org* (MDTEXT.com, South Dartmouth, 2015).
5. Bonetti, P. O., Lerman, L. O. & Lerman, A. Endothelial Dysfunction: A Marker of Atherosclerotic Risk. *Arteriosclerosis, Thrombosis, and Vascular Biology* **23,** 168–175 (2003).
6. Nakashima, Y, Fujii, H, Sumiyoshi, S, Wight, T. N. & Sueishi, K. Early Human Atherosclerosis: Accumulation of Lipid and Proteoglycans in Intimal Thickenings Followed by Macrophage Infiltration. *Arteriosclerosis, Thrombosis, and Vascular Biology* **27,** 1159–1165 (2007).
7. Falk, E. Pathogenesis of Atherosclerosis. *Journal of the American College of Cardiology* **47,** C7–C12 (2006).
8. World Health Organization. WHO | The Top 10 Causes of Death. *WHO* (2014).
9. Kenneth, D, Kochanek, M. A., Sherry, L, Murphy, B. S., Jiaquan Xu, M. D. & Betzaida, T.-V. Deaths: Final Data for 2014. *National Vital Statistics Reports* **65** (2016).

10. Vuorela, T. A., Catte, A., Niemelä, P. & Hall, A. Role of Lipids in Spheroidal High Density Lipoproteins. *PLoS Computational Biology* **6,** e1000964 (2010).

11. Murtola, T., Vuorela, T. A., Hyvönen, M. T., Marrink, S.-J., Karttunen, M. & Vattulainen, I. Low Density Lipoprotein: Structure, Dynamics, and Interactions of ApoB-100 with Lipids. *Soft Matter* **7,** 8135–8141 (2011).

12. Marrink, S.-J., de Vries, A. H. & Mark, A. E. Coarse Grained Model for Semiquantitative Lipid Simulations. *The Journal of Physical Chemistry B* **108,** 750–760 (2004).

13. Koivuniemi, A., Vuorela, T., Kovanen, P. T., Vattulainen, I. & Hyvönen, M. T. Lipid Exchange Mechanism of the Cholesteryl Ester Transfer Protein Clarified by Atomistic and Coarse-Grained Simulations. *PLoS Computational Biology* **8,** e1002299 (2012).

14. Karilainen, T., Vuorela, T. & Vattulainen, I. How Well Does BODIPY-Cholesteryl Ester Mimic Unlabeled Cholesteryl Esters in High Density Lipoprotein Particles? *The Journal of Physical Chemistry B* **119,** 15848–15856 (2015).

15. Olson, R. E. Discovery of the Lipoproteins, Their Role in Fat Transport and Their Significance as Risk Factors. *The Journal of Nutrition* **128,** 439S–443S (1998).

16. McNamara, J., Warnick, G. & Cooper, G. A Brief History of Lipid and Lipoprotein Measurements and Their Contribution to Clinical Chemistry. *Clinica Chimica Acta* **369,** 158–167 (2006).

17. Alberts, B., Johnson, A., Lewis, J., Raff, M., Roberts, K. & Walter, P. *Molecular Biology of the Cell, 5th Edition* (Garland Science, New York, 2008).

18. Lingwood, D & Simons, K. Lipid Rafts as a Membrane-Organizing Principle. *Science* **327,** 46–50 (2010).

19. Malmivuo, J. & Plonsey, R. *Bioelectromagnetism* (Oxford University Press, New York, 1995).

20. Saher, G., Brügger, B., Lappe-Siefke, C., Möbius, W., Tozawa, R.-i., Wehr, M. C., Wieland, F., Ishibashi, S. & Nave, K.-A. High Cholesterol Level Is Essential for Myelin Membrane Growth. *Nature Neuroscience* **8,** 468–475 (2005).

21. Pludowski, P., Holick, M. F., Pilz, S., Wagner, C. L., Hollis, B. W., Grant, W. B., Shoenfeld, Y., Lerchbaum, E., Llewellyn, D. J., Kienreich, K. & Soni, M. Vitamin D Effects on Musculoskeletal Health, Immunity, Autoimmunity, Cardiovascular Disease, Cancer, Fertility, Pregnancy, Dementia and Mortality-a Review of Recent Evidence. *Autoimmunity reviews* **12,** 976–989 (2013).

22. Feingold, K. R. & Grunfeld, C. in *www.endotext.org* (MDTEXT.com, South Dartmouth, 2015).

23. Boren, J, Lee, I, Zhu, W, Arnold, K, Taylor, S & Innerarity, T. L. Identification of the Low Density Lipoprotein Receptor-Binding Site in Apolipoprotein B100 and the Modulation of Its Binding Activity by the Carboxyl Terminus in Familial Defective Apo-B100. *The Journal of Clinical Investigation* **101,** 1084–1093 (1998).

24. Colvin, P. & Parks, J. Metabolism of High Density Lipoprotein Subfractions. *Current Opinion in Lipidology* **10,** 309–314 (1999).

25. Linton, M. F., Yancey, P. G., Davies, S. S., Gray Jerome, W, Linton, E. F. & Vickers, K. C. in *www.endotext.org* (South Dartmouth, 2015).

26. Ruffer, M. A. On Arterial Lesions Found in Egyptian Mummies (1580B.C.-525A.D.). *The Journal of Pathology and Bacteriology* **15,** 453–462 (1911).

27. Sandison, A. T. Degenerative Vascular Disease in the Egyptian Mummy. **6,** 77–81 (1962).

28. Zimmerman, M. R. The Paleopathology of the Cardiovascular System. *Texas Heart Institute Journal* **20,** 252–257 (1993).

29. Lobstein, J. F. *Traité D'anatomie Pathologique* (Levrault, Paris, 1829).

30. Mayerl, C., Lukasser, M., Sedivy, R., Niederegger, H., Seiler, R. & Wick, G. Atherosclerosis Research From Past to Present—on the Track of Two Pathologists with Opposing Views, Carl Von Rokitansky and Rudolf Virchow. *Virchows Archiv* **449,** 96–103 (2006).

31. Anitschkow, N & Chalatow, S. Classics in Arteriosclerosis Research: on Experimental Cholesterin Steatosis and Its Significance in the Origin of Some Pathological Processes. *Arteriosclerosis* **3,** 178–182 (1983).

32. Libby, P. Changing Concepts of Atherogenesis. *Journal of Internal Medicine* **247,** 349–358 (2000).

33. Heusch, G., Libby, P., Gersh, B., Yellon, D., Böhm, M., Lopaschuk, G. & Opie, L. Cardiovascular Remodelling in Coronary Artery Disease and Heart Failure. *Lancet* **383,** 1933–1943 (2014).

34. Murphy, A. J., Woollard, K. J., Hoang, A., Mukhamedova, N., Stirzaker, R. A., McCormick, S. P. A., Remaley, A. T., Sviridov, D. & Chin-Dusting, J. High-Density Lipoprotein Reduces the Human Monocyte Inflammatory Response. *Arteriosclerosis, Thrombosis, and Vascular Biology* **28,** 2071–2077 (2008).

35. Naqvi, T. Z., Shah, P. K., Ivey, P. A., Molloy, M. D., Thomas, A. M., Panicker, S, Ahmed, A, Cercek, B & Kaul, S. Evidence That High-Density Lipoprotein Cholesterol Is an Independent Predictor of Acute Platelet-Dependent Thrombus Formation. *The American Journal of Cardiology* **84,** 1011–1017 (1999).

36. Nofer, J.-R., Brodde, M. F. & Kehrel, B. E. High-Density Lipoproteins, Platelets and the Pathogenesis of Atherosclerosis. *Clinical and Experimental Pharmacology and Physiology* **37,** 726–735 (2010).

37. Carson, S. D. Plasma High Density Lipoproteins Inhibit the Activation of Coagulation Factor X by Factor VIIa and Tissue Factor. *FEBS Letters* **132,** 37–40 (1981).

38. Navab, M, Hama, S. Y., Cooke, C. J., Anantharamaiah, G. M., Chaddha, M, Jin, L, Subbanagounder, G, Faull, K. F., Reddy, S. T., Miller, N. E. & Fogelman, A. M. Normal High Density Lipoprotein Inhibits Three Steps in the Formation of Mildly Oxidized Low Density Lipoprotein: Step 1. *The Journal of Lipid Research* **41,** 1481–1494 (2000).

39. Navab, M, Hama, S. Y., Anantharamaiah, G. M., Hassan, K, Hough, G. P., Watson, A. D., Reddy, S. T., Sevanian, A, Fonarow, G. C. & Fogelman, A. M. Normal High Density Lipoprotein Inhibits Three Steps in the Formation of Mildly Oxidized Low Density Lipoprotein: Steps 2 and 3. *The Journal of Lipid Research* **41,** 1495–1508 (2000).

40. Nofer, J.-R., van der Giet, M., Tölle, M., Wolinska, I., von Wnuck Lipinski, K., Baba, H. A., Tietge, U. J., Gödecke, A., Ishii, I., Kleuser, B., Schäfers, M., Fobker, M., Zidek, W., Assmann, G., Chun, J. & Levkau, B. HDL Induces NO-Dependent Vasorelaxation via the Lysophospholipid Receptor S1P3. *The Journal of Clinical Investigation* **113,** 569–581 (2004).

41. Hevonoja, T, Pentikäinen, M. O., Hyvönen, M. T., Kovanen, P. T. & Ala-Korpela, M. Structure of Low Density Lipoprotein (LDL) Particles: Basis for Understanding Molecular Changes in Modified LDL. *Biochimica et Biophysica Acta* **1488,** 189–210 (2000).

42. Esterbauer, H, Gebicki, J, Puhl, H & Jürgens, G. The Role of Lipid Peroxidation and Antioxidants in Oxidative Modification of LDL. *Free Radical Biology & Medicine* **13,** 341–390 (1992).

43. Sommer, A, Prenner, E, Gorges, R, Stütz, H, Grillhofer, H, Kostner, G., Paltauf, F & Hermetter, A. Organization of Phosphatidylcholine and Sphingomyelin in the Surface Monolayer of Low Density Lipoprotein and Lipoprotein(a) as Determined by Time-Resolved Fluorometry. *Journal of Biological Chemistry* **267,** 24217–24222 (1992).

44. Schissel, S. L., Tweedie-Hardman, J, Rapp, J. H., Graham, G, Williams, K. J. & Tabas, I. Rabbit Aorta and Human Atherosclerotic Lesions Hydrolyze the Sphingomyelin of Retained Low-density Lipoprotein. *The Journal of Clinical Investigation* **98,** 1455–1464 (1996).

45. Ravandi, A, Kuksis, A & Shaikh, N. A. Glycated Phosphatidylethanolamine Promotes Macrophage Uptake of Low Density Lipoprotein and Accumulation of Cholesteryl Esters and Triacylglycerols. *Journal of Biological Chemistry* **274,** 16494–16500 (1999).

46. Lalanne, F, Pruneta, V, Bernard, S & Ponsin, G. Distribution of Diacylglycerols Among Plasma Lipoproteins in Control Subjects and in Patients with Non-Insulin-Dependent Diabetes. *European Journal of Clinical Investigation* **29,** 139–144 (1999).

47. Segrest, J. P., Harvey, S. C. & Zannis, V. Detailed Molecular Model of Apolipoprotein A-I on the Surface of High-Density Lipoproteins and Its Functional Implications. *Trends in Cardiovascular Medicine* **10,** 246–252 (2000).

48. Koppaka, V, Silvestro, L, Engler, J. A., Brouillette, C. G. & Axelsen, P. H. The Structure of Human Lipoprotein A-I. *The Journal of Biological Chemistry* **274,** 14541–14544 (1999).

49. Bhat, S., Sorci-Thomas, M. G., Alexander, E. T., Samuel, M. P. & Thomas, M. J. Intermolecular Contact Between Globular N-Terminal Fold and C-Terminal Domain of ApoA-I Stabilizes Its Lipid-Bound Conformation. *The Journal of Biological Chemistry* **280,** 33015–33025 (2005).

50. Davidson, W. S. & Hilliard, G. M. The Spatial Organization of Apolipoprotein A-I on the Edge of Discoidal High Density Lipoprotein Particles. *The Journal of Biological Chemistry* **278,** 27199–27207 (2003).

51. Panagotopulos, S. E., Horace, E. M., Maiorano, J. N. & Davidson, W. S. Apolipoprotein A-I Adopts a Belt-Like Orientation in Reconstituted High Density Lipoproteins. *The Journal of Biological Chemistry* **276,** 42965–42970 (2001).

52. Silva, R. A. G. D., Hilliard, G. M., Ling Li, Segrest, J. P. & Davidson, W. S. A Mass Spectrometric Determination of the Conformation of Dimeric Apolipoprotein A-I in Discoidal High Density Lipoproteins. *Biochemistry* **44,** 8600–8607 (2005).

53. Huang, R., Silva, R. A. G. D., Jerome, W. G., Kontush, A., Chapman, M. J., Curtiss, L. K., Hodges, T. J. & Davidson, W. S. Apolipoprotein A-I Structural Organization in High-Density Lipoproteins Isolated From Human Plasma. *Nature Structural & Molecular Biology* **18,** 416–422 (2011).

54. Blanche, P. J., Gong, E. L., Forte, T. M. & Nichols, A. V. Characterization of Human High-Density Lipoproteins by Gradient Gel Electrophoresis. *Biochimica et Biophysica Acta* **665,** 408–419 (1981).

55. Segrest, J. P., Cheung, M. C. & Jones, M. K. Volumetric Determination of Apolipoprotein Stoichiometry of Circulating HDL Subspecies. *Journal of Lipid Research* **54,** 2733–2744 (2013).

56. Duverger, N., Rader, D., Duchateau, P., Fruchart, J. C., Castro, G. & Brewer, H. B. Biochemical Characterization of the Three Major Subclasses of Lipoprotein A-I Preparatively Isolated From Human Plasma. *Biochemistry* **32,** 12372–12379 (1993).

57. Yetukuri, L., Söderlund, S., Koivuniemi, A., Seppänen-Laakso, T., Niemelä, P. S., Hyvönen, M. T., Taskinen, M.-R., Vattulainen, I., Jauhiainen, M. & Orešič, M. Composition and Lipid Spatial Distribution of HDL Particles in Subjects with Low and High HDL-Cholesterol. *Journal of Lipid Research* **51,** 2341–2351 (2010).

58. Silva, R. A. G. D., Hilliard, G. M., Fang, J., Macha, S. & Davidson, W. S. A Three-Dimensional Molecular Model of Lipid-Free Apolipoprotein A-I Determined by Cross-Linking/Mass Spectrometry and Sequence Threading. *Biochemistry* **44,** 2759–2769 (2005).

59. Davidson, W. S. & Silva, R. A. G. D. Apolipoprotein Structural Organization in High Density Lipoproteins: Belts, Bundles, Hinges and Hairpins. *Current Opinion in Lipidology* **16,** 295–300 (2005).

60. Saito, H, Dhanasekaran, P, Nguyen, D, Deridder, E, Holvoet, P, Lund-Katz, S. & Phillips, M. C. α-Helix Formation Is Required for High Affinity Binding of Human Apolipoprotein A-I to Lipids. *The Journal of Biological Chemistry* **279,** 20974–20981 (2004).

61. Phillips, J. C., Wriggers, W, Li, Z, Jonas, A & Schulten, K. Predicting the Structure of Apolipoprotein a-I in Reconstituted High-Density Lipoprotein Disks. *Biophysical Journal* **73,** 2337–2346 (1997).

62. Segrest, J. P., Jones, M. K., Klon, A. E., Sheldahl, C. J., Hellinger, M, de Loof, H. & Harvey, S. C. A Detailed Molecular Belt Model for Apolipoprotein A-I in Discoidal High Density Lipoprotein. *The Journal of Biological Chemistry* **274,** 31755–31758 (1999).

63. Klon, A., Segrest, J. P. & Harvey, S. Molecular Dynamics Simulations on Discoidal HDL Particles Suggest a Mechanism for Rotation in the Apo AI Belt Model. *Journal of Molecular Biology* **324,** 703–721 (2002).

64. Shih, A. Y., Denisov, I. G., Phillips, J. C., Sligar, S. G. & Schulten, K. Molecular dynamics simulations of discoidal bilayers assembled from truncated human lipoproteins. *Biophysical Journal* **88,** 548–556 (2005).

65. Catte, A., Patterson, J. C., Bashtovyy, D., Jones, M. K., Gu, F., Li, L., Rampioni, A., Sengupta, D., Vuorela, T., Niemelä, P., Karttunen, M., Marrink, S.-J., Vattulainen, I. & Segrest, J. P. Structure of Spheroidal HDL Particles Revealed by Combined Atomistic and Coarse-Grained Simulations. *Biophysical Journal* **94,** 2306–2319 (2008).

66. Shih, A. Y., Arkhipov, A, Freddolino, P. & Schulten, K. Coarse Grained Protein- Lipid Model with Application to Lipoprotein Particles. *The Journal of Physical Chemistry B* **110,** 3674–3684 (2006).

67. Hite, R. K., Raunser, S. & Walz, T. Revival of Electron Crystallography. *Current Opinion in Structural Biology* **17,** 389–395 (2007).

68. Prassl, R. & Laggner, P. Molecular Structure of Low Density Lipoprotein: Current Status and Future Challenges. *European Biophysics Journal* **38,** 145–158 (2008).

69. Deckelbaum, R. J., Shipley, G. G., Small, D. M., Lees, R. S. & George, P. K. Thermal Transitions in Human Plasma Low Density Lipoproteins. *Science* **190,** 392–394 (1975).

70. Deckelbaum, R. J., Shipley, G. G. & Small, D. M. Structure and Interactions of Lipids in Human Plasma Low Density Lipoproteins. *Journal of Biological Chemistry* **252,** 744–754 (1977).

71. Lund-Katz, S. & Phillips, M. C. Packing of Cholesterol Molecules in Human Low-Density Lipoprotein. *Biochemistry* **25,** 1562–1568 (1986).

72. Chen, S. H., Yang, C. Y., Chen, P. F., Setzer, D, Tanimura, M, Li, W. H., Gotto, A. M. & Chan, L. The Complete cDNA and Amino Acid Sequence of Human Apolipoprotein B-100. *The Journal of Biological Chemistry* **261,** 12918–12921 (1986).

73. Chen, G. C., Zhu, S., Hardman, D. A., Schilling, J. W., Lau, K. & Kane, J. P. Structural Domains of Human Apolipoprotein B-100. *The Journal of Biological Chemistry* **264,** 14369–14375 (1989).

74. Yang, C.-Y., Kim, T. W., Pao, Q., Chan, L., Knapp, R. D., Gotto Jr, A. M. & Pownall, H. J. Structure and Conformational Analysis of Lipid-Associating Peptides of Apolipoprotein B-100 Produced by Trypsinolysis. *Journal of Protein Chemistry* **8,** 689–699 (1989).

75. Chatterton, J. E., Phillips, M. L., Curtiss, L. K., Milne, R. W., Marcel, Y. L. & Schumaker, V. N. Mapping Apolipoprotein B on the Low Density Lipoprotein Surface by Immunoelectron Microscopy. *The Journal of Biological Chemistry* **266,** 5955–5962 (1991).

76. Segrest, J. P., Jones, M. K., Mishra, V. K., Anantharamaiah, G. M. & Garber, D. W. ApoB-100 Has a Pentapartite Structure Composed of Three Amphipathic Alpha-Helical Domains Alternating With Two Amphipathic Beta-Strand Domains. *Arteriosclerosis, Thrombosis, and Vascular Biology* **14,** 1674–1685 (1994).

77. Segrest, J. P., Jones, M. K., de Loof, H. & Dashti, N. Structure of Apolipoprotein B-100 in Low Density Lipoproteins. *The Journal of Lipid Research* **42,** 1346–1367 (2001).

78. Richardson, P. E., Manchekar, M., Dashti, N., Jones, M. K., Beigneux, A., Young, S. G., Harvey, S. C. & Segrest, J. P. Assembly of Lipoprotein Particles Containing Apolipoprotein-B: Structural Model for the Nascent Lipoprotein Particle. *Biophysical Journal* **88,** 2789–2800 (2005).

79. Kriško, A. & Etchebest, C. Theoretical Model of Human Apolipoprotein B100 Tertiary Structure. *Proteins: Structure, Function, and Bioinformatics* **66,** 342–358 (2007).

80. Heikelä, M., Vattulainen, I. & Hyvönen, M. T. Atomistic Simulation Studies of Cholesteryl Oleates: Model for the Core of Lipoprotein Particles. *Biophysical Journal* **90,** 2247–2257 (2006).

81. Atkinson, D., Deckelbaum, R. J., Small, D. M. & Shipley, G. G. Structure of Human Plasma Low-Density Lipoproteins: Molecular Organization of the Central Core. *Proceedings of the National Academy of Sciences of the United States of America* **74,** 1042–1046 (1977).

82. Hall, A., Repakova, J. & Vattulainen, I. Modeling of the Triglyceride-Rich Core in Lipoprotein Particles. *The Journal of Physical Chemistry B* **112,** 13772–13782 (2008).

83. Schlick, T. *Molecular Modeling and Simulation, 1st Edition.* (Springer, New York, 2002).

84. Cramer, C. J. *Essentials of Computational Chemistry: Theories and Models, 2nd Edition.* (John Wiley & Sons, West Sussex, England, 2004).

85. Gogonea, V, Suárez, D, van der Vaart, A & Merz, K. M. New Developments in Applying Quantum Mechanics to Proteins. *Current Opinion in Structural Biology* **11,** 217–223 (2001).

86. Leach, A. R. *Molecular Modeling: Principles and Applications, 2nd Edition.* (Prentice Hall, Harlow, 2001).

87. Abraham, M. J., van der Spoel, D, Lindahl, E, Hess, B & Team, T. G. D. *Gromacs User Manual version 5.0.7* (www.gromacs.org, 2015).

88. Guvench, O. & MacKerell, A. D. in *Molecular Modeling of Proteins* 63–88 (Humana Press, Totowa, NJ, 2008).

89. Haynes, W. M. *CRC Press Handbook of Chemistry and Physics, 95th Edition.* (CRC Press, Boca Raton, 2014).

90. Morse, P. M. Diatomic Molecules According to the Wave Mechanics. II. Vibrational Levels. *Physical Review A* **34,** 57–64 (1929).

91. Patra, M, Karttunen, M, Hyvönen, M. T., Falck, E, Lindqvist, P & Vattulainen, I. Molecular Dynamics Simulations of Lipid Bilayers: Major Artifacts Due to Truncating Electrostatic Interactions. *Biophysical Journal* **84,** 3636–3645 (2003).

92. Onsager, L. Electric Moments of Molecules in Liquids. *Journal of the American Chemical Society* **58,** 1486–1493 (1936).

93. Essmann, U., Perera, L., Berkowitz, M. L., Darden, T., Lee, H. & Pedersen, L. G. A Smooth Article Mesh Ewald Method. *The Journal of Chemical Physics* **103,** 8577–8593 (1995).

94. Schulz, R., Lindner, B., Petridis, L. & Smith, J. C. Scaling of Multimillion-Atom Biological Molecular Dynamics Simulation on a Petascale Supercomputer. *Journal of Chemical Theory and Computation* **5,** 2798–2808 (2009).

95. Hockney, R. W., Goel, S. P. & Eastwood, J. W. Quiet High-Resolution Computer Models of a Plasma. *Journal of Computational Physics* **14,** 148–158 (1974).

96. Berendsen, H. J. C., Postma, J. P. M., van Gunsteren, W. F., DiNola, A & Haak, J. R. Molecular Dynamics with Coupling to an External Bath. *The Journal of Chemical Physics* **81,** 3684–3690 (1984).

97. Nosé, S. A Molecular Dynamics Method for Simulations in the Canonical Ensemble. *Molecular Physics* **52,** 255–268 (1984).

98. Hoover, W. G. Canonical Dynamics: Equilibrium Phase-Space Distributions. *Physical Review A* **31,** 1695–1697 (1985).

99. Parrinello, M & Rahman, A. Polymorphic Transitions in Single Crystals: a New Molecular Dynamics Method. *Journal of Applied Physics* **52,** 7182–7190 (1981).

100. Nosé, S & Klein, M. L. Constant Pressure Molecular Dynamics for Molecular Systems. *Molecular Physics* **50,** 1055–1076 (1983).

101. *Encyclopedia of Life Sciences* (Nature Publishing Group, London, 2001).

102. Lindorff-Larsen, K., Piana, S., Dror, R. O. & Shaw, D. E. How Fast-Folding Proteins Fold. *Science* **334,** 517–520 (2011).

103. Lindorff-Larsen, K., Maragakis, P., Piana, S. & Shaw, D. E. Picosecond to Millisecond Structural Dynamics in Human Ubiquitin. *The Journal of Physical Chemistry B* **120,** 8313–8320 (2016).

104. Berger, O., Edholm, O. & Jähnig, F. Molecular Dynamics Simulations of a Fluid Bilayer of Dipalmitoylphosphatidylcholine at Full Hydration, Constant Pressure, and Constant Temperature. *Biophysical Journal* **72,** 2002–2013 (1997).

105. Oostenbrink, C., Villa, A., Mark, A. E. & van Gunsteren, W. F. A Biomolecular Force Field Based on the Free Enthalpy of Hydration and Solvation: the GROMOS Force-Field Parameter Sets 53A5 and 53A6. *Journal of Computational Chemistry* **25,** 1656–1676 (2004).

106. Hénin, J., Shinoda, W. & Klein, M. L. United-Atom Acyl Chains for CHARMM Phospholipids. *The Journal of Physical Chemistry B* **112,** 7008–7015 (2008).

107. Marrink, S.-J., Risselada, H. J., Yefimov, S., Tieleman, D. P. & de Vries, A. H. The MARTINI Force Field: Coarse Grained Model for Biomolecular Simulations. *The Journal of Physical Chemistry B* **111,** 7812–7824 (2007).

108. Monticelli, L., Kandasamy, S. K., Periole, X., Larson, R. G., Tieleman, D. P. & Marrink, S.-J. The MARTINI Coarse-Grained Force Field: Extension to Proteins. *Journal of Chemical Theory and Computation* **4,** 819–834 (2008).

109. Shelley, J. C., Shelley, M. Y., Reeder, R. C., Bandyopadhyay, S. & Klein, M. L. A Coarse Grain Model for Phospholipid Simulations. *The Journal of Physical Chemistry B* **105,** 4464–4470 (2001).

110. Marrink, S.-J. & Tieleman, D. P. Perspective on the Martini model. *Chemical Society Reviews* **42,** 6801–6822 (2013).

111. Izvekov, S. & Voth, G. A. A Multiscale Coarse-Graining Method for Biomolecular Systems. *The Journal of Physical Chemistry B* **109,** 2469–2473 (2005).

112. Smit, B, Hilbers, P. A. J., Esselink, K, Rupert, L. A. M., van Os, N. M. & Schlijper, A. G. Computer Simulations of a Water/Oil Interface in the Presence of Micelles. *Nature* **348,** 624–625 (1990).

113. Goetz, R. & Lipowsky, R. Computer Simulations of Bilayer Membranes: Self-Assembly and Interfacial Tension. *The Journal of Chemical Physics* **108,** 7397–7409 (1998).

114. Müller, M., Katsov, K. & Schick, M. Biological and Synthetic Membranes: What Can Be Learned From a Coarse-Grained Description? *Physics Reports* **434,** 113–176 (2006).

115. Shelley, J. C. & Shelley, M. Y. Computer Simulation of Surfactant Solutions. *Current Opinion in Colloid & Interface Science* **5,** 101–110 (2000).

116. Larson, R. G., Scriven, L. E. & Davis, H. T. Monte Carlo Simulation of Model Amphiphile-Oil–Water Systems. *The Journal of Chemical Physics* **83,** 2411–2420 (1985).

117. Larson, R. G. Monte Carlo Simulation of Microstructural Transitions in Surfactant Systems. *The Journal of Chemical Physics* **96,** 7904–7918 (1992).

118. De Jong, D. H., Singh, G., Bennett, W. F. D., Arnarez, C., Wassenaar, T. A., Schäfer, L. V., Periole, X., Tieleman, D. P. & Marrink, S.-J. Improved Parameters for the Martini Coarse-Grained Protein Force Field. *Journal of Chemical Theory and Computation* **9,** 687–697 (2012).

119. Heitjans, P & Kärger, J. *Diffusion in Condensed Matter, 2nd Edition* (Springer-Verlag, Berlin, 2005).

120. Sugita, Y., Kitao, A. & Okamoto, Y. Multidimensional Replica-Exchange Method for Free-Energy Calculations. *The Journal of Chemical Physics* **113,** 6042–6051 (2000).

121. Roux, B. The Calculation of the Potential of Mean Force Using Computer Simulations. *Computer Physics Communications* **91,** 275–282 (1995).

122. Torrie, G. M. & Valleau, J. P. Nonphysical Sampling Distributions in Monte Carlo Free-Energy Estimation: Umbrella Sampling. *Journal of Computational Physics* **23,** 187–199 (1977).

123. Kumar, S., Bouzida, D., Swendsen, R. H., Kollman, P. A. & Rosenberg, J. M. The Weighted Histogram Analysis Method for Free-Energy Calculations on Biomolecules. I. The Method. *Journal of Computational Chemistry* **13,** 1011–1021 (1992).

124. Hub, J. S., de Groot, B. L. & van der Spoel, D. g_wham - A Free Weighted Histogram Analysis Implementation Including Robust Error and Autocorrelation Estimates. *Journal of Chemical Theory and Computation* **6,** 3713–3720 (2010).

125. Neale, C., Madill, C., Rauscher, S. & Pomès, R. Accelerating Convergence in Molecular Dynamics Simulations of Solutes in Lipid Membranes by Conducting a Random Walk along the Bilayer Normal. *Journal of Chemical Theory and Computation* **9,** 3686–3703 (2013).

126. Karilainen, T., Timr, Š., Vattulainen, I. & Jungwirth, P. Oxidation of Cholesterol Does Not Alter Significantly Its Uptake into High-Density Lipoprotein Particles. *The Journal of Physical Chemistry B* **119,** 4594–4600 (2015).

127. Maldonado, E. N., Romero, J. R., Ochoa, B. & Aveldaño, M. I. Lipid and Fatty Acid Composition of Canine Lipoproteins. *Comparative Biochemistry and Physiology Part B: Biochemistry and Molecular Biology* **128,** 719–729 (2001).

128. Borhani, D., Rogers, D., Engler, J. & Brouillette, C. Crystal structure of truncated human apolipoprotein AI suggests a lipid-bound conformation. *Proceedings of the National Academy of Sciences* **94,** 12291 (1997).

129. Klon, A., Segrest, J. P. & Harvey, S. Comparative Models for Human Apolipoprotein AI Bound to Lipid in Discoidal High-Density Lipoprotein Particles†. *Biochemistry* **41,** 10895–10905 (2002).

130. Jones, D. T. Protein Secondary Structure Prediction Based on Position-Specific Scoring Matrices. *Journal of Molecular Biology* **292,** 195–202 (1999).

131. Schuler, L. D., Daura, X. & van Gunsteren, W. F. An Improved GROMOS96 Force Field for Aliphatic Hydrocarbons in the Condensed Phase. *Journal of Computational Chemistry* **22,** 1205–1218 (2001).

132. Jorgensen, W. L., Maxwell, D. & Tirado-Rives, J. Development and Testing of the OPLS All-Atom Force Field on Conformational Energetics and Properties of Organic Liquids. *Journal of American Chemical Society* **118,** 11225–11236 (1996).

133. Tieleman, D. P., Maccallum, J. L., Ash, W. L., Kandt, C., Xu, Z. & Monticelli, L. Membrane Protein Simulations with a United-Atom Lipid and All-Atom Protein Model: Lipid–Protein Interactions, Side Chain Transfer Free Energies and Model Proteins. *Journal of Physics: Condensed Matter* **18,** S1221–S1234 (2006).

134. Neale, C. & Pomes, R. Combination Rules for United-Atom Lipids and OPLSAA Proteins. *http://www.pomeslab.com/files/lipidCombinationRules.pdf* (2010).

135. Hölttä-Vuori, M., Uronen, R.-L., Repakova, J., Salonen, E., Vattulainen, I., Panula, P., Li, Z., Bittman, R. & Ikonen, E. BODIPY-Cholesterol: A New Tool to Visualize Sterol Trafficking in Living Cells and Organisms. *Traffic* **9,** 1839–1849 (2008).

136. Vasan, R. S., Pencina, M. J., Robins, S. J., Zachariah, J. P., Kaur, G., D'Agostino, R. B. & Ordovas, J. M. Association of Circulating Cholesteryl Ester Transfer Protein Activity with Incidence of Cardiovascular Disease in the Community. *Circulation* **120,** 2414–2420 (2009).

137. Polk, D. & Shah, P. K. Cholesterol Ester Transfer Protein (CETP) and Atherosclerosis. *Drug Discovery Today Therapeutic Strategies* **4,** 137–145 (2007).

138. Cannon, C. P., Shah, S., Dansky, H. M., Davidson, M., Brinton, E. A., Gotto, A. M., Stepanavage, M., Liu, S. X., Gibbons, P., Ashraf, T. B., Zafarino, J., Mitchel, Y., Barter, P. & Determining the Efficacy and Tolerability Investigators. Safety of Anacetrapib in Patients with or at High Risk for Coronary Heart Disease. *New England Journal of Medicine* **363,** 2406–2415 (2010).

139. Wassenaar, T. A., Pluhackova, K., Böckmann, R. A., Marrink, S.-J. & Tieleman, D. P. Going Backward: A Flexible Geometric Approach to Reverse Transformation from Coarse Grained to Atomistic Models. *Journal of Chemical Theory and Computation* **10,** 676–690 (2014).

140. McNamara, J. R., Small, D. M., Li, Z & Schaefer, E. J. Differences in LDL Subspecies Involve Alterations in Lipid Composition and Conformational Changes in Apolipoprotein B. *The Journal of Lipid Research* **37,** 1924–1935 (1996).

Original Papers

I

Role of Lipids in Spheroidal High Density Lipoproteins

by

Timo Vuorela, Andrea Catte, Perttu S. Niemela, Anette Hall, Marja T. Hyvönen, Siewert-Jan Marrink, Mikko Karttunen & Ilpo Vattulainen.

PLoS Computational Biology **6**, e1000964 (2010).

OPEN ACCESS Freely available online PLoS COMPUTATIONAL BIOLOGY

Role of Lipids in Spheroidal High Density Lipoproteins

Timo Vuorela[1], Andrea Catte[1,2], Perttu S. Niemelä[3], Anette Hall[1], Marja T. Hyvönen[4], Siewert-Jan Marrink[5], Mikko Karttunen[6], Ilpo Vattulainen[1,7,8]*

1 Department of Physics, Tampere University of Technology, Tampere, Finland, **2** Department of Medicine and Center for Computational and Structural Biology, University of Alabama, Birmingham, Alabama, United States of America, **3** VTT Technical Research Centre of Finland, Espoo, Finland, **4** Department of Physics, University of Oulu, Oulu, Finland, **5** Groningen Biomolecular Sciences and Biotechnology Institute and Zernike Institute for Advanced Materials, University of Groningen, Groningen, The Netherlands, **6** Department of Applied Mathematics, The University of Western Ontario, London, Ontario, Canada, **7** Department of Applied Physics, Aalto University School of Science and Technology, Espoo, Finland, **8** MEMPHYS–Center of Biomembrane Physics, Physics Department, University of Southern Denmark, Odense M, Denmark

Abstract

We study the structure and dynamics of spherical high density lipoprotein (HDL) particles through coarse-grained multi-microsecond molecular dynamics simulations. We simulate both a lipid droplet without the apolipoprotein A-I (apoA-I) and the full HDL particle including two apoA-I molecules surrounding the lipid compartment. The present models are the first ones among computational studies where the size and lipid composition of HDL are realistic, corresponding to human serum HDL. We focus on the role of lipids in HDL structure and dynamics. Particular attention is paid to the assembly of lipids and the influence of lipid-protein interactions on HDL properties. We find that the properties of lipids depend significantly on their location in the particle (core, intermediate region, surface). Unlike the hydrophobic core, the intermediate and surface regions are characterized by prominent conformational lipid order. Yet, not only the conformations but also the dynamics of lipids are found to be distinctly different in the different regions of HDL, highlighting the importance of dynamics in considering the functionalization of HDL. The structure of the lipid droplet close to the HDL-water interface is altered by the presence of apoA-Is, with most prominent changes being observed for cholesterol and polar lipids. For cholesterol, slow trafficking between the surface layer and the regimes underneath is observed. The lipid-protein interactions are strongest for cholesterol, in particular its interaction with hydrophobic residues of apoA-I. Our results reveal that not only hydrophobicity but also conformational entropy of the molecules are the driving forces in the formation of HDL structure. The results provide the first detailed structural model for HDL and its dynamics with and without apoA-I, and indicate how the interplay and competition between entropy and detailed interactions may be used in nanoparticle and drug design through self-assembly.

Citation: Vuorela T, Catte A, Niemelä PS, Hall A, Hyvönen MT, et al. (2010) Role of Lipids in Spheroidal High Density Lipoproteins. PLoS Comput Biol 6(10): e1000964. doi:10.1371/journal.pcbi.1000964

Editor: Helmut Grubmuller, Max Planck Institute for Biophysical Chemistry Gottingen, Germany

Received March 25, 2010; **Accepted** September 17, 2010; **Published** October 28, 2010

Funding: Supercomputing resources were provided by The Finnish IT Centre for Science (CSC), the SharcNet computing facility (www.sharcnet.ca), and the HorseShoe cluster at the University of Southern Denmark. This work was supported by grants from the Academy of Finland, the Natural Sciences and Engineering Research Council of Canada (NSERC), and the Netherlands Organisation for Scientific Research (NWO).

Competing Interests: The authors have declared that no competing interests exist.

* E-mail: Ilpo.Vattulainen@tut.fi

Introduction

Cardiovascular diseases are the primary cause of death in western countries [1]. One of the main causes is the lipid accumulation and plaque formation on arterial walls, called atherosclerosis. This eventually leads to the narrowing of arteries, plaque rupture, clotting, and potential death. Generally speaking, high levels of low density lipoprotein (LDL) in blood have been found to increase the risk of atherosclerosis [2,3], whereas high levels of high density lipoprotein (HDL) have been shown to reduce the risk [4,5].

Despite more than a decade of extensive studies, LDL and HDL structures are not well understood. This is largely due to their small size which ranges from about 10 (HDL) to 25 nm (LDL) rendering experimental studies of the detailed lipoprotein structures extremely difficult. This challenge is further corroborated by the soft nature of lipoparticles whose structures are transient due to thermal forces driving molecular assembly processes in living matter. The challenge is to unravel the role and mechanisms of lipoproteins in the trafficking of cholesterol and in the cholesterol-based diseases. In this work, we focus on HDL.

Let us briefly summarize the main insight one has about high density lipopproteins. HDL particles are comprised of a lipid droplet surrounded by proteins [6,7]. Apolipoprotein A-I (apoA-I) is the main protein associated with HDL, which is the main carrier of excess cholesterol from peripheral tissues to the liver, that is, for reverse cholesterol transport [5,8]. After synthesization, the ATP-binding cassette transporter A1 (ABCA1) assembles lipid-poor apoA-I molecules and lipids into discoidal HDL particles [9], after which the enzyme lecithin:cholesterolacyl transferase (LCAT) esterifies cholesterol molecules, leading to the formation of spheroidal HDL [10,11]. The spheroidal HDL is the main form of HDL responsible for cholesterol transport to the liver.

Though a number of experimental studies have been carried out to unravel the structure and dynamics of apoA-I molecules in lipid-free form [12–15] and in discoidal HDL complexes [16,17], the structure of the spheroidal HDL has remained unclear. As for

Author Summary

Cardiovascular diseases are the primary cause of death in western countries. One of the main causes is lipid accumulation and plaque formation on arterial walls, called atherosclerosis. The risk of being exposed to this condition is reduced by high levels of high density lipoprotein (HDL). The functionality of HDL has remained elusive, and even its structure is not well understood. Through extensive coarse-grained simulations, we have clarified the structure of the lipid droplet in HDL and elucidated its interactions with the apolipoprotein A-I (apoA-I) that surrounds the droplet. We have found that the structural and dynamic properties of lipids depend significantly on their location in the particle (core, intermediate region, surface). As for apoA-I, we have observed it alter the overall structure of the lipid droplet close to the HDL-water interface, with prominent changes taking place for cholesterol and other polar lipids. The nature of lipid-protein interactions is most favorable for cholesterol. Our results reveal that not only hydrophobicity but also conformational entropy are the driving forces in the formation of HDL structure, suggesting how the interplay and competition between entropy and detailed interactions may be used in nanoparticle and drug design through self-assembly.

the structure of apoA-I, a large amount of data is in favor of the so-called double belt model (see Ref. [18] and references therein), where the apoA-I proteins line along the lipid droplet. The composition of the droplet has been resolved [19,20] (see Table 1), indicating free cholesterol (CHOL), cholesteryl esters (CE), triglycerides (TG), phospholipids, and lysolipids to be its main constituents, distributed such that there is a hydrophobic interior of triglycerides and cholesteryl esters and a surface covered by polar head groups of phospholipids [21]. This is essentially the so-called *two-layer model* for HDL [6,7,22]. Furthermore, parts of the apoA-I proteins have been proposed to interact with the acyl chains of the lipids [23–27].

Currently, the role of lipids for HDL functions are only vaguely understood. This is partly due to the transient time scales associated with and the nano-scale nature of HDL. Further issues include the poor understanding of lipid organization and interplay of lipids with apoA-I. Considering findings that lipids are an integral component of protein structures, e.g., in membrane proteins that are in constant interplay with lipids [28], it is obvious that clarifying the role of lipids for HDL properties is extremely important.

Table 1. Molecular composition of HDL.

Component	N (simulation)	mol % (simulation)	mol % (experiment)
POPC	260	53.9	}56.1
PPC	10	2.1	
CE	122	25.3	25.5
CHOL	49	10.2	10.2
TG	39	8.1	8.2
ApoA-I	2		

The table shows the number of molecules (N) used in the simulations, together with the experimentally measured molar percentages in human plasma HDL [19]. While this choice reflects the relative amounts observed for the different molecular components in HDL, there is reason to stress that HDL composition is very heterogeneous and depends on, e.g., HDL size and diet [66,67]. The present study essentially represents the largest HDLs, that is HDL_2; the effect of changes in lipid and protein concentrations are discussed below in this article. The abbreviations: POPC (palmitoyl-oleoyl-phosphatidylcholine), PPC (palmitoyl-PC), CE (cholesteryl ester, here cholesteryl oleate), CHOL (free cholesterol), TG (triglyceride, here trioleate).
doi:10.1371/journal.pcbi.1000964.t001

A number of computational studies have recently been conducted to complement experiments. Previous computational studies of HDL particles have focused on discoidal particles consisting of phospholipids and two apoA-I molecules [29–32]. These studies have provided some insight into the mechanisms of assembly and the dependence of the particle shape on the lipid/protein molar fractions. In a different approach, bulk melts of cholesteryl esters [33] and triglycerides [34], as well as combination of cholesteryl esters with POPCs [35] have recently been simulated. Catte *et al.* [36] reported the first computational approach towards understanding the structure of spheroidal HDL particles. Their study clarified the conformation of apoA-I in model spheroidal HDL particles using both all-atom (AA) and coarse-grained (CG) molecular dynamics (MD) simulations. This combination of AA and CG-MD simulations led to model spheroidal HDL particles with prolate ellipsoidal shapes having sizes consistent with experimental results and suggested that cholesteryl esters stabilize the conformations of apoA-I [37]. In a more recent work, Shih et al. also combined coarse-grained simulations with atomistic ones in a series of simulations where discoidal HDL was matured into spherical HDL upon incorporation of cholesteryl esters [38]. They found that maturation results from the formation of a dynamic hydrophobic core composed of cholesteryl esters, the core being surrounded by a layer of phospholipids and apoA-I proteins. Interestingly, Shih et al. also fine-grained the coarse-grained HDL particle to atomistic description and then used atomistic simulations to consider the structure of apolipoproteins around the lipid droplet, and in particular the importance of salt bridges in apoA-I.

The main limitations of previous simulations of HDL particles are two-fold. First, the lipid composition modeled in recent simulations has been somewhat unrealistic: instead of a many-component lipid mixture, the lipid droplet has been modeled as a single-component POPC melt, or as a mixture of POPCs and cholesteryl esters [36]. The role of the many different lipid species in HDL has therefore remained unknown. Second, the time scales of HDL simulations have been too short compared to the characteristic time scales of lipid mixing and structural deformations associated with HDL. As even the time scale of lipid mixing is of the order of 1 μs (derived through the diffusion of lipids inside HDL), and the current state-of-the-art for atomistic simulations of HDL extends over 10–100 ns, it seems obvious that currently atomistic simulations are not the method of choice for dealing with HDL over large enough time scales.

Our objective is to overcome the above limitations. We have performed MD simulations of spheroidal HDL particles using the full lipid composition of human plasma HDL [19]. Instead of atom-scale simulations, we employ the coarse-grained MARTINI model [39,40] that has performed exceptionally well in a number of studies dealing with lipids and proteins [36,39–42]. We consider both the protein-free lipid droplets and the full HDL particles containing also two apoA-I molecules around the droplet, see Figures 1 and 2. Composition of the HDL system is described in Table 1 with abbreviations of all molecules included. By comparing the protein-free and the full HDL models, we can clarify the role of lipids and proteins in HDL. The principal objective is to fill the gap of detailed structural and dynamic

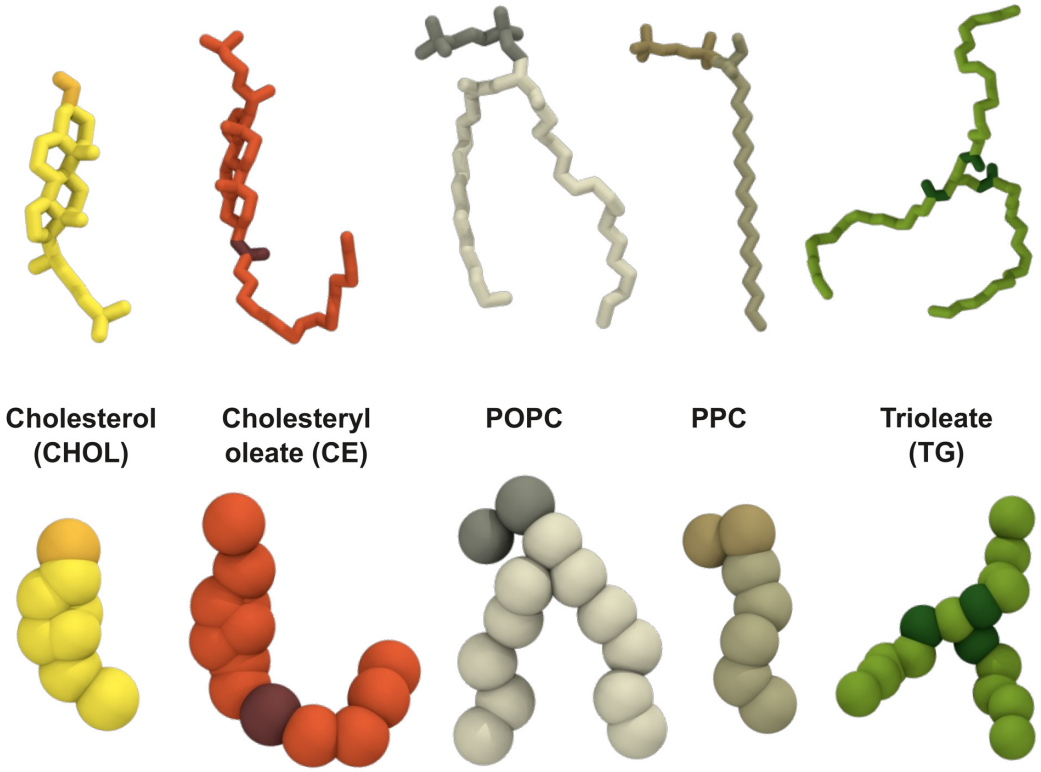

Figure 1. Descriptions of the molecules considered in the study. (Top) Atomistic (united atom) descriptions, and (bottom) the coarse-grained representations.
doi:10.1371/journal.pcbi.1000964.g001

information of lipids in spheroidal HDL particles. We also address questions related to the role of apoA-I proteins and their interactions with lipids in HDL structures. The currently incomplete understanding of the latter issue is largely due to the size heterogeneity of HDLs (diameters range from 7.2 (HDL_3) to 12 nm (HDL_2)) and the large flexibility of apoA-I. The latter renders the prediction of the positioning of different alpha helices of apoA-I on a spherical surface very difficult. The distribution of lipids inside HDL and their interplay with apoA-I are of profound interest. From a more general perspective, knowledge of the

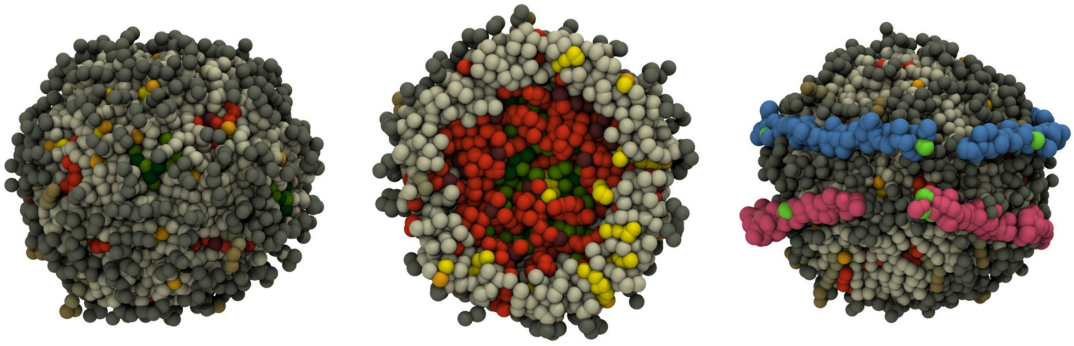

Figure 2. Example of a protein-free lipid droplet (left), its molecular distribution shown through a slice across the particle (middle), and HDL including two apoA-I proteins (right). Dark gray stands for POPC headgroup and dark brown for PPC headgroups, light gray for POPC hydrocarbon chains, light brown for PPC chains, light orange for CHOL OH-groups, bright yellow for cholesterol body, dark orange for CE ester bond, orange for CE ester body and chain, dark green for TG ester bonds, and bright green for TG chain. In HDL, proline residues in apoA-I sequences are in green.
doi:10.1371/journal.pcbi.1000964.g002

structure of spheroidal HDL is crucial for understanding the conformational changes when HDL makes the transition from discoidal to spheroidal shape, and the trafficking of CHOL and CE through the action of cholesteryl ester transfer protein [43]. Additionally, to design nanoparticles with desired surface and bulk properties, e.g., for controlled transport and release of drugs and contrast agents, it is vital to understand the conformational changes as well as the underlying mechanisms in detail [44–51].

Results

Structure of Full HDL and the Lipid Droplet

The radial density distributions shown in Figure 3 reveal the internal structure of the simulated lipoparticles. The hydrophobic CE and TG molecules are located in the core of the particle and have minimal overlap with water. The lipids with a polar head group, POPC and PPC, are mostly located at the surface region facing water, whereas most of CHOL is located just below these two lipids. Note that a small but significant concentration of CHOL is also found in the core of the particle.

Considering the size of HDL, the radii of gyration give an average of $R_g = 4.079 \pm 0.001$ nm for the droplet and $R_g = 4.278 \pm 0.001$ nm for the full HDL. Both particles are effectively spherical, as indicated by the moments of inertia (data not shown).

The apoA-I proteins are embedded onto the surface of the HDL particle, their density peaking just slightly below the headgroup region of POPC and PPC. The presence of the protein slightly disturbs the distribution of these lipids as revealed by the comparison of the lipid droplet with the full HDL particle. The distribution of hydrophobic lipids remains undisturbed. Most significant is the shifting of the distribution of CHOL, and partly PPC, towards water phase when the protein is present, while the distribution of POPC is shifted slightly towards membrane center, making room for CHOL and PPC. In the full HDL particle, water is found to distribute less to the particle compared to the droplet.

Our results clearly highlight the displacement of CHOL even further towards the interface in the full HDL particle. The data below shows that CHOL interacts prefentially with some of the protein residues, strongly promoting the partitioning of CHOL to the vicinity of apoA-I. CHOL further prefers to reside next to the water region, facilitating (hydrogen) bonding via the polar OH group. It has been proposed [52] that CHOL molecules can mediate the relief of membrane stress arising from chain-chain mismatches, since their dimerization is not favored in membranes with high surface curvature. This view is supported by the observations of Huang and Mason [53]. Their work suggests that high surface curvature requires CHOL to be at the interfacial region. Interestingly, Lemmich et al. have further found that very small amounts of CHOL (less than about 3 mol-%) may soften the interface and hence promote its fluidity [54]. In HDL, the average concentration of CHOL is about 10 mol-%, but at the interface it is about 5–10 mol-% depending on distance from the water phase (see Figure 3).

The minor but significant concentration of CHOL in the core of the particle calls for discussion. The usual assumption especially in studies of lipid membranes is that CHOL resides at the water-lipid interface due to its polar OH group. This is expected often to be the case, though there are also reported exceptions such as CHOL residing for short times in the middle of a polyunsaturated lipid bilayer [55,56], and the suggestion of CHOL in the interior of LDL [57].

To start with, one gets an impression that the density plot adheres to the two-layer model [6,7,22] wherein one assumes almost full separation of hydrophilic and hydrophobic molecules into two separate regions. While the distribution of TG fits into

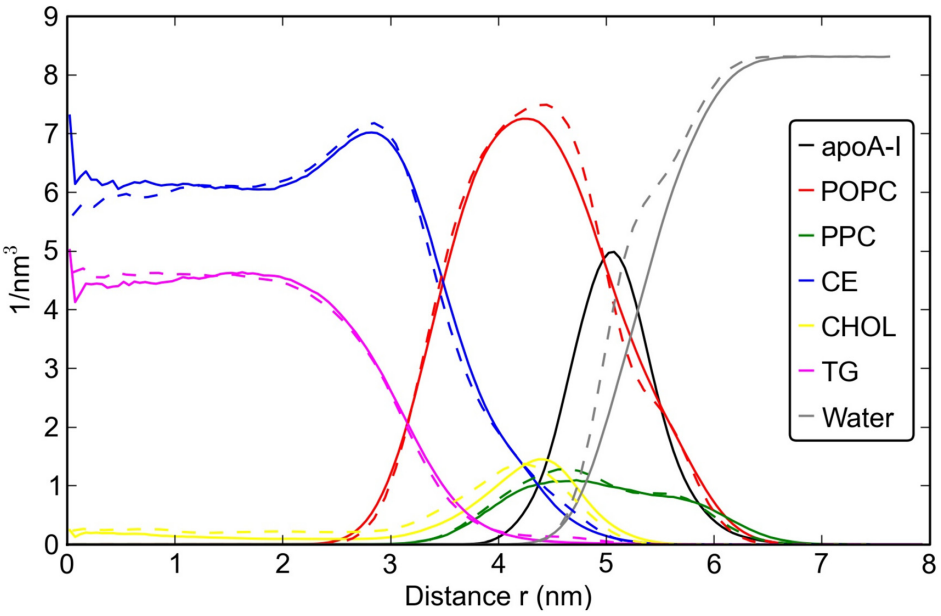

Figure 3. Radial densities showing the composition of the studied particles versus distance from the center of mass (COM) of the particle. The solid lines are for the full HDL particle, the dashed lines for the lipid droplet without apoA-I.
doi:10.1371/journal.pcbi.1000964.g003

this picture, the distribution of CE and CHOL does not. A rather significant amount of CHOL is also in the core of the particle as was discussed above. Detailed consideration further reveals that there is a significant overlap of CE with CHOL, POPC, and PPC: The radial density distributions shown in Figure 3 do not provide a sufficiently unique description of only two different structural regions inside HDL. Furthermore, by looking at the order parameters of CHOL and CE presented in Figure 4 it becomes evident that there are not only two regions but also the intermediate one between the hydrophobic and hydrophilic ones. The innermost *core* of the particle ($r<3$ nm) is clear, as there the ring structures of both CHOL and CE are oriented in a completely random fashion. The situation changes as one approaches the lipid-water interface through the *intermediate* region (3 nm $<r<5$ nm), which is characterized by significant ordering of the ring structures, in a manner where the principal axis of CE's and CHOL's ring moiety lies along the radial direction of HDL. This intermediate region overlaps with the distribution of the acyl chains of POPC and PPC, revealing that the sterol rings are also aligned with the acyl chains. Finally, at the HDL-water interface, one finds the region composed of hydrophilic headgroups of POPC and PPC that constitute the *surface* part of the lipid droplet interacting mostly with water.

The data clearly shows that instead of the two-layer model, the distribution of lipids in HDL is more complex. The structural nano-scale organization of CHOL and CE plays an important role in constituting the intermediate layer. However, there is no apparent reason to conclude that the lipid droplet in HDL would be described by a "three-layer" model either, since the intermediate region is narrow and represents a crossover from the hydrophobic to the hydrophilic environment rather than a clearly defined layer of its own. Our results for lipid dynamics are in favor of this view and will be discussed below in the context of diffusion. Meanwhile, while quantitative results have been missing, a three-layer model has earlier been proposed for LDL particles [3]. There the situation is different, though, since the diameter of LDL is roughly three times larger compared to HDL and the intermediate region can possibly be broader and more characteristic compared to HDL.

There are significant differences when the order parameters of CHOL and CE are compared (Figure 4). First, the height of the main peak is considerably lower for CE than for CHOL, indicating that the ring of CE has a lower tendency to orient itself along the acyl chains than CHOL. Second, unlike for CHOL, on the surface of the particle ($r>5$ nm) the order parameter of CE obtains negative values. These indicate the ring of CE to lie along the surface, perpendicular to the radial direction. This obviously stems from entropic reasons, since while CE strives in part to organize its structure like CHOL, also directing its weakly polar ester bond region to the surface like CHOL does for the OH group, CE also has a long oleate chain. Previous atomistic simulations of CE in bulk conditions as well as in a combined system with POPCs have shown that the oleate chain of cholesteryl oleate has essentially three different conformations with respect to the ring of CE [33,36]: one where the angle of the oleate chain (describing it as a semi-stiff rod) with respect to the principal axis of the ring is about 35 degrees, and two other modes with an angle of 90 or 150 degrees. Compared to CHOL with only one mode, CE inevitably aims to minimize free energy by promoting entropic degrees of freedom.

Another interesting observation is that apoA-I suppresses the main peak of both CHOL and CE molecules in Figure 4. The effect is an indication that the protein disturbs the ordering within the intermediate region (between the core and the surface), also facilitating the displacement of CHOL towards the water phase. This conclusion is supported by the broadening of the angle distributions of POPC in the presence of the protein (see Supporting Information (SI)).

An analysis of the internal conformations of CE molecules in Figure 5 provides a more detailed view of the situation. In the core of the particle, the most probable conformation of CE is the coil-like conformation (maximizing entropy), where the angle between the CE ring and the oleoyl chain is about 120 degrees. This is largely consistent with recent atom-scale simulations of CE in bulk conditions [33]. The behavior changes on the surface of the particle. The two peaks of the distribution on the surface correspond to two distinctly different conformations: one where the ester group of CE (corresponding to the OH-group of CHOL)

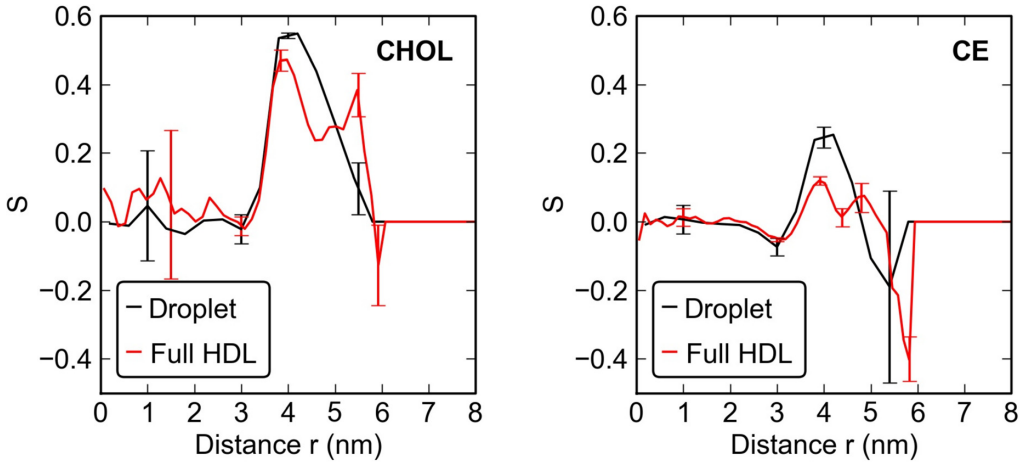

Figure 4. Order parameter S for the ring structures of CHOL (left) and CE (right). The black curves describe the lipid droplet and the red curves the full HDL.
doi:10.1371/journal.pcbi.1000964.g004

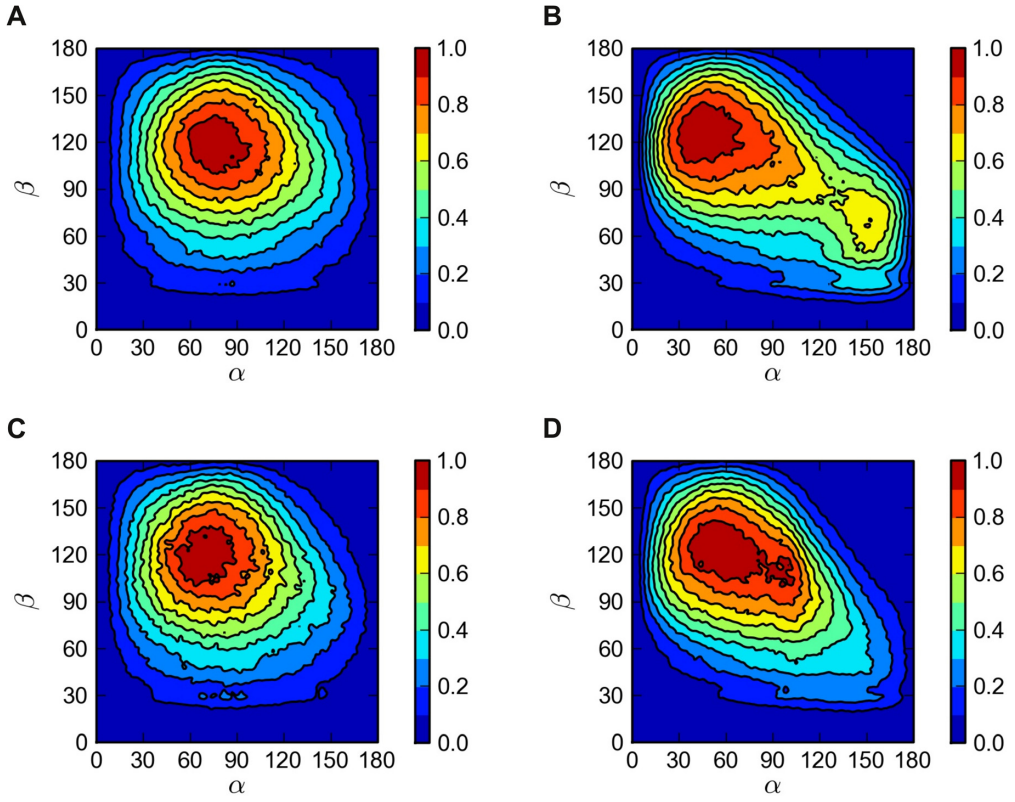

Figure 5. Distributions of CE conformations. The horizontal axis is the angle α between the CE ring and the effective normal of the lipid droplet. The vertical axis is the angle β between the ring structure and the oleate chain. The left panels (A, C) describe the core of the droplet ($r<2$ nm) and the right panels (B, D) the surface ($r>3$ nm). The pictures at the top (A, B) show the lipid droplet without apoA-I and those at the bottom (C, D) the full HDL.
doi:10.1371/journal.pcbi.1000964.g005

points towards water and the oleate chain is extended towards the solvent, and another where the ester region is pointing towards the core of the particle, while the ring and the oleoyl chain form a small angle with each other.

Also for TG, we find a change of conformation when it is shifted from the core of the particle onto the surface. In the core, the three chains of TG place themselves to a similar conformation as in a bulk melt of TG [34]. When brought to the surface, the ester bond regions seek contact with water, which brings the three chains of TG closer to each other into a more tightly packed conformation (see Figure S2). Additional data for molecular conformations are presented in Figure S1, Figure S3, Figure S4, and Figure S5.

Dynamics of Lipids Characterized by Diffusion

The large-scale dynamics within HDL and the lipid droplet are considered in terms of diffusion, characterized by the diffusion coefficient D. The diffusion coefficients were determined by considering lipid displacement distribution functions over a fixed period of time (see SI). We found that the jump length distributions for lipids in the core of the particle (TG and CE) fitted well with the three-dimensional diffusion model, yielding D_{3d}. Meanwhile, the lipids on the surface (POPC, PPC, CHOL) fitted much better with the two-dimensional description for diffusion, yielding D_{2d}. For details, see SI.

Table 2 shows the long-time diffusion coefficients of the lipid components within the lipid droplet and the full HDL particle.

Figure 6 depicts how the diffusion rate varies significantly inside the lipid droplet and/or full HDL. The diffusion is the slowest in the middle of the particle, it speeds up as the molecules get closer to the interface, and the fastest diffusion is found at the interface. The influence of apoA-I on diffusion of lipids is modest. It turns out that the lipid diffusion coefficients in the protein-free lipid droplet and the full HDL particle are almost similar. The apoA-I

Table 2. Diffusion coefficients in units of $10^{-7}\mathrm{cm}^2/\mathrm{s}$.

Component	Dimensionality	D (droplet)	D (HDL)
TG	3d	0.30 ± 0.07	0.27 ± 0.08
CE	3d	0.56 ± 0.05	0.36 ± 0.06
CHOL	2d	1.6 ± 0.2	1.3 ± 0.2
POPC	2d	1.5 ± 0.3	1.5 ± 0.1
PPC	2d	2.8 ± 0.1	2.6 ± 0.1

The dimensionality of 2d refers to diffusion along the lipid-water interface, while 3d refers to diffusion in the core of the particle.
doi:10.1371/journal.pcbi.1000964.t002

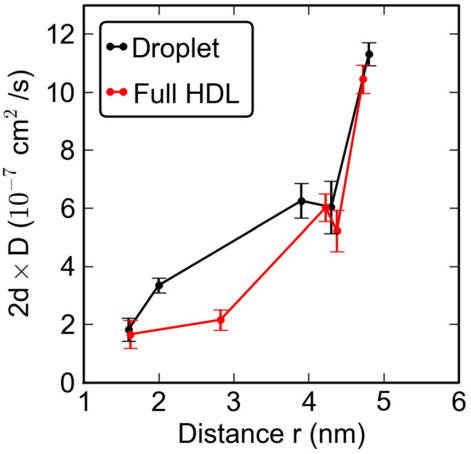

Figure 6. Diffusion coefficients of the lipid components. Each point in the plot describes the diffusion coefficient for one of the lipid types. The distance r is the average distance of the given lipid from the COM of the particle. To facilitate comparison between core (three-dimensional diffusion) and surface lipids (two-dimensional diffusion), the coefficients have been scaled with $2d$, where d is the dimension of the fit (either two or three).
doi:10.1371/journal.pcbi.1000964.g006

proteins may slow down the diffusion of lipids slightly especially close to the interfacial regions. The effect is, however, weak (see Table 2).

The diffusion coefficients of POPC, PPC and CHOL in the surface region of the particles are about $(1-3)\times10^{-7}\mathrm{cm}^2/\mathrm{s}$ and in good agreement with experimental estimates of $D\approx1\times10^{-7}\mathrm{cm}^2/\mathrm{s}$ for two-dimensional lipid bilayers in fluid phase [58]. On the other hand, the diffusion coefficients for CE and TG are smaller by a factor of 10, about $0.3\times10^{-7}\mathrm{cm}^2/\mathrm{s}$. To our knowledge, diffusion coefficients of lipids in HDL have not been experimentally determined. However, for LDL and LDL-like lipid droplets, Vauhkonen et al. used pyrene-linked PC lipids as probes to find that $D\approx(0.5-1.5)\times10^{-7}\mathrm{cm}^2/\mathrm{s}$ at the surface of lipoparticles [59], in good agreement with our findings. Massey and Pownall have further used single-chain cationic amphiphiles for considering lipid mobility at the surface regions of LDL and HDL, and while quantitative estimates for D are missing, they concluded that the diffusion at the surface is about 2–3 times slower compared to cholesterol-free POPC vesicles [60]. Recent MARTINI-model simulations for single-component PC bilayers have yielded $D\approx4\times10^{-7}\mathrm{cm}^2/\mathrm{s}$ [61], which is about a factor of 2 larger than diffusion at the surface of HDL. While the comparison of our simulation data and experiments is suggestive rather than conclusive, the qualitative agreement is striking.

Our main result regarding diffusion is that diffusion at the surface region of HDL is largely similar to diffusion of lipids in cholesterol-containing lipid bilayers in the fluid-like phase, the cholesterol concentration being roughly 10 mol%. Figure 6 also shows convincingly that the effect of apoA-I on diffusion of lipids is not significant.

Additionally, Figure 6 provides compelling evidence that the dynamics of lipids in terms of their diffusion properties is not consistent with the two-layer model. Instead of two clearly different dynamic regions, we find the diffusion coefficients to increase monotonously: diffusion rates are clearly different in the core ($r<3$ nm), in the ordered intermediate region ($r\approx4$ nm), and at the surface ($r\approx5$ nm).

Given the different proposed models for lipid distribution in HDL, the striking difference of the present findings compared to earlier studies is the role of dynamics: not only the structural and ordering properties of molecules in HDL differ across HDL, but also the dynamics in terms of molecular transport coefficients varies significantly in the different compartments. The biological relevance of this feature lies in the time scales of molecular trafficking inside HDL: while molecular transport between the surface and the intermediate region is relatively fast, the transport between the surface and the core of HDL is slower by a factor of ~10.

Role of ApoA-I in HDL

The above results show that the apoA-I proteins do not induce large changes to the lipids' properties inside the droplet. Yet, while the protein collapses onto the surface of the droplet, it does disturb the packing, ordering and, although only slightly, also the dynamics of the lipids at the surface region. What remains to be explored is the nature of the lipid-protein interactions. In this work our primary interest is the lipid component of HDL, thus we have used the standard CG MARTINI model which does not enforce the full secondary structures in apoA-I. This optimizes computational efficiency and allows us to focus on generic issues such as the partitioning of lipids around apoA-I, and the influence of apoA-I on the lipid droplet. Meanwhile, we cannot address questions related to detailed atomistic phenomena at the lipid-apoA-I interface.

Data for the surface accessible surface areas (SASAs) of apoA-I hydrophilic and hydrophobic residues (data not shown) provide evidence for the low contribution of protein hydrophobic residues (11%) to the total SASA of the protein, the main contribution coming from protein hydrophilic residues (89%). The average value of SASA of protein hydrophobic residues ($13.1\pm1.6\mathrm{nm}^2$) is in good agreement with that reported by Shih et al. [32] in a recent study on the assembly of lipids and proteins into lipoprotein particles.

The RMSFs of protein α carbons are shown in Figure 7 and reveal the mobility of different protein domains. The α-helical structure of the protein exhibits very little mobility for both chains. This rigidity of the protein is also in agreement with the observed slight disturbances produced on the lipid packing.

The number of annular lipids, as defined in the Method section, is given in Figure 8 for each lipid component. It is interesting to note that about 80% of CHOL molecules are annular (on average 40 out of 49) while only 10% of CE molecules (about 15 out of 122) are in close contact with the protein. An average of about 98 POPC molecules out of a total of 260 are annular. Overall, the results indicate that there is a preferential interaction between CHOL molecules and protein residues. This result is striking if one considers that the number of POPC molecules is larger than that of CHOL molecules.

It is known that the number of apolipoproteins in HDL depends on particle size. We characterized its role for lipid distribution through additional simulations with three apoA-Is. First, we performed a 20 microsecond simulation of the same lipid droplet with 3 apoA-I molecules placed 2 nm apart from each other. The protein molecules were found to insert themselves in the lipid droplet in the same way as was observed above, with hydrophobic moieties pointing towards the droplet. The only interesting difference was that in the structure with three apoA-Is, the C-terminus and the helix 9 of one protein molecule were not inserted in the lipid droplet. This situation is likely due to the crowded

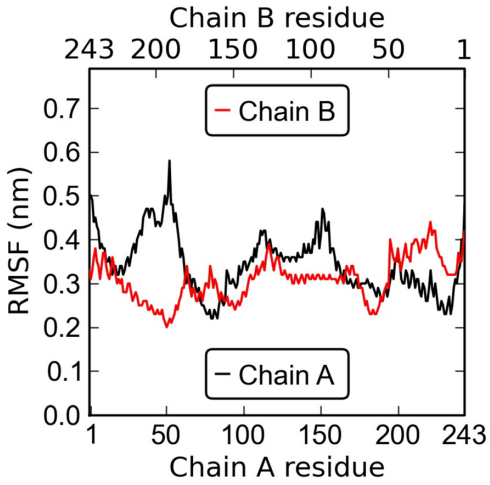

Figure 7. Root mean square fluctuation (RMSF) profiles for apoA-I alpha carbons (black, chain A; red, chain B) measured over the last 4 μs of the simulation of the full HDL particle. Experiments suggest that the alpha-helical region is likely given by the residues 44–241, and that the alpha-helical content overall is about 75–80% [6,13,18,26].
doi:10.1371/journal.pcbi.1000964.g007

arrangement of apolipoproteins, or due to the limited time scale of the simulation. The addition of a third apoA-I molecule does also affect the interaction of cholesterol with apoA-I: Almost 100% of the cholesterol molecules (47 ± 1 out of 49) are in contact with the three proteins. That is, the addition of the third apoA-I molecule enhances the average number of annular cholesterol molecules from about 80% (observed with 2 apoA-I molecules) to about 96% of the total unesterified cholesterol in the particle.

The lipid-protein interactions of different moieties of each lipid component showed that POPC, PPC and TG molecules interact with apoA-I residues preferentially through the acyl chains (POPC and PPC glycerol backbone has also a high number of contacts with apoA-I), while CHOL and CE molecules interact with the protein mainly through the sterol ring (see Table S1). To better understand the nature of the interaction between CHOL and apoA-I we also measured the number of lipid-protein contacts per residue (hydrophobic and hydrophilic), shown in Figure 9. It is clear that there is a preferential interaction of CHOL molecules with apoA-I hydrophobic residues, in particular tryptophane (Trp) and phenylalanine (Phe) having aromatic side chains, but also valine (Val) and leucine (Leu). Highly preferred interaction with Trp and Phe is understandable through findings of aromatic ring pairing in e.g. known protein structures [62]. We also observe a relevant number of contacts with apoA-I hydrophilic residues with aromatic side chains such as tyrosine (Tyr) and histidine (His). This is not surprising, as Tyr has a hydrophobicity comparable to Phe as has been shown experimentally by Wimley and White [63] through the determination of a hydrophobicity scale for proteins at membrane interfaces. There are less contacts of CHOL molecules with the other apoA-I hydrophilic residues, namely serine (Ser), threonine (Thr) and asparagine (Asp) being the most attractive ones. These results are in good agreement with the observed large number of contacts of the sterol ring of CHOL molecules with protein residues.

The sterol ring of CHOL molecules can intercalate or interact with the aromatic side chains of protein residues as observed for CE in a recent study by Catte et al. [36]. This interaction between CHOL molecules and apoA-I was also observed experimentally by Dergunov et al. [64]. The authors estimated the degree of exclusion of CHOL molecules from the boundary lipid region in

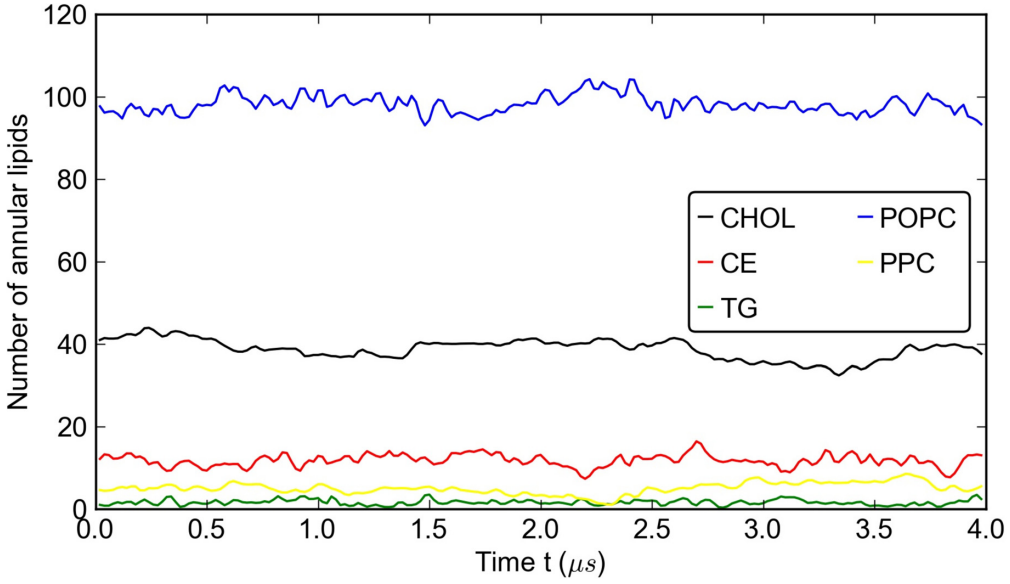

Figure 8. Number of annular lipid molecules over the last 4 μs of the simulation of the full HDL particle: POPC (blue), CHOL (red), CE (orange), PPC (purple) and TG (green).
doi:10.1371/journal.pcbi.1000964.g008

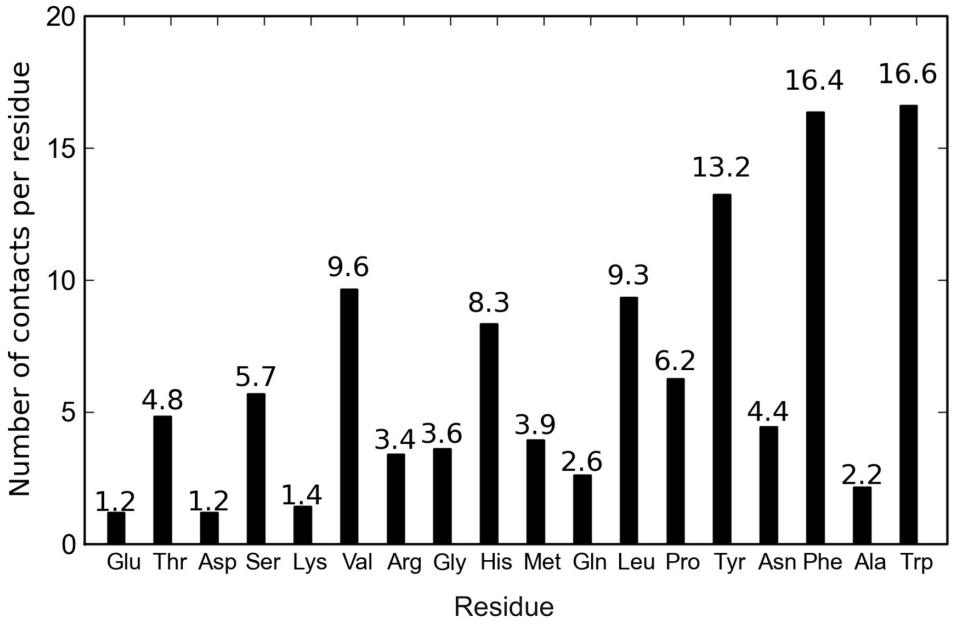

Figure 9. Number of contacts of CHOL molecules with apoA-I residues normalized per residue. See text for details. Isoleucine and cysteine are absent in the human apoA-I sequence considered here [13].
doi:10.1371/journal.pcbi.1000964.g009

reconstituted discoidal HDL particles containing different apolipoproteins and observed an increase in the order A-I<E<A-II. The partial exclusion of CHOL molecules operated by apoA-I and the corresponding CHOL distribution among surface and bulk lipids are in good agreement with our findings as depicted through a series of snapshots in Figure 10 (see also SI).

The binding between CHOL molecules and apoA-I residues is quite weak, which permits exchange among apoA-I -bound and free CHOL molecules on the time scale of the simulation. We characterized this trafficking process by computing the distributions of lifetimes between CHOL-protein and CE-protein contacts. The average lifetime was found to be 146 ns for CHOL

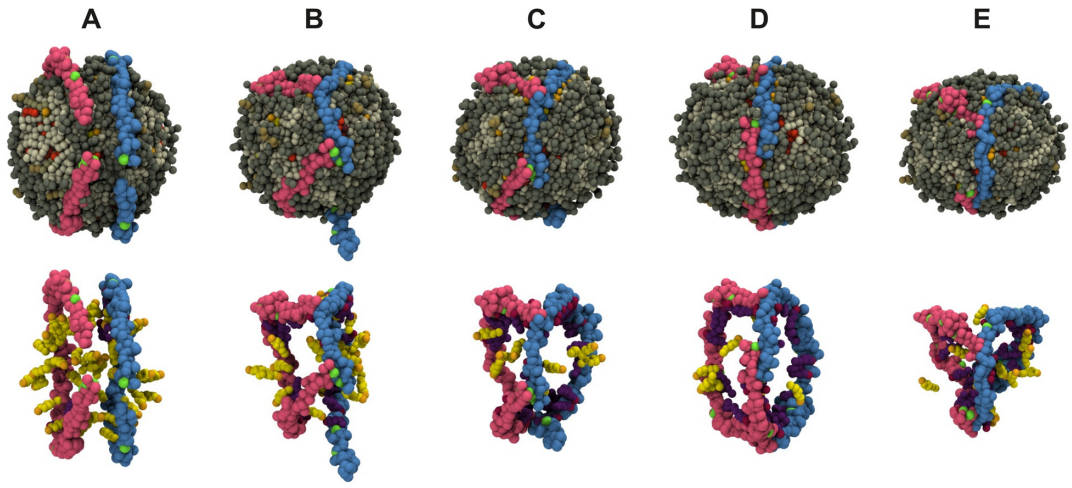

Figure 10. Illustrative snapshots of HDL structure. (Top) Different snapshots of the full HDL simulation: (A) 0 μs, (B) 0.4 μs, (C) 1.4 μs, (D) 12.4 μs, and (E) 19.04 μs. (Bottom) Snapshots displayed at the top of the figure showing here only the apoA-I molecules, and annular and bulk CHOL molecules. The two apoA-I chains are in light red (chain A) and light blue (chain B) with proline residues in green. Annular CHOL molecules are shown in purple with a dark red hydroxyl group. Bulk CHOL molecules are depicted in yellow with an orange hydroxyl group.
doi:10.1371/journal.pcbi.1000964.g010

and 15 ns for CE. While the errors are of the same order as the lifetime due to a limited number of samples, and the fact that the distribution for CHOL is broad as there are cases where the CHOL-protein contact is maintained throughout the simulation, the results highlight the stability of CHOL-protein binding with respect to that of CE. The relatively large lifetime of the CHOL-protein binding also highlights that once CHOL has migrated to the vicinity of apoA-I, it remains there for a long period of time. For comparison, the average non-contact lifetime for CHOL-protein pairs, describing the characteristic time for CHOL to not be in contact with any parts of apoA-I was found to be about 175 ns. That is, CHOL molecules reside close to the water-HDL interface and on average spend half of their time in contact with apoA-I.

The above results are in good agreement with NMR experiments performed on human HDL, which indicate that CHOL molecules are present in two distinct environments [65]. More specifically, Lund-Katz et al. found that the cholesterol molecules dissolved in the core of HDL are relatively disordered and mobile, while the cholesterol molecules located among phospholipid molecules in the surface of the particle undergo relatively restricted, anisotropic motions. This view is in line with our simulation results discussed earlier in this article. Lund-Katz et al. thus proposed that cholesterol molecules are in two different microenvironments, undergoing fast exchange between these two regions, equilibrating between the surface and the core of HDL in the time scale of milliseconds or more. While the time scales proposed by Lund-Katz et al. are beyond those that are accessible via simulations, we have found that there is local exchange taking place at times up to microseconds. However, the time scales we have found via simulations should be regarded as the lower limit, since the diffusion coefficients we have found for the core of HDL imply that the exchange of cholesterols between the core and surface regions has to be larger than 1 μs.

Discussion

In this study, we elucidated the structure and dynamics of spheroidal high density lipoparticles with a realistic lipid composition corresponding to human serum HDL. We found that the traditional two-region model for HDL is not accurate enough. Instead, we found the distribution of the different lipid types in HDL to be more complex.

The innermost core of HDL is mainly occupied by TG and CE, which as hydrophobic lipids constitute a randomly oriented melt. However, in contrast to the common view, the inner core was also found to contain a rather significant fraction of free cholesterol partitioned into the disordered melt. The outermost surface region constitutes the interface with water, which is mostly occupied by the polar headgroups of POPC and PPC. Between these two is the intermediate region occupied by CHOL, partly also CE, and the acyl chains of POPC and PPC. However, there is no apparent reason to consider the intermediate region as a "third layer", since it is narrow, unclear to define spatially, and represents a crossover from the hydrophobic to the hydrophilic environment rather than a true layer of its own. Yet it has properties that are distinct from those in the core and at the surface.

This is most obvious in two aspects: ordering of steroid moieties and molecular diffusion. Unlike in the core, in the intermediate region the bulky rings of CHOL and CE are strongly ordered along with the acyl chains. This ordering extends also to the surface region of HDL, highlighting the difficulty to define the intermediate region as a true layer of its own. This view is also supported by the diffusion data, which illustrates that the diffusion of molecules takes place at a clearly different pace in the different regions. In the core and in the intermediate region of the particle, diffusion was found to be three-dimensional, while the diffusion of lipids at the HDL-water interface turned out to be two-dimensional in nature. Quantitatively, diffusion in the core of the particle was observed to be slow, as in a polymer melt, and to speed up monotonously as one crosses the intermediate region and ends up in the interfacial region.

The perspective arising from our results is novel, providing the first molecular scale view to the nano-scale organization of lipids in HDL. The present results indicate that the spatial distribution of lipids within HDL provides only a narrow perspective to the complexity of lipid organization. To understand this issue, one has to pay considerable attention not only to density distributions but also conformational and orientational degrees of freedom of the lipids, and their dynamics within HDL.

Events where CE and TG penetrate to the surface were found to be rare. In the few observed cases when it occurred, their conformation was significantly changed. In the core of the particle, both CE and TG were observed to be capable of obtaining more coil-like conformations. This indicates that the formation of the HDL core is not only driven by the hydrophobic effect, but that conformational entropy has a significant effect.

When comparing the simulation of the full HDL (with apoA-I) to the lipid droplet (without apoA-I), we found that the overall structure of the lipid droplet was not significantly changed by the presence of the protein. Rather, we found a disturbance in the behavior of the surface lipids. In particular, the order of CHOL and CE molecules decreased and the conformations of the acyl chains of PC lipids got broader. Diffusion of the surface lipids was slightly perturbed by the protein, but the effect was minor.

The low contribution of the SASA of apoA-I hydrophobic residues to the total SASA of the protein and the large number of contacts of hydrophobic moieties of each lipid component with apoA-I evidence that the hydrophobic forces drive the insertion of the protein and contribute to the stability of the full HDL. Interestingly, we found that a large number of CHOL molecules interact with apoA-I, mainly through their sterol ring and especially with hydrophobic residues having an aromatic side chain. We also observed fast exchange among protein-free and protein-bound CHOL molecules. This result is in good agreement with experimental findings for human HDL particles [65].

It is tempting to discuss the physiological relevance of the above-discussed molecular level findings, especially the preferable interaction of the sterol ring moiety with the aromatic amino acids, and the observation that CHOL molecules spend about half of their time in contact with apoA-I, trafficking relatively rapidly back and forth in the vicinity of apoA-I. Such interaction is prone to have impact on the availability of sterols and lipids for related transfer proteins and enzymes, such as the cholesteryl ester transfer protein (CETP) and cholesteryl esterases. This interaction may be even more important in the process of cholesterol efflux, which is the critical part of reverse cholesterol transport, where the accumulated cholesterol is removed from macrophages.

For future purposes for characterizing the properties of HDL, as well as HDL under enzymatic reactions, our results bring about a useful view to consider. We have found that the interfacial region of HDL close to the water phase is rather well defined in terms of its molecular composition: it can be described as a model layer composed of PCs, lyso-PCs, CHOLs, and the apolipoproteins A-I. The diffusion results discussed in this study indicate that the lateral diffusion along the interfacial layer is largely consistent with diffusion taking place in model membranes, whose molecular composition is of the same type. These features suggest that both

the physical and chemical properties of HDL could be explored with reasonable accuracy through studies of (planar) model membranes, which are considerably easier to characterize compared to nano-sized HDLs. Clearly, the insight gained in this manner would be limited, since a number of inherent features would be missing, such as the curved nature of the HDL-water interface and its effect on apoA-I. Nonetheless, there is reason for optimism, encouraging experiments and simulations to use model membranes for better understanding of lipoprotein properties, including both HDL and LDL.

The view presented in this article for HDL structure and dynamics paves way to extend the scope of computational studies for HDL, and to gain a much deeper understanding of HDL properties in a number of conditions related to health. For instance, there is reason to assume that the molecular composition in HDL depends to some extent on factors such as diet and lifestyle. In altered HDL the lipid composition can be abnormal due to e.g. dyslipidemia [66]. Characterization of molecular composition of HDL of subjects with varying degrees of health would allow coarse-grained simulation studies of HDL in these subject groups, using the present results as a reference. Preliminary studies in this spirit have very recently been reported and discussed by Yetukuri et al. [67], who found that an elevated triglyceride concentration in low-HDL subjects also affected its distribution in HDL, increasing the concentration of triglycerides markedly at the lipid-water interface next to apolipoproteins. Such results based on large-scale coarse-grained models can further be fine-grained to atomistic description to study the atom-scale features that are relevant e.g. in lipid-protein interactions, and the implications on HDL stability due to reactions of enzymes such as phospholipases. Work in this direction has already been initiated by Shih et al., who recently fine-grained coarse-grained models for matured HDL particles comprised of apoA-Is, phopholipids, and cholesteryl esters [38]. Similar work is in progress for the present HDL models.

Altogether, considering the complexity of HDL, our study highlights the importance of lipid-apoA-I interactions, and in particular the specificity of apoA-I for free cholesterol and its esters. The molecular-scale insight of HDL structure and dynamics found and confirmed in our study largely stems from the ordering and dynamical phenomena taking place close to the HDL-water interface, being in part driven by the interactions between cholesterol and apoA-I. Evidently, they have a prominent role to play in a number of transport processes dealing with cholesterol.

Methods

Simulation Models

Construction of the models was implemented in two stages. First, we constructed lipid droplets (without the apoA-I proteins) using coarse-grained descriptions of lipids and water. Second, the studies of pure lipid droplets were complemented by models where the droplet was surrounded by two apoA-I proteins. Below, we describe the main stages of the model construction.

The initial structure for the lipid droplet was obtained by placing the set of lipid molecules (see Table 1) randomly into a three-dimensional simulation box without water or any other solvent. As CE, we used cholesterol oleate, while TG was chosen as trioleate. The system was then simulated under NpT conditions in order to reach proper density. The resulting molecular melt was next hydrated with $\sim$100,000 water particles and the energy was minimized, after which the system was equilibrated for 8 μs. After equilibration, the system was simulated over a period of 4 μs that was used for analysis. All time scales shown here represent the realistic effective time (simulation time multiplied by the scaling factor of four) [39].

For POPC, PPC, CHOL and water, we used standard components of the coarse-grained MARTINI force field [39]. The parameters for CE and TG are those corresponding to cholesteryl-oleate and trioleate respectively, and they come from a combination of standard MARTINI-components and careful adjustments of the key particle types and angle potentials (see SI). The adjustments were justified by comparing structural properties of the molecules in bulk with extensive atomic-scale simulations [33,34], see SI for details. Sphingomyelin (SM) in ref. [19] has been included in the POPC contribution, as SM's properties in the MARTINI description do not differ considerably from those of POPC.

Next, all-atom apoA-I molecules were generated using as a reference the molecular belt model of apoA-I for discoidal HDL [68–72]. The hydrophobic faces of the amphipathic helices were oriented toward the interior of the alpha helical ring but for the N-terminal part of apoA-I; the first 32 residues of the N-terminus were rotated, as in the lipid-mimetic solution NMR structure of apoA-I [22,73], in order to have their hydrophobic face oriented towards the lipid droplet surface. These all-atom models of apoA-I were coarse grained using a pre-released version of the MARTINI force field for proteins [40] for the assignment of beads to every amino acid residue (see also ref. [36]). To obtain the initial structure of the full HDL, two coarse grained apoA-I molecules were added to the equilibrated lipid droplet (discussed above) in a double-belt conformation at a distance of 4 nm from each other.

After energy minimization, the HDL particle was subjected to very short equilibration runs using different time steps to get a stable system for a simulation with a time step of 25 fs. Finally, the particle was simulated for a total of 19 μs, of which the last 4 μs was used for analysis.

To confirm the validity of the results, the simulations for HDL discussed in this article were complemented by several additional simulations that were started from different initial configurations. Each simulation covered a multi-microsecond time scale, and the results were found to be consistent with those discussed in this article.

The molecular dynamics simulations were performed with the GROMACS 3.3.1 package [74]. Time steps of 20 fs and 25 fs were used for integrating the equations of motion of the lipid droplet and of the full HDL, respectively. For production runs, the Nosé-Hoover thermostat [75,76] and the Parrinello-Rahman barostat [77] were used to ensure proper NpT conditions ($T=310$ K, $p=1$ atm). Water and the lipids were coupled to separate thermostats, and the whole system was coupled to the barostat isotropically. Time constant of $\tau=1.0$ ps was used for all couplings. For non-bonded interactions, we used the standard distance of 1.2 nm [36]. The Lennard-Jones interaction was shifted smoothly to zero after 0.9 nm.

Analysis Methods

The equilibration of the simulated lipoparticles was monitored through the numbers of intermolecular contacts between different lipid types and the radial density distributions as a function of time. The intermolecular contacts between different molecular groups were calculated using a 0.8 nm cutoff for all beads. The radial density distributions describe the number densities of the coarse-grained beads. The orientation order of CHOL and CE ring structures was measured by the order parameter $S=\langle 3\cos^2\phi-1\rangle/2$, where ϕ is the angle between the molecular axis and the effective normal of the lipoparticle at the location of the molecule in question. Being more specific, the molecular axis in this definition for CHOL is drawn from

the beginning of CHOL (carbon in the ring of CHOL attached to the short chain) to the carbon connected to the hydroxyl group. The effective normal is the vector from the center of mass (COM) of the lipoparticle to the center of the molecular axis. For CE, an additional measure is the angle between the molecular (ring, see above) axis and the vector from the beginning to the end of the oleoyl chain.

Diffusion was analyzed by measuring the jump-length distributions of the COM positions of the lipids over a time scale t. Two types of Gaussian functions were fitted to the distributions, the two-dimensional (2d):

$$P_{2d}(r,t) = \frac{r}{2D_{2d}t}\exp\left(-\frac{r^2}{4D_{2d}t}\right),$$

and the three-dimensional (3d):

$$P_{3d}(r,t) = \frac{4\pi r^2}{(4\pi D_{3d}t)^{3/2}}\exp\left(-\frac{r^2}{4D_{3d}t}\right).$$

The diffusion coefficient D from the best fitting function (P_{2d} or P_{3d}) is reported, which in practice means that lipids at the water-lipid interface were found to undergo 2d diffusion, while those under the interface diffused in a 3d manner. Also, different time scales were tested and the measured D was observed to level off at long times, an indication of diffusive behavior in the hydrodynamic (long-time) limit. "Long" times here refer to times of the order of 100 ns, where D is found to level off to a well defined constant value. Examples of data for P_{2d} and P_{3d} are shown in SI, including also a more detailed description of how to choose the diffusion time scale in the intermediate region under the lipid-water surface (see Text S1, and Figure S6).

In many-component systems such as the present one, the diffusion of different molecular components may take place at different rates, and it is not obvious that CG models account for this aspect correctly. For the MARTINI model used here, we have previously confirmed that this is not an issue. For instance, Niemela et al. [78] recently used atomistic and coarse-grained models to show that the protein diffusion coefficient was about 10 times smaller compared to that of lipids, and the diffusion mechanisms of lipids and proteins was similar in both models. Ramadurai et al. [79] studied the influence of membrane thickness (hydrophobic mismatch) with several peptides using both FCS measurements and coarse-grained simulations and found essentially quantitative agreement for the peptide diffusion coefficients after the MARTINI results had been scaled by a factor of 4. The simulations were also in agreement with experiments for the trend predicted with increasing hydrophobic mismatch. Further, Apajalahti et al. [61] considered the lateral diffusion of lipids in many-component protein-free membranes and found the diffusion of lipids in raft-like membrane domains (in the liquid-ordered phase) to be about 10 times slower compared to diffusion in domains that were in the liquid-disordered phase. Therefore, diffusion has been studied in several multi-component lipid systems, and the MARTINI models have been found to be consistent with experiments.

The solvent accessible surface area (SASA) of hydrophobic, hydrophilic and all-protein residues were measured using a radius of the solvent probe of 0.56 nm (the all-atom 0.14 nm radius of the solvent probe is converted to the coarse-grained one because one water bead corresponds to four water molecules) inside the GROMACS program g_sas. The SASA values were averaged over the entire trajectory used for analysis. The root mean square fluctuations (RMSFs) of protein alpha carbons were measured for both apoA-I chains to monitor protein flexibility.

Lipid-protein interactions were monitored through the number of intermolecular contacts and their lifetimes for every lipid component with the protein. Annular lipid molecules, defined as those with any bead within 8 Å of any protein bead, were monitored over the analyzed trajectory. The average percentage of the number of contacts of each lipid component with the protein residues were estimated separately for each of the following moieties of every lipid component: POPC (polar head group, glycerol backbone, oleoyl and palmitoyl chains), PPC (polar head group, glycerol backbone and palmitoyl chain), CHOL (short acyl chain, sterol ring), CE (short acyl chain, sterol ring, and oleate chain) and TG (glycerol backbone, *sn*–1, *sn*–2, and *sn*–3 chains). Cholesterol-protein interactions were also tested by measuring the average number of contacts per protein residue of the cholesterol molecule with hydrophilic and hydrophobic protein residues. Additionally, for evaluation of CHOL-protein and CE-protein lifetimes, we accounted for cases where the distance between the molecules fluctuated around 8 Å: for an annular lipid, if its distance from apoA-I exceeded 8 Å temporarily for less than 10 frames (0.1 ns), the coupling was considered unbroken.

Here our primary interest is the lipid part of HDL, for which reason we have used the standard CG MARTINI model which does not enforce the full secondary structures in apoA-I. This computational efficient approach allows us to focus on generic issues such as the partitioning of lipids around apoA-I, as well as the influence of apoA-I on the disttributions of lipids in a droplet. By fine graining our equilibrated structures back to atomistic level, one could employ atom-scale simulations to elucidate the more detailed aspects of the system.

Supporting Information

Figure S1 POPC angle distributions showing the orientation of the P-N vector and hydrocarbon chains with respect to the effective normal.
Found at: doi:10.1371/journal.pcbi.1000964.s001 (0.18 MB PDF)

Figure S2 Distributions of TG conformations in different regions of HDL. Distributions are given in terms of the angle between the hydrocarbon *sn*-1 and *sn*-3 chains, and the angle between the *sn*-1 and *sn*-2 chains.
Found at: doi:10.1371/journal.pcbi.1000964.s002 (0.63 MB PDF)

Figure S3 Conformations of cholesteryl ester and triglyceride in different parts of the droplet.
Found at: doi:10.1371/journal.pcbi.1000964.s003 (0.24 MB PDF)

Figure S4 Angle distributions describing cholesteryl ester conformations.
Found at: doi:10.1371/journal.pcbi.1000964.s004 (0.11 MB PDF)

Figure S5 Angle distributions characterizing conformations of triglyceride molecules.
Found at: doi:10.1371/journal.pcbi.1000964.s005 (0.14 MB PDF)

Figure S6 Displacement distributions for CE (Panel A) and POPC (Panel B) together with the fits of P_{2d} and P_{3d}.
Found at: doi:10.1371/journal.pcbi.1000964.s006 (0.19 MB PDF)

Table S1 Average percentages of different moieties of each lipid component interacting with apoA-I.
Found at: doi:10.1371/journal.pcbi.1000964.s007 (0.01 MB PDF)

Text S1 Description of additional data (for Figures S1, S2, S3, S4, S5, S6 and Table S1), details of coarse-grained model construction, and description of diffusion analysis.

Found at: doi:10.1371/journal.pcbi.1000964.s008 (0.05 MB PDF)

Acknowledgments

Chantelle Oliver is thanked for valuable comments and suggestions.

Author Contributions

Conceived and designed the experiments: TV AC PSN AH MTH SJM MK IV. Performed the experiments: TV AC. Analyzed the data: TV AC. Contributed reagents/materials/analysis tools: TV AC PSN AH. Wrote the paper: TV AC PSN AH MTH SJM MK IV.

References

1. Mokdad AH, Marks JS, Stroup DF, Gerberding JL (2004) Actual causes of death in the United States, 2000. JAMA 291: 1238–1245.
2. Castelli WP, Garrison RJ, Wilson PW, Abbott RD, Kalousdian S, et al. (1986) Incidence of coronary heart disease and lipoprotein cholesterol levels. The Framingham Study. JAMA 256: 2835–2838.
3. Hevonoja T, Pentikäinen MO, Hyvönen MT, Kovanen PT, Ala-Korpela M (2000) Structure of low density lipoprotein (LDL) particles: Basis for understanding molecular changes in modified LDL. Biochim Biophys Acta 1488: 189–210.
4. Colvin PL, Parks JS (1999) Metabolism of high density lipoprotein subfractions. Curr Opin Lipidol 10: 309–314.
5. Linsel-Nitschke P, Tall AR (2005) HDL as a target in the treatment of atherosclerotic cardiovascular disease. Nat Rev Drug Discov 4: 193–205.
6. Lund-Katz S, Liu L, Thuahnai ST, Phillips MC (2003) High density lipoprotein structure. Front Biosci 8: d1044–1054.
7. Jackson RL, Morrisett JD, Gotto AM (1976) Lipoprotein structure and metabolism. Physiol Rev 56: 259–316.
8. von Eckardstein A, Nofer JR, Assmann G (2001) High density lipoproteins and arteriosclerosis - role of cholesterol efflux and reverse cholesterol transport. Arterioscler Thromb Vasc Biol 21: 13–27.
9. Oram JF, Heinecke JW (2005) ATP-binding cassette transporter A1: A cell cholesterol exporter that protects against cardiovascular disease. Physiol Rev 85: 1343–1372.
10. Jonas A (2000) Lecithin cholesterol acyltransferase. Biochim Biophys Acta 1529: 245–256.
11. Peelman F, Vinaimont N, Verhee A, Vanloo B, Verschelde JL, et al. (1998) A proposed architecture for lecithin cholesterol acyl transferase (LCAT): Identification of the catalytic triad and molecular modeling. Protein Sci 7: 587–599.
12. Rogers DP, Roberts LM, Lebowitz J, Datta G, Anantharamaiah GM, et al. (1998) The lipid-free structure of apolipoprotein A-I: Effects of amino-terminal deletions. Biochemistry 37: 11714–11725.
13. Brouillette CG, Anantharamaiah GM, Engler JA, Borhani DW (2001) Structural models of human apolipoprotein A-I: A critical analysis and review. Biochim Biophys Acta 1531: 4–46.
14. Silva RA, Hilliard GM, Fang J, Macha S, Davidson WS (2005) A three-dimensional molecular model of lipid-free apolipoprotein A-I determined by cross-linking/mass spectrometry and sequence threading. Biochemistry 44: 2759–2769.
15. Ajees AA, Anantharamaiah GM, Mishra VK, Hussain MM, Murthy HMK (2006) Crystal structure of human apolipoprotein A-I: Insights into its protective effect against cardiovascular diseases. Proc Natl Acad Sci USA 103: 2126–2131.
16. Davidson WS, Silva RA (2005) Apolipoprotein structural organization in high density lipoproteins: Belts, bundles, hinges and hairpins. Curr Opin Lipidol 16: 295–300.
17. Saito H, Dhanasekaran P, Nguyen D, Deridder E, Holvoet P, et al. (2004) Alpha-helix formation is required for high affinity binding of human apolipoprotein A-I to lipids. J Biol Chem 279: 20974–20981.
18. Gangani D, Silva RA, Huang R, Morris J, Fang J, Gracheva EO, et al. (2008) Structure of apolipoprotein A-I in spherical high density lipoproteins of different sizes. Proc Natl Acad Sci USA 105: 12176–12181.
19. Maldonado EN, Romero JR, Ochoa B, Avelda MI (2001) Lipid and fatty acid composition of canine lipoproteins. Comp Biochem Physiol B, Biochem Mol Biol 128: 719–729.
20. Kotronen A, Velagapudi VR, Yetukuri L, Westerbacka J, Bergholm R, et al. (2009) Serum saturated fatty acids containing triacylglycerols are better markers of insulin resistance than total serum triacylglycerol concentrations. Diabetologia 52: 684–690.
21. Edelstein C, Kezdy FJ, Scanu AM, Shen BW (1979) Apolipoproteins and the structural organization of plasma lipoproteins: Human plasma high density lipoprotein-3. J Lipid Res 20: 143–153.
22. Cushley RJ, Okon M (2002) NMR studies of lipoprotein structure. Annu Rev Biophys Biomol Struct 31: 177–206.
23. Mishra VK, Palgunachari MN, Segrest JP, Anantharamaiah GM (1994) Interactions of synthetic peptide analogs of the class A amphipathic helix with lipids. Evidence for the snorkel hypothesis. J Biol Chem 269: 7185–7191.
24. Segrest JP, Garber DW, Brouillette CG, Harvey SC, Anantharamaiah GM (1994) The amphipathic alpha helix: A multifunctional structural motif in plasma apolipoproteins. Adv Protein Chem 45: 303–369.
25. Palgunachari MN, Mishra VK, Lund-Katz S, Phillips MC, Adeyeye SO, et al. (1996) Only the two end helixes of eight tandem amphipathic helical domains of human apoA-I have significant lipid affinity. Implications for HDL assembly. Arterioscler Thromb Vasc Biol 16: 328–338.
26. Mishra VK, Palgunachari MN, Datta G, Phillips MC, Lund-Katz S, et al. (1998) Studies of synthetic peptides of human apolipoprotein A-I containing tandem amphipathic α-helixes. Biochemistry 37: 10313–10324.
27. Anantharamaiah GM, Mishra VK, Garber DW, Datta G, Handattu SP, et al. (2007) Structural requirements for antioxidative and anti-inflammatory properties of apolipoprotein A-I mimetic peptides. J Lipid Res 48: 1915–1923.
28. Hite RK, Raunser S, Walz T (2007) Revival of electron crystallography. Curr Opin Struct Biol 17: 389–395.
29. Shih AY, Denisov IG, Phillips JC, Sligar SG, Schulten K (2005) Molecular dynamics simulations of discoidal bilayers assembled from truncated human lipoproteins. Biophys J 88: 548–556.
30. Catte A, Patterson JC, Jones MK, Jerome WG, Bashtovyy D, et al. (2006) Novel changes in discoidal high density lipoprotein morphology: A molecular dynamics study. Biophys J 90: 4345–4360.
31. Shih AY, Arkhipov A, Freddolino PL, Schulten K (2006) Coarse grained protein-lipid model with application to lipoprotein particles. J Phys Chem B 110: 3674–3684.
32. Shih AY, Arkhipov A, Freddolino PL, Sligar SG, Schulten K (2007) Assembly of lipids and proteins into lipoprotein particles. J Phys Chem B 111: 11095–11104.
33. Heikelä M, Vattulainen I, Hyvönen MT (2006) Atomistic simulation studies of cholesteryl oleates: Model for the core of lipoprotein particles. Biophys J 90: 2247–2257.
34. Hall A, Repakova J, Vattulainen I (2008) Modelling of the triglyceride rich core in lipid droplets. J Phys Chem B 112: 13772–13782.
35. Koivuniemi A, Heikelä M, Kovanen PT, Vattulainen I, Hyvönen MT (2009) Atomistic simulations of phosphatidylcholines and cholesteryl esters in high-density lipoprotein-sized lipid droplet and trilayer: Clues to cholesteryl ester transport and storage. Biophys J 96: 4099–4108.
36. Catte A, Patterson JC, Bashtovyy D, Jones MK, Gu F, et al. (2008) Structure of spheroidal HDL particles revealed by combined atomistic and coarse grained simulations. Biophys J 94: 2306–2319.
37. Sparks DL, Lund-Katz S, Phillips MC (1992) The charge and structural stability of apolipoprotein A-I in discoidal and spherical recombinant high density lipoprotein particles. J Biol Chem 267: 25839–25847.
38. Shih AY, Sligar SG, Schulten K (2009) Maturation of high-density lipoproteins. J R Soc Interface 6: 863–871.
39. Marrink SJ, Risselada HJ, Yefimov S, Tieleman DP, de Vries AH (2007) The MARTINI force field: Coarse grained model for biomolecular simulations. J Phys Chem B 111: 7812–7824.
40. Monticelli L, Kandasamy S, Periole X, Larson R, Tieleman DP, et al. (2008) The MARTINI coarse grained force field: Extension to proteins. J Chem Theor Comp 4: 819–834.
41. Risselada HJ, Marrink SJ (2008) The molecular face of lipid rafts in model membranes. Proc Natl Acad Sci USA 105: 17367–17372.
42. Ollila OHS, Risselada HJ, Louhivuori M, Lindahl E, Vattulainen I, et al. (2009) 3D pressure field in lipid membranes and membrane-protein complexes. Phys Rev Lett 102: 078101.
43. Qiu X, Mistry A, Ammirati MJ, Chrunyk BA, Clark RW, et al. (2007) Crystal structure of cholesteryl ester transfer protein reveals a long tunnel and four bound lipid molecules. Nat Struct Mol Biol 14: 106–113.
44. Peer D, Karp JM, Hong S, Farokhzad OC, Margalit R, et al. (2007) Nanocarriers as an emerging platform for cancer therapy. Nature Nanotech 2: 751–760.
45. Oda MN, Hargreaves PL, Beckstead JA, Redmond KA, van Antwerpen R, et al. (2006) Reconstituted high density lipoprotein enriched with the polyene antibiotic amphotericin B. J Lipid Res 47: 260–267.
46. Lou B, Liao XL, Wu MP, Cheng PF, Yin CY, et al. (2005) High-density lipoprotein as a potential carrier for delivery of a lipophilic antitumoral drug into hepatoma cells. World J Gastroenterol 11: 954–959.
47. Frias JC, Williams KJ, Fisher EA, Fayad ZA (2004) Recombinant HDL-like nanoparticles: A specific contrast agent for MRI of atherosclerotic plaques. J Am Chem Soc 126: 16316–16317.
48. Frias JC, Ma Y, Williams KJ, Fayad ZA, Fisher EA (2006) Properties of a versatile nanoparticle platform contrast agent to image and characterize atherosclerotic plaques by magnetic resonance imaging. Nano Lett 6: 2220–2224.
49. Kratzer I, Wernig K, Panzenboeck U, Bernhart E, Reicher H, et al. (2007) Apolipoprotein A-I coating of protamine-oligonucleotide nanoparticles increases particle uptake and transcytosis in an *in vitro* model of the blood-brain barrier. J Control Release 117: 301–311.
50. Briley-Saebo KC, Mulder WJM, Mani V, Hyafil F, Amirbekian V, et al. (2007) Magnetic resonance imaging of vulnerable atherosclerotic plaques: Current imaging strategies and molecular imaging probes. J Magn Reson Imaging 26: 460–479.

51. Canet-Soulas E, Letourneur D (2007) Biomarkers of atherosclerosis and the potential of MRI for the diagnosis of vulnerable plaque. Magn Reson Mater Phys 20: 129–142.
52. Rukmini R, Rawat SS, Biswas SC, Chattopadhyay A (2001) Cholesterol organization in membranes at low concentrations: Effects of curvature stress and membrane thickness. Biophys J 81: 2122–2134.
53. Huang C, Mason JT (1978) Geometric packing constraints in egg phosphatidylcholine vesicles. Proc Natl Acad Sci USA 75: 308–310.
54. Lemmich J, Mortensen K, Ipsen JH, Honger T, Bauer R, et al. (1997) The effect of cholesterol in small amounts on lipid bilayer softness in the region of the main phase transition. Eur Biophys J 25: 293–304.
55. Harroun TA, Katsaras J, Wassall SR (2008) Cholesterol is found to reside in the center of a polyunsaturated lipid membrane. Biochemistry 47: 7090–7096.
56. Marrink SJ, de Vries A, Harroun TA, Katsaras J, Wassall SR (2008) Cholesterol shows preference for the interior of polyunsaturated lipid membranes. J Am Chem Soc 130: 10–11.
57. Lund-Katz S, Phillips MC (1986) Packing of cholesterol molecules in human low-density lipoprotein. Biochemistry 25: 1562–1568.
58. Filippov A, Orädd G, Lindblom G (2003) The effect of cholesterol on the lateral diffusion of phospholipids in oriented bilayers. Biophys J 84: 3079–3086.
59. Vauhkonen M, Sassaroli M, Somerharju P, Eisinger J (1989) Lateral diffusion of phospholipids in the lipid surface of human low-density lipoprotein measured with a pyrenyl phospholipid probe. Eur J Biochem 186: 465–471.
60. Massey JB, Pownall HJ (1998) Surface properties of native human plasma lipoproteins and lipoprotein models. Biophys J 74: 869–878.
61. Apajalahti T, Niemela P, Govindan PN, Miettinen MS, Salonen E, et al. (2010) Concerted diffusion of lipids in raft-like membranes. Faraday Disc 144: 411–430.
62. Thomas A, Meurisse R, Charloteaux B, Brasseur R (2002) Aromatic side-chain interactions in proteins. I. Main structural features. Proteins: Struct Func Gen 48: 628–634.
63. Wimley WC, White SH (1996) Experimentally determined hydrophobicity scale for proteins at membrane interfaces. Nature Struct Biol 3: 842–848.
64. Dergunov AD, Dobretsov GE, Visvikis S, Siest G (2001) Protein-lipid interactions in reconstituted high density lipoproteins: Apolipoprotein and cholesterol influence. Chem Phys Lipids 113: 67–82.
65. Lund-Katz S, Phillips MC (1984) Packing of cholesterol molecules in human high-density lipoproteins. Biochemistry 23: 1130–1138.
66. Kontush A, Chapman MJ (2006) Functionally defective high-density lipoprotein: A new therapeutic targest at the crossroads of dyslipidemia, inflammation, and atherosclerosis. Pharmacol Rev 58: 342–374.
67. Yetukuri L, Soderlund S, Koivuniemi A, Seppanen-Laakso T, Niemela PS, et al. (2010) Composition and lipid spatial distribution of high density lipoprotein particles in subjects with low and high HDL-cholesterol. J Lipid Res 51: 2341–2351.
68. Segrest JP, Jones MK, Klon AE, Sheldahl CJ, Hellinger M, et al. (1999) A detailed molecular belt model for apolipoprotein A-I in discoidal high density lipoprotein. J Biol Chem 274: 31755–31758.
69. Borhani DW, Rogers DP, Engler JA, Brouillette CG (1997) Crystal structure of truncated human apolipoprotein A-I suggests a lipid-bound conformation. Proc Natl Acad Sci USA 94: 12291–12296.
70. Segrest JP, Harvey SC, Zannis V (2000) Detailed molecular model of apolipoprotein A-I on the surface of high-density lipoproteins and its functional implications. Trends Cardiovasc Med 10: 246–252.
71. Klon AE, Segrest JP, Harvey SC (2002) Comparative models for human apolipoprotein A-I bound to lipid in discoidal high-density lipoprotein particles. Biochemistry 41: 10895–10905.
72. Klon AE, Segrest JP, Harvey SC (2002) Molecular dynamics simulations on discoidal HDL particles suggest a mechanism for rotation in the apoA-I belt model. J Mol Biol 324: 703–721.
73. Okon M, Frank PG, Marcel YL, Cushley RJ (2002) Heteronuclear NMR studies of human serum apolipoprotein A-I part I. Secondary structure in lipid-mimetic solution. FEBS Lett 517: 139–143.
74. Lindahl E, Hess B, van der Spoel D (2001) GROMACS 3.0: A package for molecular simulation and trajectory analysis. J Mol Mod 7: 306–317.
75. Nosé S (1984) A molecular dynamics method for simulations in the canonical Ensemble. Mol Phys 52: 255–268.
76. Hoover WG (1985) Canonical dynamics: Equilibrium phase-space fistributions. Phys Rev 31: 1695–1697.
77. Parrinello M, Rahman A (1981) Polymorphic transitions in single crystals: A new molecular dynamics method. J Appl Phys 52: 7182–7190.
78. Niemela PS, Miettinen M, Monticelli L, Hammaren H, Bjelkmar P, et al. (2010) Membrane proteins diffuse as dynamic complexes with lipids. J Am Chem Soc 132: 7574–7575.
79. Ramadurai S, Holt A, Schafer LV, Krasnikov VV, Rijkers DTS, et al. (2010) Influence of hydrophobic mismatch and amino acid composition on the lateral diffusion of transmembrane peptides. Biophys J 99: 1447–1454.

II

Low Density Lipoprotein: Structure, Dynamics, and Interactions of ApoB-100 with Lipids

by

Teemu Murtola, Timo Vuorela, Marja T. Hyvönen, Siewert-Jan Marrink, Mikko Karttunen & Ilpo Vattulainen.

Soft Matter **7**, 8135-8141 (2011).

View Article Online / Journal Homepage / Table of Contents for this issue
Dynamic Article Links

Soft Matter

Cite this: *Soft Matter*, 2011, **7**, 8135

www.rsc.org/softmatter

PAPER

Low density lipoprotein: structure, dynamics, and interactions of apoB-100 with lipids†

Teemu Murtola,[ab] Timo A. Vuorela,[c] Marja T. Hyvönen,[d] Siewert-Jan Marrink,[e] Mikko Karttunen[f] and Ilpo Vattulainen[*acg]

Received 2nd March 2011, Accepted 6th June 2011
DOI: 10.1039/c1sm05367a

Low-density lipoprotein (LDL) transports cholesterol in the bloodstream and plays an important role in the development of cardiovascular diseases, in particular atherosclerosis. Despite its importance to health, the structure of LDL is not known in detail. This is worrying since the lack of LDL's structural information makes it more difficult to understand its function. In this work, we have combined experimental and theoretical data to construct LDL models comprised of the apoB-100 protein wrapped around a lipid droplet of about 20 nm in size. The models are considered by near-atomistic multi-microsecond simulations to unravel structural as well as dynamical properties of LDL, with particular attention paid to lipids and their interactions with the protein. We find that the distribution and the ordering of the lipids in the LDL particle are rather complex. The previously proposed 2- and 3-layer models turn out to be inadequate to describe the properties of the lipid droplet. At the surface of LDL, apoB-100 is found to interact favorably with cholesterol and its esters. The interactions of apoB-100 with core molecules, in particular cholesteryl esters, are rather frequent and arise from hydrophobic amino acids interacting with the ring of cholesteryl esters, and also in part from the rather loose packing of lipids at the surface of the lipoparticle. The loose packing may foster the function of transfer proteins, which transport lipids between lipoproteins. Finally, the comparison of the several apoB-100 models in our study suggests that the properties of lipids in LDL are rather insensitive to the conformation of apoB-100. Altogether, the findings pave the way for further studies of LDL to better understand the central steps in the emergence of atherosclerosis.

Introduction

Low-density lipoprotein (LDL) particles transport cholesterol and its esters in the human bloodstream. Clinically, LDL plays a central role in the development of cardiovascular diseases, in particular atherosclerosis. In the initial stages of atherogenesis, LDL-derived lipids accumulate in the arterial intima, and high LDL levels have been shown to increase the risk of atherosclerosis.[1,2] This together with formation of plaque on arterial walls leads to the narrowing of arteries, rupture, clotting, and potential death.

On average, LDL particles (see Fig. 1) have a diameter of 22 nm and contain ~3000 lipids. Their density ranges between 1.019 and 1.063 g ml^{-1} (ref. 3), highlighting that quite a heterogeneous group of particles can be called LDL. Most abundant lipid species in LDL are triglycerides and cholesteryl esters assumed to reside in the core of the particle, while different phospholipids are expected to be located on the surface,[3] the location of unesterified cholesterol being less well understood. Further, there is also a single copy of apolipoprotein B-100 (apoB-100) which, with 4536 residues, is one of the largest monomeric proteins known.

While the general features of the structures of LDL and apoB-100 have been determined experimentally,[4,5] detailed understanding of their structures, dynamics, and hence also *function* is lacking. Molecular simulations could be expected to shed some light on these issues since they have recently been shown to provide detailed insight into many lipid-based biological systems.[6] Yet, as far as LDL is concerned, there is reason to stress that this quest is exceptionally challenging. First, given that the diffusion of lipids at the LDL surface is of the order of 10^{-7} cm^2

[a]*Aalto University School of Science and Technology, Finland*
[b]*Department of Biochemistry and Biophysics, Stockholm University, Sweden*
[c]*Department of Physics, Tampere University of Technology, POB 692, FI-33101 Tampere, Finland. E-mail: Ilpo.Vattulainen@tut.fi*
[d]*Department of Physics, University of Oulu, Finland*
[e]*Groningen Biomolecular Sciences and Biotechnology Institute & Zernike Institute for Advanced Materials, University of Groningen, The Netherlands*
[f]*Department of Applied Mathematics, University of Western Ontario, Canada*
[g]*MEMPHYS, University of Southern Denmark, Denmark*

† Electronic supplementary information (ESI) available: Description of models, simulations, analysis, and additional results. See DOI: 10.1039/c1sm05367a

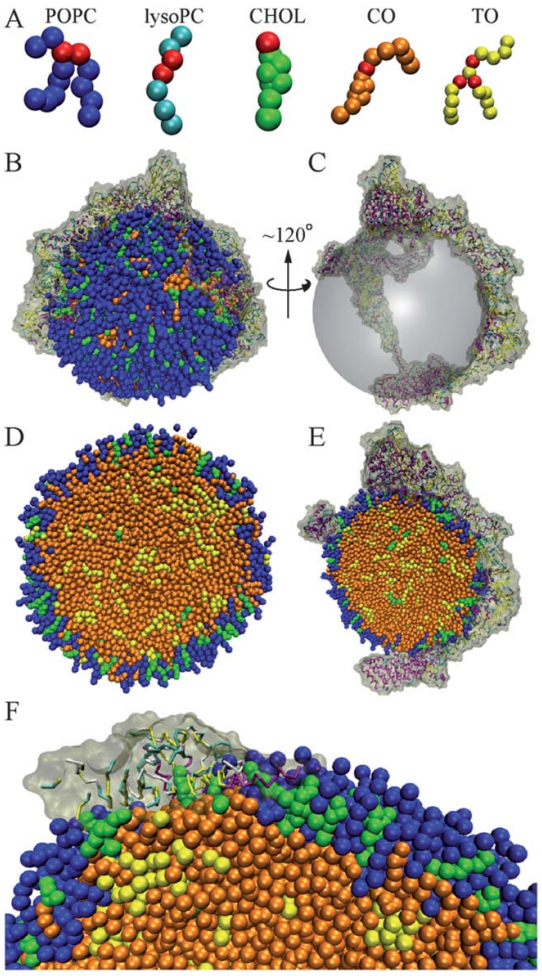

Fig. 1 LDL particle structure. (A) Lipids. Red beads show the location of glycerol (PC, lysoPC), hydroxyl (CHOL), and ester (CO, TO) groups. (B) Full LDL from the final structure of S1r. Lipids shown in similar colours as in (A), without red highlights, and PC and lysoPC coloured blue. ApoB-100 shown in tan, with the lipovitellin domain (first 1000 residues) pointing up. (C) Same as (B), except that lipids are shown as transparent spheres. (D) LDL simulated without the protein, cut through the middle. Note how the core penetrates to the surface. (E) Same as (B), except that the lipid part has been cut through the middle. The core penetrates to the lipid surface under the protein. (F) Close-up image of the surface from (B).

s^{-1} (ref. 7), the diffusion time across LDL is of the order of microseconds. Any simulation should hence cover at least several microseconds to equilibrate the lipid distribution. Second, as the precise structure of apoB-100 is not known, one should simulate more than one protein structure and compare their differences. Further, due to the major size of the system, atom-scale simulations of LDL are not currently feasible.

Due to these reasons, we have chosen to use the MARTINI approach[8,9] to describe LDL on a coarse-grained (CG) level (see Fig. 1 and Materials and Methods section). A similar approach has earlier been used in studies of high density lipoproteins (HDL, diameter of 7–8 nm),[10–15] which have also been simulated in atomic detail.[11,16–18] Related work on simulations of lipid droplet biogenesis,[19] and properties of triglyceride[20] and cholesteryl ester melts[21] in the hydrophobic core of lipoproteins has also been recently discussed. Nonetheless, so far LDL has not been studied at all through molecular simulations.

Our objective in this work is to fill this gap, thereby providing insight into the structural as well as dynamical properties of LDL in semi-atomistic detail. We focus on lipids and their interactions with apoB-100. We find that the distribution and ordering of the lipids in the LDL particle are rather complex, and the previously proposed 2- and 3-layer models (see, *e.g.* ref. 3) are inadequate to describe the properties of the lipid droplet in LDL. The dynamics of lipids is also untrivial and depends on the location of lipids in the particle. At the surface of LDL, apoB-100 is found to interact favorably with cholesterol and its esters. The interactions of apoB-100 with core molecules, in particular cholesteryl esters, are rather frequent and arise from hydrophobic amino acids interacting with the ring of cholesteryl esters, and also in part from the rather loose packing of lipids at the surface of the lipoparticle. The loose packing is expected to foster the function of transfer proteins, which transport lipids between lipoproteins. Finally, the distribution of lipids is found to be rather insensitive to the conformation of apoB-100.

The models we have developed for LDL and the results discussed in this article provide a solid basis for further simulations of LDL functions, such as the effect of enzymatic modifications and oxidation due to free radicals that promote the development of atherosclerosis.

Materials and methods

We have run five MD simulations with GROMACS[22] starting from different initial structures (Table 1), each simulation spanning several microseconds. All the systems have the same lipid composition, corresponding to an average LDL particle:[3] 1600 cholesteryl oleates (CO), 180 trioleates (TO), 600 unesterified cholesterols (CHOL), 630 double-tailed phospholipids (PC), and 80 lysolipids (lysoPC). The force field used in this work is based on the MARTINI approach.[8,9]

In the MARTINI description for proteins, the secondary structures have to be constructed separately, and here we realized this with the elastic network model.[23] The downside of this

Table 1 Description of LDL simulations performed

System	Length	Lipids	apoB-100 structure
LD	18 μs	Random droplet	No apoB-100
S1	10 μs	LD at 8 μs	From ref. 22, missing residues manually from PSIPRED
S1r	10 μs	LD at 8 μs	Same as S1 but different placement at surface
S2	6 μs	LD at 8 μs	Residues 1–1000 from ref. 21, 1000–2000 an amphiphilic β-sheet, otherwise as S1
S2r	10 μs	LD at 8 μs	Same as S2 but different placement at surface

approach is the fact that the secondary structures will remain fixed. However, in this work where we focus on lipids and their interactions with apoB-100, this is not a major limitation.

We first simulated only the lipid droplet (LD) in water, *i.e.*, without apoB-100. The structure of the LD in this simulation after 8 μs was used as the initial lipid droplet for the other four simulations that contain apoB-100 (Fig. 1). Here, two different secondary structures were constructed for the protein, referred to as S1 and S2. S1 was mainly based on the theoretical models by Krisko and Etchebest.[24] The domains (~10% of all residues) were constructed using secondary structure prediction from PSIPRED.[25] The second model (S2) used the homology model of Richardson *et al.*[26] for the first 1000 residues, and a continuous amphipathic β-sheet for residues 1000–2000. The remaining part was modelled as in S1. For both secondary structures, two different initial placements of the protein were constructed, referred to as S1 and S1r (and S2 and S2r, respectively). Fig. 1B showing the structure for the protein that lays on the particle surface is in line with the low-resolution model, which is based on neutron scattering studies of desolubilized apoB.[27] Analysis focuses on systems S1r and S2r, as S1 and S2 were found to behave very similarly.

All further details are given in the ESI†.

Results and discussion

Molecular distribution and order within LDL

As for the reference system (without apoB-100), Fig. 2 (left panel) shows the average radial distribution of the different molecules in LD. The curves show the number density of beads as a function of the distance from the centre of the droplet for each molecule type separately. Also shown is the total lipid bead density. The figure clearly depicts how the particle is partitioned into a surface monolayer consisting mostly of PC, lysoPC and CHOL lipids, and a hydrophobic core that contains CO and TO, as well as around 13% of the CHOL lipids. Note, however, that the core lipids (CO and TO) penetrate the surface monolayer, having non-negligible densities up to the water phase. This is to be expected, because there are about 1300 PC, lysoPC, and CHOL lipids in total, while the total surface area is ~1000 nm^2 (for a radius of 9 nm). Therefore, the area per lipid in the surface monolayer is well above the equilibrium area for these lipids in a lipid bilayer. In fact, the area per lipid is similar in magnitude to a value that has been observed to lead to formation of small, transient pores in monolayers,[28] but different compositions of the layers prevent any quantitative comparison. Nevertheless, we observe small transient pores to form, exposing some of the core lipids on the surface, see snapshots in Fig. 1D and E.

The results for the surface area of lipids suggest some ideas that would be worth testing later, using either other simulations or experiments. First, would it be possible that the surface of LDL is like a lipid layer under low surface pressure. If this was the case, then some aspects of lipoproteins could be characterized using, *e.g.*, lens lipid membrane[29] like layers instead. Second, given the looser packing at the surface, is it possible that the protein can to a significant extent interact with the neutral molecules (TO, CO) in the core of the particle. This possibility would be highly relevant for lipid transfer, since transfer proteins such as the cholesteryl ester transfer protein (CETP)[30] first bind to the lipoprotein surface and then allow lipids to migrate to their binding pocket/tunnel. The looser is the lipoprotein surface, the more efficient can the transfer process be expected to be.

Notably, lysoPCs reside further out from the centre as compared to PCs. This conclusion holds even after accounting for the fact that the headgroup is a larger part of lysoPC than PC. Similar observations have also been made for CG vesicles.[31]

Fig. 3 (left panel) depicts the average orientation of the ring structures of CO and CHOL *vs.* distance from the centre of the droplet. The orientation is measured as $S = (1/2)\,\langle 3\cos^2\theta - 1\rangle$, where θ is the angle between the radial unit vector and a vector from the head/ester group to the first bead in the tail. The distance and the radial unit vector are measured using the centre of the mentioned vector. A value of zero indicates a completely random distribution, while one signifies perfect radial alignment, and −0.5 stands for alignment parallel to the surface. The blue dashed lines show the region where the surface monolayer resides. The core is largely unordered with all orientations equally likely. Within the monolayer, the molecules are mainly aligned along the normal, *i.e.*, they sit upright between the lipids. Close to the outer boundary, there are a few molecules, thus the large peaks are mainly due to poor statistics. The alignment of

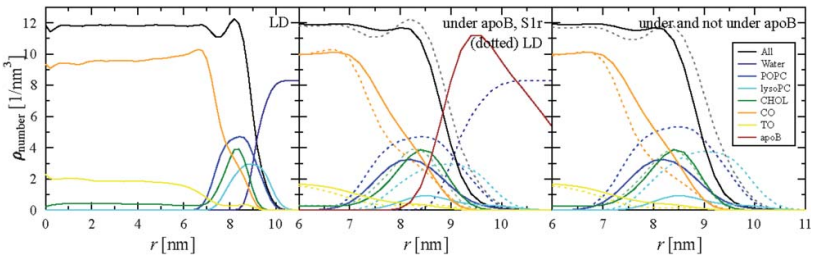

Fig. 2 Number density of particles *vs.* distance from the centre of the droplet (r): all lipids (black), POPC (blue), PPC (cyan, scaled by 10), CHOL (green), CO (orange), TO (yellow), water (dark blue, not in right panel), protein (brown, only middle panel). The left panel shows the distribution in LD without apoB-100. The middle panel shows how the distribution changes under apoB-100. The dotted lines are identical to those in the left panel; the solid lines show the distribution in regions where there is protein on the surface. The right panel compares the distribution between the regions covered and not covered by apoB-100 in S1r. The solid line is identical to the middle panel. The dotted line shows the distribution in regions not covered by apoB-100.

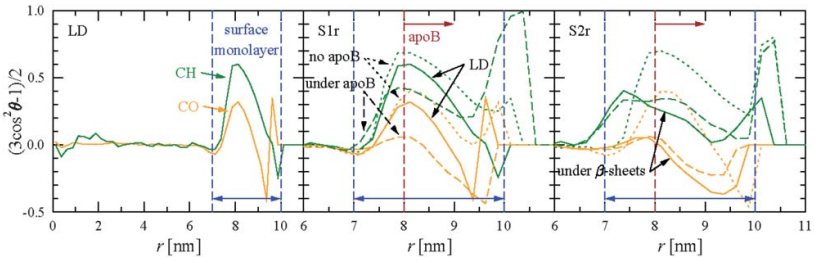

Fig. 3 Order parameter of the angle between the CHOL plane and the local normal for CHOL (green) and CO (orange) *vs.* distance from the center of the droplet. The left panel shows the situation in the absence of apoB-100. The middle panel shows the effect of apoB-100 in S1r. The solid lines are identical to the left panel, while the dashed and dotted lines show the situation in regions covered and not covered by apoB-100, respectively. The right panel shows the effect of protein secondary structure on the ordering in S2r. The dotted and dashed lines show the order parameter in regions covered and not covered by apoB-100, respectively. The solid line represents regions where apoB-100 has β-strands close to the lipid surface.

CO along the normal is weaker than for CHOL. This comes from the fact that the hydrophilic part of CO is in the middle of the molecule, thus rendering it difficult to place the molecule in the surface monolayer such that the ring structure would be upright and the hydrophilic part on the surface. The hydroxyl group in CHOL is also more hydrophilic than the ester linkage in CO. The four protein simulations all behave quite similarly, thus we focus on the system S1r to identify the main effects of the protein on the lipids. We note that the lipid droplet remains spherical, as measured by the radii of gyrations calculated along the principal axes of the droplet (results not shown).

Fig. 2 (middle panel) shows how the surface composition changes close to apoB-100: the figure compares the radial densities in LD (left panel) to those in S1r. The latter are calculated only for sections under apoB-100, defined as the parts of the particle that are within 2° of any protein atom when seen from the centre of the LD. A complementary comparison is shown in the right panel: it shows the radial densities for S1r, calculated for sections under and not under apoB-100.

The total lipid density shows that the radius of the droplet is slightly smaller below the protein. This comes from reduction of the PC and lysoPC densities, while the core lipids (CO and TO) as well as CHOL actually move closer to apoB-100. These observations suggest that the protein prefers to interact directly with the core of the particle, displacing the surface monolayer, see below. This also means that in the systems that contain the protein, the surface monolayer has a significantly lower area per lipid. This has an effect on its composition: in these systems, the core lipids do not penetrate as often to the surface (Fig. 1D).

Fig. 3 (middle panel) shows how the protein affects CO and CHOL orientation under it. The order parameter in regions without apoB-100 is higher than in LD, in line with the common notion that smaller area per lipid on the surface increases order. Under the protein, order parameter is lower, and in particular the CO molecules prefer orientations parallel to the surface ($S < 0$).

Dynamics and lipid–protein interactions

For dynamics, we estimated the diffusion coefficients for the different molecules in different parts of the lipid droplet, see Table 2. By considering particle displacement distributions over fixed time intervals, we readily identified core lipids to undergo 3D diffusion, while lipids at the surface diffused in a 2D manner (see ESI†). Table 2 shows clearly that the diffusion speeds up monotonically as one leaves the core and approaches the surface, the diffusion coefficient increasing by a factor of 10. At the surface, the diffusion coefficient is in line with the experiments by Vauhkonen *et al.*,[7] who used pyrene-linked PCs as probes to find $D = (0.5–1.5) \times 10^{-7}$ cm^2 s^{-1} at the surface of lipoparticles.

The addition of the protein does not significantly affect the diffusion in the core of the droplet, but considerably slows down the motion on the surface. This effect is most pronounced close to the protein, but can also be seen for other parts of the surface as well as in the core lipids close to the surface. The overall slowing down can be explained by noting that the area per lipid in the surface monolayer reduces considerably upon addition of the protein. Close to the protein, there may be specific interactions, *e.g.*, between hydrophilic beads in the protein and in the lipids. The slowing down is stronger for CHOL than for CO, which also supports the picture that CHOL interacts strongly with some parts of the protein. Here, we refer to Fig. 4 which shows the number of contacts between CHOL/CO and different

Table 2 Diffusion coefficients are in units of 10^{-8} cm^2 s^{-1}. The distance r from the center of the lipid droplet/LDL is given in units of nm. Error estimates are of the order of 5%. Values for CHOL have been computed over all molecules, although 13% of them lay in the core. In the last column are given diffusion coefficients separately for molecules that are either near or far from apoB-100 (in the system LD, there is no protein, thus only one value is given)

Molecule	System	$r < 2$	$2 < r < 4$	$4 < r < 6$	$r > 6$ Near/far apoB
CO	LD	1.8	2.0	3.0	4.2
	S1r	1.9	2.0	2.5	2.5/3.4
	S2r	1.9	1.9	2.3	2.4/3.0
TO	LD	1.1	1.4	2.1	3.3
	S1r	1.2	1.4	1.7	1.9/2.4
	S2r	1.1	1.2	1.5	1.7/1.9
CHOL	LD				8.8
	S1r				3.7/6.4
	S2r				3.5/5.8
PC	LD				8.0
	S1r				3.5/5.6
	S2r				3.0/5.0
Lyso-PC	LD				14.0
	S1r				5.7/10.0
	S2r				5.3/9.0

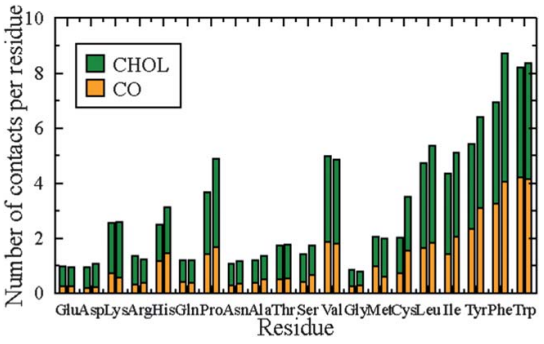

Fig. 4 Average number of contacts between different amino acids of apoB-100 and CHOL or CO molecules for systems S1r (left bars) and S2r. Each pair of beads within 0.8 nm of each other constitutes one contact.

amino acids in apoB. The figure demonstrates that the majority of the contacts between CHOL/CO and the protein occur at hydrophobic amino acids. Note that the figure carries a certain bias towards larger amino acids (Trp, Phe, Tyr, His) since they contain more beads, but even if these are ignored, the general conclusions still hold. We also separated contributions from the sterol rings and the rest of the molecule. For CO, there is no clear preference for either, but for CHOL the rings form much more contacts with the protein than the CHOL tails, even when we account for the tails having fewer beads than the rings. The CO bars in Fig. 4 can also be used to assess which amino acids interact preferentially with the core (with similar conclusions as above); this is because TO forms only few contacts with the protein (Fig. 2, middle panel), and these do not influence the image significantly. A similar figure with secondary structure classes on the *x*-axis (not shown) indicates that some helices, and in the case of S2 also some β-sheets, are the main secondary structure elements interacting with the core. These regions are easily identified as the C-terminal extended helical region, where most of the helices lay on the interface as single helices, and the extended β-sheet (residues 1000–2000) in S2, which by construction lays flat on the surface.

Influence of protein conformation on lipids

As the three-dimensional structure of apoB-100 is not well known, we considered two different models for the protein. The comparison of our results for the different models indicates that all the protein systems behave qualitatively in a similar manner. There are only minor differences between S1 and S1r (S2 and S2r): it takes some time for the protein to bind to the surface in S1/S2, and how these systems equilibrate slower than S1r/S2r. The main difference between the two secondary structure models (S1r and S2r) is in the area covered by the protein: S1r covers, on average, ∼35% of the surface, while S2r covers ∼40%. This difference comes mainly from the extended β-sheet in model S2 that is much thinner than the same region in S1, so it spans a larger surface area: in S2r, the residues 1000 to 2000 cover 13% of the particle surface, while this figure is 8% for S1r. The effect of the protein structure on the radial densities is also minor. However, there are larger differences in the CHOL orientations (Fig. 3, right). Again, the difference comes from the presence of the large β-sheet in S2, which orders the cholesterols a bit deeper in the core. This extended ordering is not present for CO.

We conclude that the three-dimensional conformation of apoB-100 does not play a significant role for lipid distribution and orientation in LDL. Further results for lipid diffusion (data not shown) result in the same conclusion. This largely implies that we cannot conclude one of the protein models to be better than the other, as the observed differences in lipid properties are not significant to the extent that we could say one of the models to be physically unreasonable.

Are there "core ridges" under the β-sheets?

Segrest *et al.* proposed in 2001 an appealing idea of "core ridges" under the β-sheets of apoB-100.[4] This model depicts cholesteryl esters to distribute not only in the core of LDL but also under the β-sheets of apoB-100. Further, CO molecules under the β-sheets would be aligned along the surface plane, and organize to form strong smectic-like liquid crystal phases.

When we compare our simulation data to the ideas underlying the core ridge model, we first find that the core molecules (CO, TO) extend further outwards from the center of the LDL particle when they are close to the protein. Also, the order parameters for the COs and CHOLs under the β-sheets are lower than elsewhere under the protein, meaning that the rings of COs and CHOLs prefer to orient parallel to the β-sheets and therefore also the LDL surface. Further, the diffusion of lipids that are under the protein is slower compared to lipids that are elsewhere in the surface region. These findings are in general agreement with the idea of core ridges proposed by Segrest *et al.*[4]

Meanwhile, the simulation data indicate that the effect of the β-sheets spans the surface monolayer, but does not affect the structure significantly deeper in the core. The ordering of the lipids and the extent of the ordered layers of molecules are not as pronounced as the core ridge model suggests. The effect that we observe is quite weak, while Segrest *et al.* proposed strong, smectic-like organization of COs.

What can we say about the protein itself?

Because of the limitations of our model (uncertainty in the apoB structure and its fixed secondary structure), it is not possible to study the protein itself in detail. Yet, let us discuss how the protein evolves during the simulations. First, on a global scale, the protein conformation remains unmodified. The RMSD values between the initial and final protein structures are ∼1.5 nm. The protein also expands to cover 2–3% more of the total particle surface. The observed RMSD is not large considering the protein's size and flexibility: the protein consists of several domains that can move more or less freely relative to each other, and the domains also form a chain with a total contour length of about 70 nm instead of a compact globule. Experimentally it is also known that apoB-100 can adapt to large changes in the particle diameter (from 70 nm in VLDL down to 20 nm in LDL), also supporting the view that the protein is quite flexible. Finally, the two large β-sheets in the lipovitellin domain (the first 1000 residues in S2) spread out to follow the lipid surface, in agreement with the proposition of Richardson *et al.*[26]

Transition from core to surface: can LDL be characterized by a two- or three-layer model?

Given that we now have a complete view of the results for lipids' structure as well as dynamics in LDL, and we also have some understanding of the role of apoB-100 in LDL, let us comprise this information to consider the model that best matches our findings. In this respect it is widely accepted that apoB-100 resides on the surface of LDL, but there are several conflicting propositions of how the protein interacts with the lipids.[3,4] There has also been discussion on whether a two-layer (core + surface monolayer) or a three-layer picture is more correct.[3]

We find that the protein resides on the surface and displaces the surface monolayer, but does not penetrate into the core. Also, the core near the surface is more ordered than deep inside the particle, in particular close to large β-sheet structures. The protein thus displaces the surface layer nearly completely from under it, and also influences the lipids under the protein by decreasing the tail density and partially orienting the CHOL rings along the surface.

Further, as for lipids, our simulations show that CO and TO mainly reside in the core, though small amounts of these lipids are also found close to the surface. CO molecules are randomly oriented in the core, but under the surface and at the surface they are rather strongly oriented to stand upright along the radial normal direction of the particle. The orientation of cholesterol is largely similar to that of CO, though cholesterol is almost entirely in the surface region and only occasionally in the inside of the particle. Polar phospholipids occupy the surface of LDL, where they are abundant and highly ordered as the acyl chains have to pack themselves tightly. Finally, when one considers the diffusion of the lipids, it is slow in the core and speeds up the more the closer one is to the surface.

Altogether, the data support a picture for the lipids where there is (1) a hydrophobic core composed of randomly oriented CO, TO, and some CHOL, (2) an ordered intermediate hydrophobic layer composed of PC tails, CHOL, and some CO, and (3) a surface layer composed mostly of the PC headgroups. However, assigning a fixed number of layers is quite arbitrary, since there is no unique way to define the boundaries between them. Instead of being in favor of either the two- or three-layer model, we consider it more appropriate to conclude that there is a broad transition from the core to the polar surface region.

Concluding remarks

In conclusion, our study provides the first molecular-scale model for LDL structure and dynamics based on extensive near-atomistic simulations, with emphasis on lipids' distribution and interactions with apoB-100. The results highlight the importance of lipids in understanding LDL function. Not only the surface lipids but also the core lipids play an important role in LDL, as interactions between lipids and apoB-100 drive core lipids to the surface. This may have biological significance for trafficking as carriers such as cholesteryl ester transfer proteins embrace cholesteryl esters and triglycerides from LDL and HDL to their binding pocket for transport. The rather loose packing at the surface and the observed fast diffusion at the LDL surface compared to the core would promote this for lipids close to the surface layer.

The detailed structural and dynamical simulation data show that there is no simple model in terms of two or three well-defined layers in the lipid droplet of LDL to describe the distribution and structural as well as dynamical properties of the lipids. Instead an appropriate paradigm is more complex, describing LDL with a hydrophobic core and polar surface regions, and a broad transition between them. At the surface, the simulations are in partial agreement with the idea of core ridges proposed by Segrest *et al.*,[4] suggesting that cholesteryl esters are attracted by apoB-100 to come close to it and align themselves along the surface plane. However, we did not observe significant layers of ordered cholesteryl ester molecules under apoB-100.

The results provide a solid basis for further simulations of LDL functions, such as the effect of enzymatic modifications and oxidation due to free radicals that promote the development of atherosclerosis. Of major biological importance is to understand the coupling between lipid composition of LDL and its structure and function, as the lipid composition depends on the subject's diet and living habits.[14,32]

As for applications, the view presented here promotes the development of LDL-based molecular transporters and atherosclerosis blockers. In all these aspects, the LDL model found in this work can be employed as a basis for full atomistic and even *ab initio* simulations through systematic fine-graining of the coarse-grained model to an atomistic representation.

Acknowledgements

We acknowledge A. Koivuniemi, L. Monticelli, P. Niemelä and S. Ollila. A. Krisko and C. Etchebest are thanked for sharing their data. This work has been supported by the Academy of Finland and The Swedish Research Council. Computational resources were provided by the Finnish IT Center for Science, HECToR (UK, DEISA initiative), and Sharcnet.

References

1 P. L. Colvin and J. S. Parks, *Curr. Opin. Lipidol.*, 1999, **10**, 309.
2 P. Linsel-Nitschenke and A. R. Tall, *Nat. Rev. Drug Discovery*, 2005, **4**, 193.
3 T. Hevonoja, M. O. Pentikäinen, M. T. Hyvönen, P. T. Kovanen and M. Ala-Korpela, *Biochim. Biophys. Acta, Mol. Cell Biol. Lipids*, 2000, **1488**, 189.
4 J. P. Segrest, M. K. Jones, H. D. Loof and N. Dashti, *J. Lipid Res.*, 2001, **42**, 1346.
5 R. Prassl and P. Laggner, *Eur. Biophys. J.*, 2009, **38**, 145.
6 I. Vattulainen and T. Rog, *Cold Spring Harbor Perspect. Biol.*, 2011, **3**, a004655.
7 M. Vauhkonen, M. Sassaroli, P. Somerharju and J. Eisinger, *Eur. J. Biochem.*, 1989, **186**, 465.
8 S. J. Marrink, H. J. Risselada, S. Yefimov, D. P. Tieleman and A. H. de Vries, *J. Phys. Chem. B*, 2007, **111**, 7812.
9 L. Monticelli, S. K. Kandasamy, X. Periole, R. G. Larson, D. P. Tieleman and S. J. Marrink, *J. Chem. Theory Comput.*, 2008, **4**, 819.
10 A. Y. Shih, A. Arkhipov, P. L. Freddolino and K. Schulten, *J. Phys. Chem. B*, 2006, **110**, 3674.
11 A. Y. Shih, P. L. Freddolino, A. Arkhipov and K. Schulten, *J. Struct. Biol.*, 2007, **157**, 579.
12 A. Catte, J. C. Patterson, D. Bashtovyy, M. K. Jones, F. Gu, L. Li, A. Rampioni, D. Sengupta, T. Vuorela, P. Niemelä, M. Karttunen, S. J. Marrink, I. Vattulainen and J. P. Segrest, *Biophys. J.*, 2008, **94**, 2306.

13 A. Y. Shih, S. G. Sligar and K. Schulten, *J. R. Soc. Interface*, 2009, **6**, 863.
14 L. Yetukuri, S. Soderlund, A. Koivuniemi, T. Seppanen-Laakso, P. S. Niemelä, M. T. Hyvönen, M. R. Taskinen, I. Vattulainen, M. Jauhiainen and M. Oresic, *J. Lipid Res.*, 2010, **51**, 2342.
15 T. Vuorela, A. Catte, P. S. Niemelä, A. Hall, M. T. Hyvönen, S. J. Marrink, M. Karttunen and I. Vattulainen, *PLoS Comput. Biol.*, 2010, **6**, e1000964.
16 A. Y. Shih, I. G. Denisov, J. C. Phillips, S. G. Sligar and K. Schulten, *Biophys. J.*, 2005, **88**, 548.
17 A. Catte, J. C. Patterson, M. K. Jones, W. G. Jerome, D. Bashtovyy, Z. Su, F. Gu, J. Chen, M. P. Aliste, S. C. Harvey, L. Li, G. Weinstein and J. P. Segrest, *Biophys. J.*, 2006, **90**, 4345.
18 A. Koivuniemi, M. Heikelä, P. T. Kovanen, I. Vattulainen and M. T. Hyvönen, *Biophys. J.*, 2009, **96**, 4099.
19 H. Khandelia, L. Duelund, K. I. Pakkanen and J. H. Ipsen, *PLoS One*, 2010, **5**, e12811.
20 A. Hall, J. Repakova and I. Vattulainen, *J. Phys. Chem. B*, 2008, **112**, 13772.
21 M. Heikelä, I. Vattulainen and M. T. Hyvönen, *Biophys. J.*, 2006, **90**, 2247.
22 B. Hess, C. Kutzner, D. van der Spoel and E. Lindahl, *J. Chem. Theory Comput.*, 2008, **4**, 435.
23 X. Periole, M. Cavalli, S. J. Marrink and M. Ceruso, *J. Chem. Theory Comput.*, 2009, **5**, 2531.
24 A. Krisko and C. Etchebest, *Proteins: Struct., Funct., Bioinf.*, 2007, **66**, 342.
25 D. T. Jones, *J. Mol. Biol.*, 1999, **292**, 195.
26 P. E. Richardson, M. Manchekar, N. Dashti, M. K. Jones, A. Beigneux, S. G. Yong, S. C. Harvey and J. P. Segrest, *Biophys. J.*, 2005, **88**, 2789.
27 A. Johs, M. Hammel, I. Waldner, R. P. May, P. Laggner and R. Prassl, *J. Biol. Chem.*, 2006, **281**, 19732.
28 V. Knecht, M. Muller, M. Bonn, S. J. Marrink and A. E. Mark, *J. Chem. Phys.*, 2005, **122**, 024704.
29 A. H. Rantamäki, J. Telenius, A. Koivuniemi, I. Vattulainen and J. M. Holopainen, *Prog. Retinal Eye Res.*, 2011, **30**, 204.
30 X. Qiu, A. Mistry, M. J. Ammirati, B. A. Chrunyk and R. W. Clark, et al., *Nat. Struct. Mol. Biol.*, 2007, **14**, 106.
31 S. J. Marrink and A. E. Mark, *J. Am. Chem. Soc.*, 2003, **125**, 15233.
32 J. R. McNamara, D. M. Small, Z. Li and E. J. Schaefer, *J. Lipid Res.*, 1996, **37**, 1924.

III

Lipid Exchange Mechanism of the Cholesteryl Ester Transfer Protein Clarified by Atomistic and Coarse-Grained Simulations

by

Artturi Koivuniemi, Timo Vuorela, Petri T. Kovanen,
Ilpo Vattulainen & Marja T. Hyvönen.

PLoS Computational Biology **8**, e1002299 (2012).

OPEN ACCESS Freely available online PLoS COMPUTATIONAL BIOLOGY

Lipid Exchange Mechanism of the Cholesteryl Ester Transfer Protein Clarified by Atomistic and Coarse-grained Simulations

Artturi Koivuniemi[1]*, Timo Vuorela[1], Petri T. Kovanen[2], Ilpo Vattulainen[1,3,4], Marja T. Hyvönen[3,5]

1 Department of Physics, Tampere University of Technology, Tampere, Finland, **2** Wihuri Research Institute, Helsinki, Finland, **3** Department of Applied Physics, Aalto University School of Science and Technology, Espoo, Finland, **4** MEMPHYS – Centre for Biomembrane Physics, University of Southern Denmark, Odense, Denmark, **5** Department of Physics, University of Oulu, Oulu, Finland

Abstract

Cholesteryl ester transfer protein (CETP) transports cholesteryl esters, triglycerides, and phospholipids between different lipoprotein fractions in blood plasma. The inhibition of CETP has been shown to be a sound strategy to prevent and treat the development of coronary heart disease. We employed molecular dynamics simulations to unravel the mechanisms associated with the CETP-mediated lipid exchange. To this end we used both atomistic and coarse-grained models whose results were consistent with each other. We found CETP to bind to the surface of high density lipoprotein (HDL) -like lipid droplets through its charged and tryptophan residues. Upon binding, CETP rapidly (in about 10 ns) induced the formation of a small hydrophobic patch to the phospholipid surface of the droplet, opening a route from the core of the lipid droplet to the binding pocket of CETP. This was followed by a conformational change of helix X of CETP to an open state, in which we found the accessibility of cholesteryl esters to the C-terminal tunnel opening of CETP to increase. Furthermore, in the absence of helix X, cholesteryl esters rapidly diffused into CETP through the C-terminal opening. The results provide compelling evidence that helix X acts as a lid which conducts lipid exchange by alternating the open and closed states. The findings have potential for the design of novel molecular agents to inhibit the activity of CETP.

Citation: Koivuniemi A, Vuorela T, Kovanen PT, Vattulainen I, Hyvönen MT (2012) Lipid Exchange Mechanism of the Cholesteryl Ester Transfer Protein Clarified by Atomistic and Coarse-grained Simulations. PLoS Comput Biol 8(1): e1002299. doi:10.1371/journal.pcbi.1002299

Editor: Roland L. Dunbrack, Fox Chase Cancer Center, United States of America

Received May 2, 2011; **Accepted** October 27, 2011; **Published** January 12, 2012

Funding: Tampere University of Technology paid the salary of Artturi Koivuniemi during this work. The funders had no role in study design, data collection and analysis, decision to publish, or preparation of the manuscript.

Competing Interests: The authors have declared that no competing interests exist.

* E-mail: artturi.koivuniemi@vtt.fi

Introduction

Cholesteryl ester transfer protein (CETP) is a 476-residue-long glycoprotein which promotes the transfer of cholesteryl esters (CEs), triacylglycerols (TGs) and phospholipids (PLs) between the different lipoprotein fractions (high density lipoprotein (HDL), low density lipoprotein (LDL), and very low density lipoprotein (VLDL)) in human blood plasma. CETP is believed to mediate the transfer by a hetero-exchange mechanism in which CEs are carried from HDL to VLDL and LDL particles, and TGs are carried in the opposite direction from VLDL and LDL to HDL particles, resulting in CE depletion and TG enrichment of HDL [1]. Interestingly, CETP is structurally homologous to the phospholipid transfer protein (PLTP), the lipopolysaccharide binding protein (LBP), and the bactericidal/permeability-increasing protein (BPI) [1]. As all these proteins are able to bind phospholipids, similarity in their transportation mechanisms has been suggested. Importantly, however, CETP is the only protein able to transfer neutral lipids (cholesteryl esters and triglycerides) in human plasma [2].

The broad interest to understand CETP and its lipid trafficking properties stems from the fact that it has a potentially protective role in the development of cardiovascular diseases, in particular atherosclerosis, which are currently the main cause of death in Western countries, claiming ~17 million lives a year. The role of CETP in the development of atherosclerosis became evident when it was found that CETP deficiency and the inhibition of CETP lower LDL and increase HDL levels in human plasma [3]. High HDL levels have been clinically found to be inversely correlated with the development of atherosclerosis, since HDL particles are considered crucial components in the transport of cholesterol from atherosclerotic plaques back into the systemic circulation. Unfortunately, the clinical trial with the first oral anti-atherogenic drug candidate with a CETP-inhibitory activity, torcetrapib, was unsuccessful because of its potentially lethal side effects [4]. Treatment with torcetrapib increased blood pressure and circulating aldosterone levels and also altered serum electrolyte levels. However, subsequent studies indicated that these adverse effects of torcetrapib were unrelated to the inhibition of CETP and are not necessarily shared by the other members of the class of CETP inhibitors. Indeed, a recent clinical trial showed that another CETP inhibitor, anacetrapib, effectively raises HDL and has an acceptable side-effect profile in patients with coronary heart disease or risk factors for coronary heart disease [5]. Importantly, a recent meta-analysis of 92 studies involving 113,833 participants concluded that the CETP genotypes that have lower CETP activity are associated with a decreased coronary risk [6].

Considering the central role of CETP in the development of coronary atherosclerosis and its complications, we face an outstanding challenge to better understand the mechanisms

Author Summary

Coronary heart disease is a major cause of death in the Western societies. One of the most promising interventions to prevent and slow down the progress of coronary heart disease is the elevation of high density lipoprotein (HDL) levels in circulation. Animal models together with early clinical studies have shown that the inhibition of cholesteryl ester transfer protein (CETP) is a promising strategy to achieve higher HDL levels. However, drugs with acceptable side-effects for CETP-inhibition do not yet exist, although the next generation CETP inhibitor (anacetrapib) has great potential in this regard. In this study, our objective is to gain more detailed information regarding the interactions of CETP with lipoprotein particles. We show how the CETP-lipoprotein complex is formed and how lipid exchange between CETP and lipoprotein particles takes place. Our findings help to understand in a mechanistic way how CETP-mediated lipid exchange occurs and how it could be exploited in the design of new and more efficient molecular agents against coronary heart disease.

associated with CETP functions. Recently, Qiu et al. resolved the X-ray structure of CETP showing that it carries CE molecules inside a long hydrophobic tunnel, whose ends are plugged by phospholipids (Figure 1) [7]. This kind of hydrophobic tunnel is unique among proteins, and it was speculated that CEs diffuse into and out from the tunnel through the two tunnel openings, which are closed by PLs during the transportation in aqueous surroundings. In addition, based on the X-ray structure it has been speculated that CETP is attached to lipoproteins via its concave surface where also the two hydrophobic tunnel openings reside [7]. Further, it has been proposed that the formation of CETP-lipoprotein complexes is modulated by pH, surface pressure, and the ionic interactions between CETP and phospholipids [8,9]. Fluorescence quenching has been used to demonstrate that the interaction between tryptophan residues of CETP and PLs could be important in the attachment [10]. Regarding the lipid exchange mechanism of CETP, helix X has been suggested to play a role in lipid loading and unloading by acting as a lid at the C-terminal tunnel opening, being in the open state when the exchange of lipids takes place, and in the closed state when CETP detaches from the lipoprotein surface to become surrounded by aqueous medium [5]. Various mutational studies further suggest that helix X is possibly crucial in the transfer of CEs and TGs but not in the transfer of PLs [11,12].

The above findings and suggestions are appealing and insightful, but call for better understanding of the structure-function relationship and of the dynamics that drive CE, TG and PL transfer. In essence, atomic and molecular scale insight into the lipid exchange between CETP and lipoproteins is limited, which largely stems from exceptional difficulties to experimentally probe the related transient processes in the nanometer scale. In the current study, our objective is to complement experiments through atomistic and coarse-grained molecular dynamics simulations to investigate the binding of CETP to a small lipid droplet and a planar lipid trilayer, and to determine the initial stages of the lipid exchange mechanism. By doing so, we can follow the lipid exchange in atomic detail, shed light on its mechanism, consider the effect of lipoprotein curvature, and unravel the dynamics of the related processes. These mechanisms and phenomena are considered over a multitude of time scales by bridging atomistic and coarse-grained simulations, which are shown to provide consistent results. The present study paves the way for future simulations to elucidate interactions of anacetrapib with CETP and CETP-lipoprotein complexes, with an objective to unlock its inhibitory mechanism. Given the significant role of CETP in

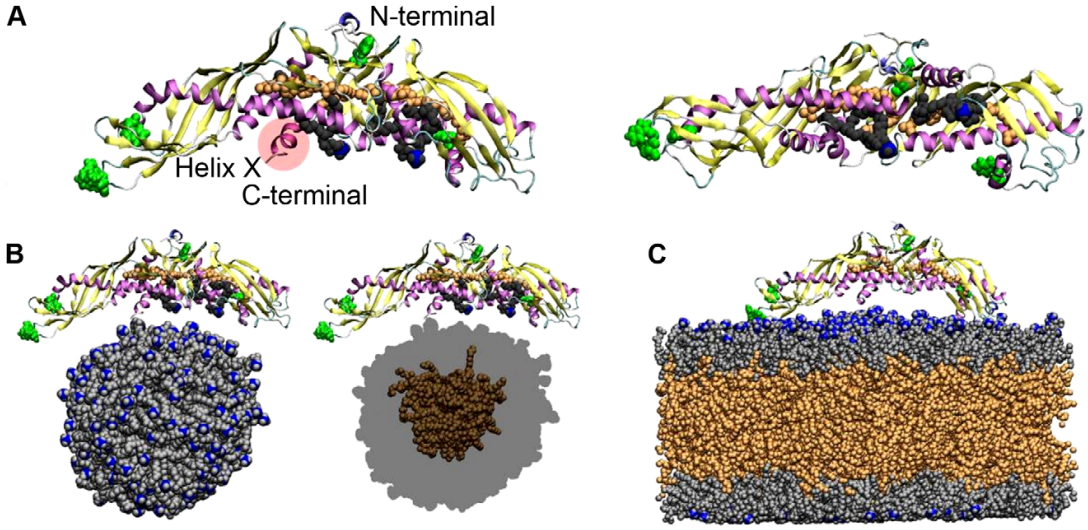

Figure 1. Structure of CETP and starting configurations for simulations. A) X-ray structure of CETP from the side (left) and bottom (right). Two DOPCs (grey and blue spheres) plug the tunnel openings that lead to the hydrophobic tunnel where two CETP-bound CEs (orange spheres) are located. Helix X is labelled and marked with a red sphere. B) The starting configuration for droplet simulations. C) The starting configuration for lipid trilayer simulation. POPCs and DOPCs are coloured as grey, CEs are orange, head group nitrogens are blue, and Trp residues green. Water molecules were removed from the snapshots for clarity.
doi:10.1371/journal.pcbi.1002299.g001

cardiovascular diseases, the broad interest of the topic is hoped to attract substantial interest to extend the present work.

Results

Flexible structure of CETP helps it to bind to curved lipoproteins

We carried out three 100 ns atomistic simulations for fully hydrated systems containing CETP with different interior lipid compositions and a small pre-equilibrated HDL-sized lipid droplet composed of POPCs and CEs (A1, A2, A3; Figure 1; see Materials and Methods). In addition to these spherical droplets, CETP was simulated with a pre-equilibrated planar POPC-CE trilayer system (A4; Figure 1C) to study the effect of less curved lipoprotein particles, like VLDL and LDL, on the conformation of CETP.

Root mean square deviation (RMSD) profiles indicate that the structures do not deviate considerably from the X-ray structure (Figure 2B). The radius of gyration fluctuated between 3.2 and 3.5 nm, and its profiles together with snapshots from simulation trajectories show that the conformation of CETP is able to bend to bind to surfaces with different curvatures (Figure 2A). In the case of spherical A3 the curvature of CETP is clearly higher than in the planar A4 system, and it became apparent that the conformation of CETP is not able to rearrange sufficiently to fully match the planar surface. Nonetheless, our results imply that the structure of CETP is elastic and facilitates the binding of CETP to different lipoprotein surfaces with varying curvatures. Yet, due to its inherent curvature that closely matches the curvature of HDL, CETP prefers to bind to HDL-sized particles compared to larger VLDL-sized particles. Consequently, we propose that the free energy change associated with the binding of CETP to HDL is more favorable compared to the formation of a CETP-VLDL complex.

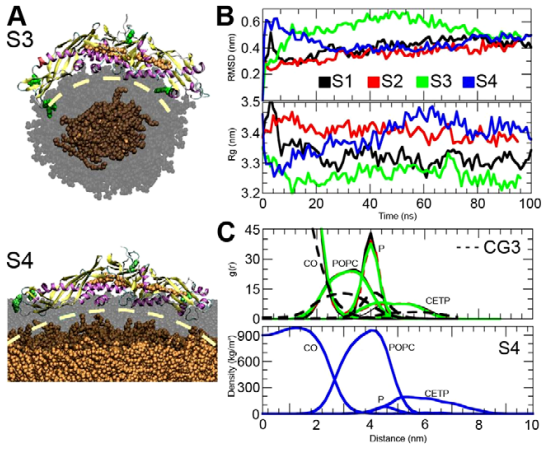

Figure 2. The binding of CETP to lipid surfaces with different curvatures. A) Snapshots from the end of atomistic simulations A3 and A4. POPCs are transparent and grey, and COs are orange. Water molecules were omitted for clarity. CETP is rendered using secondary structures and Trp residues are marked with green color. Dashed and yellow lines present the curvature of CETP. B) RMSD and radii of gyration profiles for CETP in droplet and trilayer simulations. C) Radial distribution functions and density profiles for the droplet and trilayer systems, respectively.
doi:10.1371/journal.pcbi.1002299.g002

Radial distribution functions and density profiles indicate that CETP does not penetrate deeper than to the level of POPC phosphate groups (Figure 2C). Therefore, in all atomistic simulations the core CEs were observed not to interact directly with CETP, as instead they were found to reside only in the core. This suggests that the surface-core lipid ratio is important for the exchange of neutral lipids by CETP.

During the simulation A2, CETP-bound DOPCs did not diffuse into the lipid droplet. However, we found that during the simulation S1 the hydrophobic tunnel of CETP collapsed, which strongly suggests that the structure of CETP is not stable without interior lipids (See Figure S2 and Text S2). This finding is important regarding the lipid exchange process of CETP as it suggests that during the neutral lipid exchange, the hydrophobic cavity is not empty at any point. We return to this matter later.

Salt bridges and tryptophans stabilize CETP-lipoprotein complexes

In atomistic lipid droplet simulations, we calculated the number of salt bridges that formed between CETP and POPCs as a function of time, in order to characterize the key charged residues involved in the attachment of CETP. The number of salt bridges that formed between the positively charged lysine residues of CETP and the negatively charged phosphate (P) groups of POPCs stabilized to a level of 12–20 (Figure 3A). Salt bridging of lysines is much more efficient in A2 and A3 than in A1 (19–20 compared to 12, see Figure 3A). The number of salt-bridges between arginines and P groups was on average two or three. Additionally, we calculated the number of salt bridges formed by the negatively charged Asp and Glu residues and found that Asp residues were able to form 6–8 and Glu residues 2–4 salt bridges with the positively charged choline groups. Amino acids that form most of the salt bridges are shown in Figure 3, revealing that they are mainly located at the edge of the concave surface of CETP.

In the spirit of the earlier Trp quenching study [10], we inspected more carefully the behavior of Trps during binding. In all droplet simulations, Trp299 formed hydrogen bonds with POPCs (Figure 3B). Trp264 stayed buried inside the structure of the protein and Trp162 was able to interact with the water molecules. In A1 and A2, Trp105 and Trp106 were located facing the water phase, while in A3 the flap Ω_5 interacted with POPCs by anchoring Trps 105 and 106 to the carbonyl region of POPC surface, highlighted in Figure 2. In the trilayer simulation only two Trp residues (105 and 299) were able to interact with the POPC surface.

Our results highlight the importance of electrostatic interactions between CETP and phospholipids in the formation of CETP-droplet complexes. The results provide compelling evidence that three Trp residues anchor CETP to lipid droplets, introducing additional stability to CETP-lipoprotein complexes where the curvature of CETP and a lipoprotein matches.

Coarse-grained simulations reveal that the ratio of surface and core lipids in lipid droplets is an important modulator of CETP activity

Interpretation of atomistic simulations requires care due to the limited time and length scales that are feasible through atomistic studies. For example, the diffusion of lipids in HDLs is slow compared to the time scales we have simulated and, thus, claims regarding the principal binding site and penetration depth of CETP must be carefully considered. In order to add liability to our atomistic simulations, we also carried out coarse-grained simulations, covering time scales beyond 2 μs.

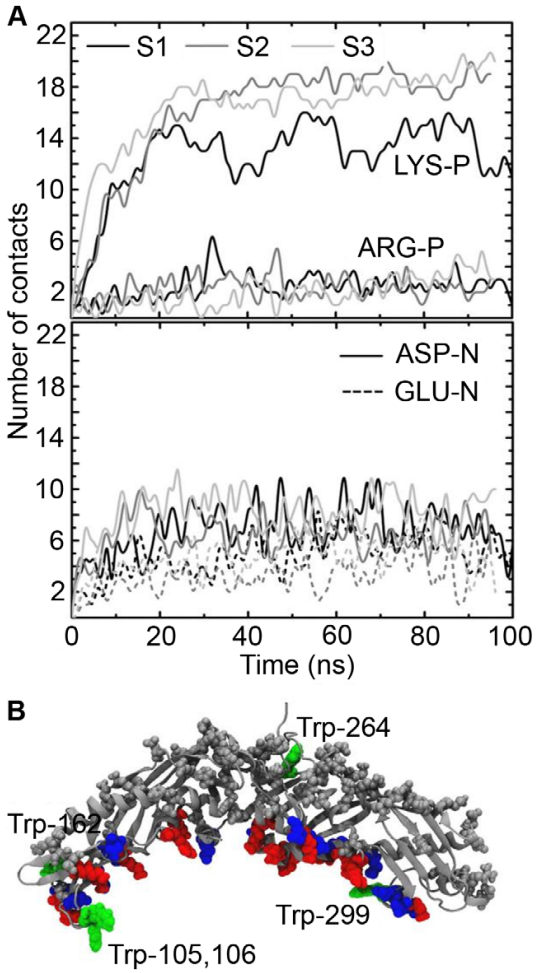

Figure 3. Electrostatic interactions between CETP and lipid droplet. A) Number of salt bridges formed between the charged residues of CETP and the head groups of POPCs as a function of time. The upper profile shows the number of contacts between the positively charged residues and P atoms of POPCs, and the lower profile shows the number of contacts between the negatively charged amino acids and N atoms of POPCs. B) Salt bridge-forming positively (red) and negatively (blue) charged amino acids marked to the structure of CETP. Trp residues are labeled and green.
doi:10.1371/journal.pcbi.1002299.g003

CG simulations support and validate atomistic simulations by showing that the concave surface is the principal lipoprotein binding site of CETP. We did not observe any deviations from this conclusion during the three independent 2-microsecond simulations. Radial distribution functions shown in Figure 2 depict a similar distribution of molecules as in atomistic simulations.

However, intriguingly we found that POPCs which were in contact with the concave surface of CETP migrated away from the tunnel openings, forming a small hydrophobic patch under the concave surface (Figure 4A). In essence, CETP drives phospholipids to diffuse away from the slightly hydrophobic tunnel openings to its edges where most of the salt bridge-forming amino acids reside. We analyzed the spatial densities of the polar beads

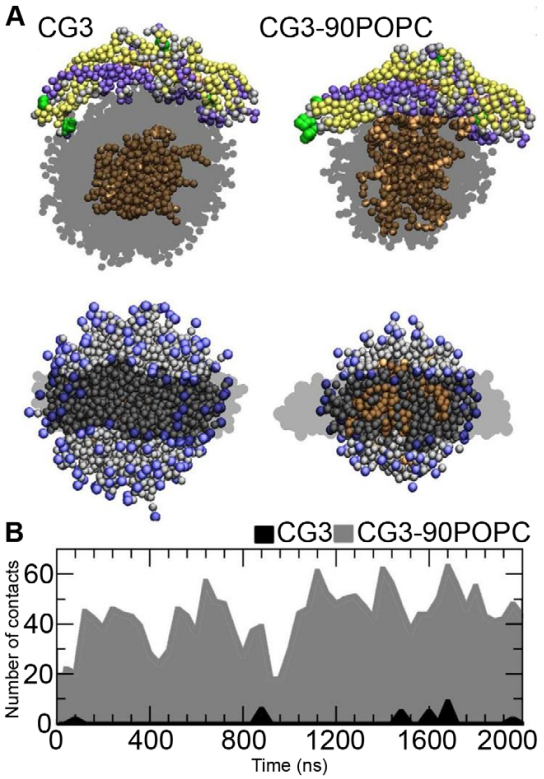

Figure 4. Interaction of CETP with core lipids. A) Snapshots from the coarse-grained simulations CG3 (left) and CG3-90POPC (right). The upper snapshots show side views and the lower ones top views of CETP bound to a lipid droplet. In the latter, the hydrophobic patch under CETP is clearly visible. The structure of CETP has been rendered using secondary structure information in upper snapshots (β-sheets are yellow, α-helixes violet and random coils gray) or as dark transparent phantom in lower snapshots. The green spheres are Trp residues. POPCs are transparent in the upper snapshots, while those in the bottom snapshots are visible as grey (the choline head groups are visible as blue). CEs are rendered with orange spheres. Water molecules were omitted for clarity. B) Number of contacts between core CEs and CETP with different surface-core lipid ratios as a function of time.
doi:10.1371/journal.pcbi.1002299.g004

(GL1, GL2, and NC3, PO4, using the descriptions of the Martini model) of POPCs to clarify the patch formation more clearly. The spatial density map revealed the formation of a hydrophobic patch under the concave surface, and specifically in the region where the N- and C-terminal tunnel openings reside (see Figure S1 and Text S1 in Supporting Information (SI)).

The time associated with the formation of the hydrophobic patch is difficult to estimate accurately, since the process fluctuates depending on the dynamics of the CETP-droplet complex. In practice we found the patch to emerge in roughly 10–40 ns, and it increased to a size of about 1 nm×3 nm in 100–500 nanoseconds, depending on the system studied (see Figure S1). At longer times the patch fluctuated quite a lot but there was a trend showing a slow increase in size, suggesting that the total formation time may be of the order of microseconds.

To gain further support for patch formation, as predicted by CG simulations, we repeated the analysis with two additional CG

simulations where we used PME for electrostatics with the non-polarizable Martini water model, and PME with the polarizable Martini water model [13]. With the polarizable water model the solubility of charged species to apolar media should be better described compared to the standard Martini model. In both additional CG simulations, hydrophobic patch formation was observed too (Figure S1).

Given that the patch emerged in CG simulations in tens of nanoseconds, and the atomistic simulations lasted for 100 ns, we returned to our atomistic simulation data to consider this aspect in atomic detail. We analyzed the spatial density profile of POPC head groups and observed similar hydrophobic patch formation. For example, in A3 we noticed that a small hydrophobic patch was formed under CETP already in ~20 ns, and the patch slowly grew in size and number as in ~80–100 ns there were two patches close to one another (data not shown). The fact that also 100 ns atomistic simulations show the hydrophobic patch formation confirms that the CETP-lipoprotein interaction is strong specifically under the concave surface and promotes the formation of a path between the droplet core and CETP.

The hydrophobic patch formation exposes the hydrophobic parts of the lipids to the concave surface where the hydrophobic tunnel openings are located. However, hardly any of the CEs were in contact with CETP, as can be seen from Figure 4. Thus, we reduced the number of POPCs from 180 to 90 (CG3-90POPC) and simulated the system again for 2 μs in order to see if the lower surface pressure of a lipid droplet would promote the solubility of CEs to the surface lipid monolayer and the interaction between CETP and CEs. Indeed, the contacts between core CEs and CETP increased. Clearly, the concave surface of CETP has some affinity for CEs, over random thermal fluctuations, as the hydrophobic patch under CETP guides core CEs to the concave surface. However, the surface pressure must be low enough for CEs to localize to the surface monolayer and CETP to bind to the surface. This implies that the ratio of surface and core lipids (surface pressure) and the formation of the small hydrophobic patch under CETP are important factors modulating the core lipid transfer activity of CETP.

Structure fluctuations show that the hinge region of helix X is highly mobile

Root mean square fluctuations (RMSFs) of the protein backbone were analyzed after 40 ns of atomistic lipid droplet simulations to find the regions, which wobble the most after CETP attached to the surface of the lipid droplet (Figure 5). This was done as follows. First, the RMSF of backbone atoms was computed by fitting the atomic positions to the reference structure (average structure of CETP after its binding to the lipid droplet surface) and then calculating the average distance deviation from the reference structure. The RMSFs of individual backbone atoms were then averaged per residue to determine the residual RMSF profile. Similar results were observed in all droplet simulations. The N- and C-terminal ends and loop regions (marked by omegas) of CETP showed high fluctuations, as expected. We also found that in the helix X region (residues 460–476) the conformational fluctuations peaked near the residue 462. This region has previously been proposed to be a potential hinge region of helix X with elevated B-factors [7]. In addition, it was found that the flaps Ω_1 and Ω_2 resulted in high fluctuations to the RMSF profile as was also proposed based on the B-factors of the X-ray structure of CETP [7]. In addition to the suggested high fluctuations, we found that another five regions of CETP were also highly fluctuating in each simulation. These regions were Ω_3 (residues 380–400), Ω_4 (residues 40–50), Ω_5 (residues 90–110), Ω_6 (residues 150–170), and Ω_7 (residues 230–260). All regions are found in the loops, and hence high fluctuations can be expected. Previously it has been speculated that the hinge region could promote the needed flexibility to helix X that is important in the lipid exchange process [5]. To study further the role of helix X in lipid exchange, we did two additional atomistic simulations to probe its role in the lipid exchange process, see below.

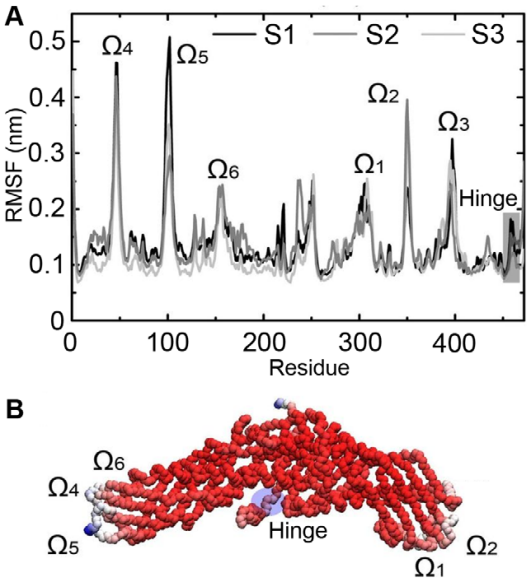

Figure 5. Dynamical properties of CETP. A) Root mean square fluctuations for atomistic droplet simulations. Loop regions are marked with omegas and the hinge region of helix X has been slightly darkened. B) Residual B-factors mapped to the backbone structure of CETP. Red color indicates the most rigid structures, whereas white and blue indicate the most flexible structural regions. The hinge region of helix X is marked with a transparent blue sphere.
doi:10.1371/journal.pcbi.1002299.g005

Helix X regulates the accessibility of cholesteryl esters inside CETP

Earlier point and deletion mutations suggest that helix X is important in the transfer of core lipids, while it is not needed in phospholipid transfer [12]. Since we found that the hydrophobic patch was formed under the concave surface of CETP in both CG and atomistic simulations, we asked if the fully formed hydrophobic patch could induce changes to the conformation of helix X. To test this hypothesis, we did one additional atomistic simulation with 90 POPCs (that is, starting from the system A3-90POPC) where we expanded the hydrophobic patch under the concave structure by removing POPCs near the two tunnel openings of CETP, so that helix X was only able to interact with the hydrophobic parts of POPCs and CEs. Here, it is worth to mention that atomistic simulations are the only method of choice for this purpose, since this kind of conformational change can not take place in our CG simulations, where we used the elastic network model to keep the secondary structure of CETP stable [14]. We found that the conformation of helix X rearranged and became buried inside the hydrophobic cavity of CETP, where it interacted with CETP-bound CE (Figure 6). This conformational change generated a hydrophobic pathway from the droplet surface

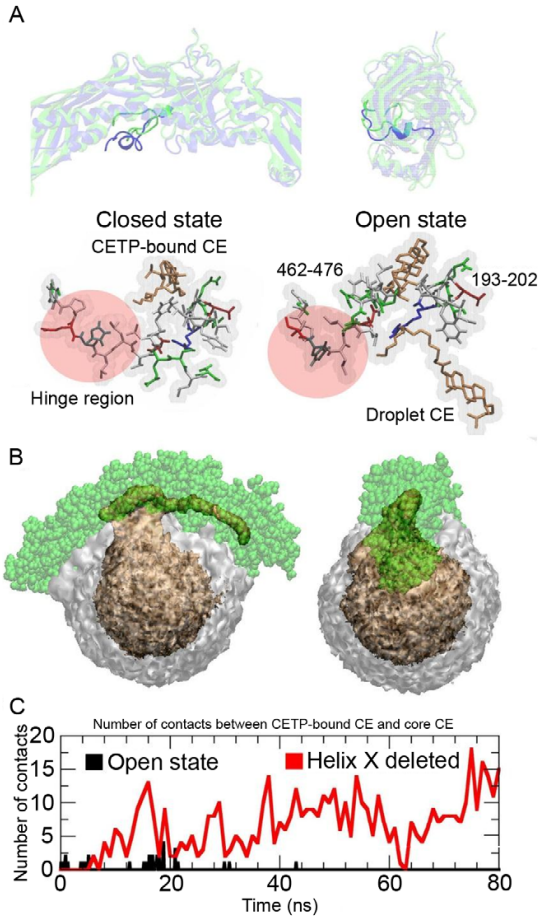

Figure 6. Hypothesis for the initial event of helix X assisted core lipid exchange. A) Two RMSD-fitted snapshots from the simulation A3-90POPC showing the rearrangement of helix X (darkened colour). The green conformation is for the open state and the blue one for the closed state. A more detailed structure of helix X and the role of the hinge region during the conformational change (red and transparent region) are shown in the lower snapshots. CEs are shown as orange sticks. The residues 462–476 and 193–202 of CETP have been rendered using sticks, and coloring is based on the polarity of residues. B) Spatial number density of POPCs (grey and transparent) and CEs (orange) during the simulation A3-90POPC. Core CEs diffuse into the hydrophobic tunnel of CETP (green spheres) without helix X. C) Number of contacts between core CEs and interior CE-473 when helix X is in the open state (black) or completely removed (red).
doi:10.1371/journal.pcbi.1002299.g006

to the tunnel, increasing the accessibility of core CEs to the hydrophobic tunnel of CETP.

To further assess the regulatory role of helix X, we created a deletion mutant of CETP, in which the residues 462–476 (helix X) were removed from the structure, and we simulated this structure for 80 ns. Deletion mutation simulation revealed that three CEs readily diffused into CETP when helix X was completely removed from the structure (see the spatial density maps and the number of contacts plot in Figures 6B and 6C). This provides further support for the view that helix X acts as a lid at the C-terminal tunnel opening, and that its conformation regulates the accessibility of CEs to the hydrophobic tunnel.

Discussion

Previously, the role of electrostatic interactions in the formation of isolable CETP-lipoprotein complexes was demonstrated by Pattnaik et al., who showed that (in addition to CETP-HDL complexes) CETP was able to form isolable complexes with LDL and VLDL particles when negative surface charge was increased by phospholipase A_2 digestion or by acylation of phospholipid amino groups. They reached the conclusion that the phospholipid phosphate groups are the primary sites for the interaction of lipoproteins with CETP [8]. They also found that the formation of isolated CETP-HDL complexes was hindered by decreasing the pH, introducing positive divalent ions into the solution, or by digesting lipoproteins by phospholipase C. Moreover, Nishida et al. reported that the affinity of CETP for various lipoproteins is governed by a delicate balance of electrostatics and hydrophobic interactions [15]. The importance of electrostatic interaction in CETP binding has been shown also by several point mutation studies applied to the positively charged lysine residues of CETP [16]. Our results are in agreement with experiments, as in the present simulations most of the salt-bridges with the negatively charged phosphate groups of POPCs were formed by the Lys residues at the concave surface, when CETP fastened to the lipid surface. However, also Glu and Asp residues formed salt-bridges with the positively charged choline groups of POPCs, although the ratio of salt-bridges formed by the positively and negatively charged amino acids is approximately 1.8, indicating that mostly the positively charged amino acids contribute to the formation of CETP-lipoprotein complexes. Another important factor playing a role in the binding of CETP is Trp residues located in the flaps Ω_5 and Ω_1 that were found to become buried into the lipid matrix. Most likely Trp residues add more stability to the CETP-lipoprotein complexes by anchoring CETP to a lipoprotein surface. Interestingly, Desmuraux et al. made mutations to the structurally similar flap Ω_5 region (Trp-91, Phe-92 and Phe-93) of PLTP and showed that the phospholipid transfer activity of PLTP from liposomes to HDL particles decreased up to 60% [17]. This finding together with our results suggests that the flexible flap Ω_5 region of CETP and Trp residues therein are crucial in the binding of CETP to HDL particles, playing an important role in the CETP-mediated lipid transfer.

Penetration depth of CETP is an important factor in CETP-mediated lipid exchange, as it determines how efficiently the neutral core lipids are able to interact with CETP. Previous studies have shown that the exclusion pressure of CETP is lower than the exclusion pressure of other apolipoproteins, like apoA-I [9,10]. Moreover, it has been argued that the weaker penetration of CETP to the emulsion particles compared to apoA-I makes the activation energy of the attachment and detachment of CETP lower, rendering the transportation process more efficient [9,10]. Our atomistic and CG simulation results showed that CETP is not able to bury its amino acid residues deeper than to the level of the phosphate groups of POPCs. The above findings therefore imply that core lipids have to diffuse to or reside at the surface to enter CETP. Therefore, the amount of core lipids at the lipoprotein surface is an important factor modulating the activity of CETP, as has been suggested previously based on liposome studies [18], and it can be promoted by defects as is outlined below. The number of surface-located neutral lipids can be regulated by the lipid and apolipoprotein composition of lipoprotein particles.

Interestingly, we found that when CETP attaches to the surface by the aid of electrostatic interactions, the head groups of POPCs moved aside, providing access to the hydrophobic lipid region. In this manner, the two tunnel openings of the concave surface are exposed to the hydrophobic lipid matrix of the lipoprotein. The hydrophobic patch formation facilitates, by generating a defect to the surface monolayer, the diffusion of core lipids to the surface monolayer region located under CETP (Figure 6B). Thus, the localization of neutral lipids at the surface monolayer itself is not crucial to allow CETP to exchange neutral lipids between lipoproteins but the neutral lipids can enter CETP through the formation of the hydrophobic patch. Consequently, we envision that the activity of CETP could be inhibited by nonpolar drugs that are transferred into the hydrophobic tunnel of CETP through the hydrophobic core of lipoproteins. Further, we observed that the concave surface interacted directly with CEs that diffused more readily to the hydrophobic tunnel openings when the surface-core lipid ratio was decreased.

Finally, we found CEs to diffuse into the hydrophobic tunnel of CETP and interact with CETP-bound CE when the conformation of helix X was in the open state or completely removed. A previous mutational study argued that CETP is not able to transfer neutral lipids when helix X is removed from the structure [11,12]. However, CETP is able to transfer phospholipids without helix X. Our results showed that the conformation of helix X rearranges, and helix X moves inside the hydrophobic tunnel of CETP where it can interact with CETP-bound CE. Given this, we suggest that there are two important functional properties of helix X that make the neutral lipid exchange possible. First, helix X is able to facilitate the neutral lipid exchange by opening the hydrophobic pathway from a lipoprotein surface to the hydrophobic tunnel of CETP. Second, helix X promotes the diffusion of neutral lipids from the hydrophobic tunnel to lipoproteins by filling the volume of CETP-bound neutral lipid when it diffuses out from CETP. Afterwards, another neutral lipid from the lipoprotein core or inside CETP could take the place of helix X after which the C-terminal tunnel opening closes again. We propose that helix X is needed to prevent the structure of CETP from collapsing as was registered in the simulation A1 without the CETP-bound lipids. The above reasons would explain why helix X is important in the neutral lipid exchange, but not in the exchange of phospholipids.

It is tempting to contemplate the possible roles of helix X in the inhibition of CETP. It has been reported that dalcetrapib, a novel CETP inhibitor, binds covalently to CETP by forming a disulphide bond with Cys-13, which is located inside the hydrophobic tunnel of CETP [19]. In addition, it has been suggested that the disulphide bond formation is a necessary requirement for the dalcetrapib-mediated CETP inhibition. However, that is not the case with torcetrapib or anacetrapib (another novel CETP inhibitors), both of which bind reversibly to CETP [19]. Yet, all inhibitors stabilize HDL-CETP complexes, which has been found to be the second major inhibitory mechanism of the neutral lipid transfer exerted by the synthetic CETP inhibitors [19]. Based on our simulations, we can hypothesize that helix X is locked to the open state when inhibitors are bound to CETP. The driving force for this could be the small size of an inhibitor that enforces helix X to be located inside the hydrophobic tunnel and, thus, prevents collapse of the lipid pocket. Another reason could be the more favorable interaction between helix X and the inhibitor inside the tunnel, which could conceivably force the conformation of helix X to the open state, or change the conformation distribution to favor the open state. Consequently, the detachment of CETP from the surface of HDL would be hindered since the helix X is not able to shield the hydrophobic tunnel opening of the lipid pocket when CETP is completely in the aqueous phase. In addition, the open state could prevent the binding of phospholipids to the C-terminal tunnel opening, which, based on the X-ray structure of CETP, is known to be occupied by phospholipids when CETP is not attached to a lipoprotein surface. A reduced ability of CETP to bind and transport phospholipids could further stabilize the HDL-CETP complex.

In summary, we have provided a detailed atomistic picture regarding the initial steps in the lipid exchange mechanism of CETP and, furthermore, we have offered a plausible mechanism for the exchange of neutral lipids mediated by CETP. Overall, our work paves the way for additional future studies to elucidate interactions of the available promising CETP inhibiting drugs, such as anacetrapib and dalcetrapib, with CETP and CETP-lipoprotein complexes. Our findings for the factors that affect the lipid exchange process can also be exploited in the design of novel molecular agents capable of inhibiting the activity of CETP, one possible strategy being the design of nonpolar drugs which can be transferred into the hydrophobic tunnel of CETP. Together with recent simulation models for both HDL and LDL [20], these ideas are a reasonable goal already at present.

Materials and Methods

System setup

The coordinate file of CETP in the PDB format with an accession code 2OBD was acquired from the RCSB Protein Data Bank. In addition to the protein, the structure provides information of the lipids carried by CETP: there are two CEs located inside the long hydrophobic tunnel of CETP, and two dioleoylphosphatidylcholine (DOPC) lipids that cover the two endings of the hydrophobic tunnel. The charge state of CETP was chosen to represent the physiological pH that is 7.4. A detailed explanation of the protein structure is given elsewhere [7].

For atomic-scale simulations, three different setups were constructed by combining pre-equilibrated lipid droplets consisting of 180 palmitoyloleoyl-PC (POPC) and 35 CE molecules [21]. In each system, CETP was placed approximately at a distance of 1 nm from the surface of the lipid droplet (Figure 2). In the first simulated system (A1), the two DOPCs and CEs were removed from CETP. In the second simulation (A2), both DOPCs and CEs were included, while in the third simulation (A3) only CEs were kept inside CETP. We also simulated CETP with a planar trilayer system composed of 512 POPCs and 796 CEs (A4). The droplet systems were solvated with ~180,000 water molecules at a salt concentration of 0.2 M including counter ions, while the trilayer system included ~50,000 water molecules. Altogether, the systems included ~500,000 atoms. Finally, three additional atomistic systems were constructed to characterize the role of helix X in lipid exchange in more detail (see text). First, we studied the effect of the hydrophobic patch on the structure of helix X by removing half of the POPCs from A3 at 100 ns (A3-90POPC). Second, we also considered CETP through its helix X deletion mutant to probe the regulatory role of the helix. Third, we used A3-90POPC as a basis and removed some of the surface lipids to model the complete formation of a hydrophobic patch under the concave surface of CETP. The context of these simulations to the studied processes will become clear in the discussion below.

In addition to atomistic simulations, we carried out four coarse-grained (CG) simulations. First, the system A3 was directly coarse grained (in the text, we refer to this simulation as CG3) by using a script that is available at the homepage of the Martini force field. Second, 90 POPCs were removed from CG3, ending up in the

system denoted as CG3-90POPC. The systems CG3 and CG3-90POPC were simulated under standard Martini model (see below) conditions with regard to electrostatics (using truncation of electrostatic interactions) and the water model that is non-polarizable. To clarify the influence of long-range interactions and the water model, we simulated two additional systems. That is, in the third case we focused on the system CG3 which was simulated with full electrostatics using the particle mesh Ewald (PME) method [22]. Finally, in the fourth coarse-grained model, we simulated the system CG3 using both PME and the polarizable Martini water model [13].

Simulation parameters and force field

The GROMACS simulation package with version 4.0 was used in the simulations [23]. In atomistic studies, we used the Nose-Hoover thermostat [24,25] with a coupling constant of 1.0 ps to set the temperature to 330 K in which the particle core is certainly in liquid state. The pressure was set to 1 bar using the Parrinello-Rahman barostat [26] with isotropic pressure coupling and a coupling constant of 0.1 ps. The van der Waals interactions were chosen to have a cutoff at 1.0 nm. Electrostatic interactions were evaluated by the particle mesh Ewald technique with a real space cut-off of 1.0 nm [22]. Water molecules were described using the SPC water model. All non-water bonds were constrained using the LINCS algorithm [27] and the SETTLE algorithm [28] was used to constrain water molecules, allowing the use of a time step of 2 fs in the integration of equations of motion. Berger parameters [29] were used for lipids, while the GROMOS53A6 force-field [30] was employed for the protein. Combination rules were introduced for the interactions between lipids and the protein. The four leading atomistic systems (A1–A4) were simulated for 100 ns, and the last two ones that focused on helix X for 80 ns. The total simulation time of atomistic simulations was 0.56 μs.

CG simulations were also carried out with GROMACS, using the Martini force field with an extension to proteins [31,32]. The ElNeDyn elastic network model was used to keep the structure of CETP stable [14]. The Berendsen thermostat and barostat were used with time constants of 1.0 ps. Temperature was set to 320 K and isotropic pressure coupling was used with pressure set to 1 bar. Cut-off distance for electrostatic interactions was set to 1.2 nm. For Lennard-Jones interactions we used a cut-off of 1.2 nm, and Lennard-Jones interactions were shifted to zero from 0.9 nm. Time step was 25 fs. The simulation time of each CG system was beyond 2 μs, and the times reported here are given in units of the effective Martini time. All rendered figures were done by VMD [33].

Supporting Information

Figure S1 Spatial density maps for one of the atomistic systems and for two additional coarse-grained models.
(TIF)

Figure S2 Number of intrinsic contacts of CETP as a function of time.
(TIF)

Text S1 Description of additional data for Figure S1.
(PDF)

Text S2 Description of additional data for Figure S2.
(PDF)

Acknowledgments

We would like to thank CSC – The IT Center for Science for providing supercomputer facilities.

Author Contributions

Conceived and designed the experiments: AK TV PK IV MH. Performed the experiments: AK TV. Analyzed the data: AK. Contributed reagents/materials/analysis tools: AK TV. Wrote the paper: AK TV PK IV MH.

References

1. Tall AR (1993) Plasma cholesteryl ester transfer protein. J Lipid Res 34: 1255–1274.
2. Hesler CB, Tall AR, Swenson TL, Weech PK, Marcel YL, et al. (1988) Monoclonal antibodies to the M_r 74,000 cholesteryl ester transfer protein neutralize all of the cholesteryl ester and triglyceride transfer activities in human plasma. J Biol Chem 263: 5020–5023.
3. Polk D, Shah PK (2008) Cholesterol ester transfer protein (CETP) and atherosclerosis. Drug Discov Today Ther Strateg 4: 137–145.
4. Tall AR, Yvan-Charvet L, Wang N (2007) The failure of torcetratib: Was it the molecule or the mechanism. Arterioscler Thromb Vasc Biol 27: 257–260.
5. Cannon CP, Shah S, Dansky HM, Davidson M, Brinton EA, et al. (2010) Safety of anacetrapib in patients with or at high risk for coronary heart disease. N Engl J Med 363: 2406–2415.
6. Vasan RS, Pencina MJ, Robins SJ, Zachariah JP, Kaur G, et al. (2009) Association of circulating cholesteryl ester transfer protein activity with incidence of cardiovascular disease in the community. Circulation 120: 2414–2420.
7. Qiu X, Mistry A, Ammirati MJ, Chrunyk BA, Clark RW, et al. (2007) Crystal structure of cholesteryl ester transfer protein reveals a long tunnel and four bound lipid molecules. Nat Struct Mol Biol 14: 106–113.
8. Pattnaik NM, Zilversmit DB (1979) Interaction of cholesteryl ester exhange protein with human plasma lipoproteins and phoshpholipid vesicles. J Biol Chem 254: 2782–2786.
9. Weinberg RB, Cook VR, Jones JB, Kussie P, Tall AR (1994) Interfacial properties of recombinant human cholesterol ester transfer protein. J Biol Chem 269: 29588–29591.
10. Rajaram OV, Sawyer WH (1996) Penetration of an emulsion surface by cholesteryl ester transfer protein. Eur Biophys J 25: 31–36.
11. Wang S, Wang X, Deng L, Rassart E, Milne RW, et al. (1993) Point mutagenesis of carboxyl-terminal amino acids of cholesteryl ester transfer protein. J Biol Chem 268: 1955–1959.
12. Wang S, Deng L, Milne RW, Tall AR (1992) Identification of a sequence within the C-terminal 26 amino acids of cholesteryl ester transfer protein responsible for binding a neutralizing monoclonal antibody and necessary for neutral lipid transfer activity. J Biol Chem 267: 17487–17490.
13. Yesylevskyy SO, Schafer LV, Sengupta D, Marrink SJ (2010) Polarizable water model for the coarse-grained MARTINI force field. PLoS Comput Biol 6: e1000810. 10.1371/journal.pcbi.1000810.
14. Periole X, Cavalli M, Marrink S, Ceruso MA (2009) Combining an elastic network with a coarse-grained molecular force field: Structure, dynamics, and intermolecular recognition. J Chem Theory Comput 5: 2531–2543.
15. Nishida HI, Arai H, Nishida T (1993) Cholesterol ester transfer mediated by lipid transfer protein as influenced by changes in the charge characteristics of plasma lipoproteins. J Biol Chem 268: 16352–16360.
16. Jiang X, Bruce C, Cocke T, Wang S, Boguski M, et al. (1995) Point mutagenesis of positively charged amino acids of cholesteryl ester transfer protein: Conserved residues within the lipid transfer/lipopolysaccharide binding protein gene family essential for function. Biochemistry. pp 7258–7263.
17. Desrumaux C, Labeur c, Verhee A, Tavernier J, Vandekerckhove J, et al. (2001) A hydrophobic cluster at the surface of the human plasma phospholipid transfer protein is critical for activity on high density lipoproteins. J Biol Chem 276: 5908–5915.
18. Morton RE, Greene DJ (2003) The surface cholesteryl ester content of donor and acceptor particles regulates CETP: A liposome-based approach to assess the substrate properties of lipoproteins. J Lipid Res 44: 1364–1372.
19. Ranalletta M, Bierilo KK, Chen Y, Milot D, Chen Q, et al. (2010) Biochemical characterization of cholesteryl ester transfer protein inhibitors. J Lipid Res 51: 2739–2752.
20. Vuorela T, Catte A, Niemela PS, Hall A, Hyvonen MT, et al. (2010) Role of lipids in spheroidal high density lipoproteins. PLoS Comput Biol 6: e1000964.
21. Koivuniemi A, Heikelä M, Kovanen PT, Vattulainen I, Hyvönen MT (2009) Atomistic simulations of phosphatidylcholines and cholesteryl esters in high-density lipoprotein-sized lipid droplet and trilayer: Clues to cholesteryl ester transport and storage. Biophys J 96: 4099–4108.
22. Essmann U, Perera L, Berkowitz ML, Darden T, Lee H, et al. (1995) A smooth particle mesh ewald method. J Chem Phys 103: 8577–8593.
23. Hess B, Kutzner C, van der Spoel D, Lindahl E (2008) GROMACS 4: Algorithms for highly efficient, load-balanced, and scalable molecular simulation. J Chem Theory Comput 4: 435–447.

24. Nose S, Klein ML (1983) Constant pressure dynamics for molecular systems. Mol Phys 52: 1055–1076.
25. Hoover WG (1985) Canonical dynamics: Equilibrium phase-space distributions. Phys Rev A 31: 1695–1697.
26. Shinoda W, Fukada T, Okazaki S, Okada I (1995) Molecular dynamics simulation of the dipalmitoylphosphatidylcholine (DPPC) lipid bilayer in the fluid phase using the nosé-parrinello-rahman NPT ensemble. Chem Phys Lett 232: 308–322.
27. Hess B, Bekker H, Berendsen HJC, Fraaije JGEM (1997) LINCS: A linear constraint solver for molecular simulations. J Comp Chem 18: 1463–1472.
28. Miyamoto S, Kollman PA (1992) Settle: An analytical version of the SHAKE and RATTLE algorithm for rigid water models. J Comp Chem 13: 952–962.
29. Berger O, Edholm O, Jähnig F (1997) Molecular dynamics simulations of a fluid bilayer of dipalmitoylphosphatidylcholine at full hydration, constant pressure, and constant temperature. Biophys J 72: 2002–2013.
30. Schuler LD, Daura X, van Gunsteren W (2001) An improved GROMOS96 force field for aliphatic hydrocarbons in the condensed phase. J Comp Chem 22: 1205–1218.
31. Marrink SJ, de Vries AH, Mark AE (2004) Coarse grained model for semi-quantitative lipid simulations. J Phys Chem B 108: 750–760.
32. Monticelli L, Kandasamy SK, Periole X, Larson RG, Tieleman DP, et al. (2008) The MARTINI coarse grained forcefield:Extension to proteins. J Chem Theory Comput 4: 819–834.
33. Humprey W, Dalke A, Schulten K (1996) VMD - visual molecular dynamics. J Molec Graphics 14: 33–38.

IV

How Well Does BODIPY-Cholesteryl Ester Mimic Unlabeled Cholesteryl Esters in High Density Lipoprotein Particles?

by

Topi Karilainen, Timo Vuorela & Ilpo Vattulainen.

Journal of Physical Chemistry B **119**, 15848-15856 (2015).

THE JOURNAL OF PHYSICAL CHEMISTRY B
Article
pubs.acs.org/JPCB

How Well Does BODIPY-Cholesteryl Ester Mimic Unlabeled Cholesteryl Esters in High Density Lipoprotein Particles?

Topi Karilainen,[†] Timo Vuorela,[†] and Ilpo Vattulainen*[,†,‡,§]

[†]Department of Physics, Tampere University of Technology, P.O. Box 692, FI-33101 Tampere, Finland
[‡]MEMPHYS-Center for Biomembrane Physics, University of Southern Denmark, Odense, Denmark
[§]Department of Physics, University of Helsinki, P.O. Box 43, FI-00014 Helsinki, Finland

Supporting Information

ABSTRACT: We compare the behavior of unlabeled and BODIPY-labeled cholesteryl ester (CE) in high density lipoprotein by atomistic molecular dynamics simulations. We find through replica exchange umbrella sampling and unbiased molecular dynamics simulations that BODIPY labeling has no significant effect on the partitioning of CE between HDL and the water phase. However, BODIPY-CE was observed to diffuse more slowly and locate itself closer to the HDL-water interface than CE due to the BODIPY probe that is constrained to the surface region, and because the CE body in BODIPY-CE prefers to align itself away from the HDL surface. The implications as to the suitability of BODIPY to explore lipoprotein properties are discussed.

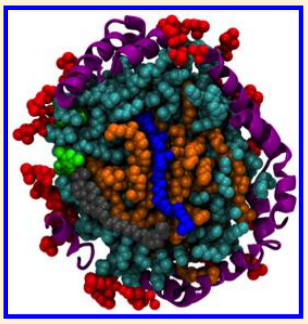

1. INTRODUCTION

Bioimaging has become one of the versatile techniques in considerations of cellular systems.[1−3] "Seeing is believing", as many say; thus, there is considerable interest to develop and use techniques that render visualization of the various transport processes in cells possible, thereby also helping in the clarification of physiological and pathophysiological changes in the body.

Fluorescent probes are one of the means used for this purpose.[4−6] When bound to their host molecules such as lipids or proteins, they allow one to follow the motion of the host molecule in question, which in turn can reveal a wealth of information on cellular processes. The probes have a number of advantages as they enable highly sensitive studies of local and time-dependent phenomena with limited invasion, and the fluorescence signal of the probe can be modulated to yield information on phenomena based on activation, too. Especially the emergence and establishment of super-resolution microscopy have generated a lot of momentum for the development and use of novel fluorescent probes that have consequently become indispensable tools in modern cell biology to investigate nanoscale dynamical processes.

Unfortunately, the advantages of fluorescent probes also have a price. Perhaps the greatest concern is the inevitable fact that labeling changes the nature of the host molecules attached to probes. Therefore, the labeled molecule may not interact with its surroundings in a similar manner as the unlabeled (pristine) counterpart, and the information given by the probe may not reflect the environment that it is designed to gauge. Obviously, the probe would be the better the less it perturbs the host molecule and its vicinity.

Given that the size of fluorescent probes is typically of the order of nanometers, the atomistic molecular dynamics (MD) simulation[7,8] is definitely the method of choice to investigate how significantly probes alter the properties of the system they gauge. Until now this approach has been used mainly in the context of lipids, where previous studies have largely focused on probes embedded in lipid membranes. Studies of, e.g., pyrene, diphenylhexatriene, BODIPY, and Texas Red, have shown[9−14] that probe-induced perturbations are local and extend typically only a few nanometers away from the probe. Yet, as the perturbations can be locally significant, the data measured based on probes has to be interpreted with great care.[15]

Here we consider this issue in the context of the high density lipoprotein (HDL). The role of HDL is important in preventing cardiovascular disease, since it carries cholesterol and cholesteryl esters (CEs) from cells to the liver in circulation,[16] and by doing so it also works against the formation of atherosclerotic plaques by removing excess cholesterol and its esters.[17] Meanwhile, low density lipoprotein (LDL) acts as the reverse of HDL, carrying cholesterol and CE molecules in the blood to be taken up by cells. Cholesteryl ester is transferred between HDL and LDL in a process mediated by the cholesteryl ester transfer protein. Besides being a key

Received: October 18, 2015
Revised: December 2, 2015
Published: December 4, 2015

DOI: 10.1021/acs.jpcb.5b10188
J. Phys. Chem. B 2015, 119, 15848−15856

molecule in cholesterol transport, CE is a major component of atherosclerotic plaques.[18,19]

Mature HDL particles that transport cholesteryl ester are spherical and have a size range from 7.5 to 11 nm in diameter.[20,21] The amphipathic surface of a HDL particle consists of apolipoprotein molecules and a monolayer of phospholipids and cholesterol. Under its surface, there is a hydrophobic core of cholesteryl esters and triglycerides as a disordered melt. The numbers of apolipoprotein molecules and lipids vary with the size of the HDL particle.[21−23] Although it is difficult to directly study HDL due to its small size and heterogeneity, recent experimental and computational studies have provided insight into its structure and dynamics.[24−29]

The molecular-level understanding of the mechanisms related to HDL and cholesterol transport is essential for designing effective treatments for diseases caused by high levels of cholesterol. As discussed above, fluorescent probes are a very useful tool for revealing these mechanisms. During the past decade, dipyrromethene difluoride (BODIPY) probes have been found to be useful in the study of cholesterol-related systems.[4,30] Specifically, a compound where the BODIPY moiety is linked to the carbon-24 in cholesterol has been shown to reproduce some key features of cholesterol including membrane partitioning and trafficking.[4,31−34]

In order to study cholesterol transport in a lipoprotein environment, it is important to label also the esterified form of cholesterol. Recently, this has been done with a cholesteryl 1-pyrenedecanoate probe in reconstituted discoidal HDL particles.[35] To our knowledge, the behavior of esterified BOPIPY-labeled cholesterol in lipoproteins has not yet been characterized. However, access to an effective and well-characterized fluorescent CE analogue would be paramount for efforts to study cholesterol transport.

In this study, we unravel how the structural and dynamical properties of BODIPY-labeled CE differentiate from those of unlabeled CE inside spherical HDL particles. To this end, we consider atomistic simulation models studied through the replica exchange umbrella sampling (REUS) technique as well as conventional (unbiased) molecular dynamics simulations. REUS calculations have been shown to increase the accuracy of free energy results compared to regular umbrella sampling,[36,37] thus it is an ideal technique to elucidate how BODIPY influences the partitioning of CE to HDL. Meanwhile, unbiased atomistic MD simulations are used in this work to get a detailed picture about BODIPY-induced changes in the structural organization and the diffusive dynamics inside HDL. We show that BODIPY labeling has no significant effect on the partitioning of CE between HDL and the water phase. However, due to the hydrophilic nature of the BODIPY moiety, BODIPY-CE was observed to diffuse more slowly and locate itself closer to the HDL-water interface than CE due to the double constraint of keeping the BODIPY probe in the surface region and the CE body away from it. We close the article by briefly discussing the implications of the observed findings.

2. METHODS AND ANALYSIS

2.1. Model Systems. We modeled HDL particles with different lipid compositions through a series of replica exchange umbrella sampling (REUS) simulations and unbiased molecular dynamics (MD) simulations. In each simulation, there was a single HDL particle solvated in water. Our atomistic model of the HDL particle was taken from a previous study[28] and contained a hydrophobic core (see below) surrounded by 56 1-palmitoyl-2-oleoylphosphatidylcholine (POPC) molecules, and two apolipoprotein A-I chains on the surface of the particle. The apoA-I proteins were placed in a hairpin arrangement. The HDL particle was solvated by 48 000 water molecules.

In pristine HDL, the hydrophobic core was comprised of 16 cholesteryl ester (CE) molecules that in our simulations were chosen to be cholesteryl oleate. In modified HDL, one or three of the CE molecules were replaced with BODIPY-cholesteryl ester (BODIPY-CE). In this paper, we use the notation 13/3, 15/1, and 16/0 to describe the numbers of CE and BODIPY-CE molecules, respectively, in each system. Notably, in two model systems an additional CE or BODIPY-CE molecule was pulled into the HDL particle, making the total number of CE and BODIPY-CE molecules 17. The chemical structures of CE and BODIPY-CE are shown in Figure 1. All performed REUS and unbiased simulations are summarized in Table 1. The details of system preparation and simulations are given in sections 2.3 and 2.4.

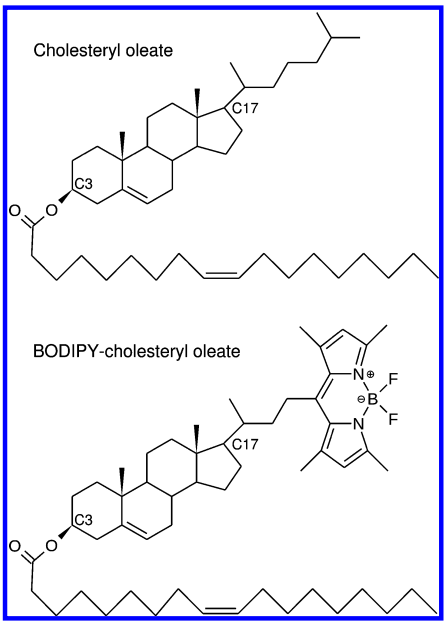

Figure 1. Chemical structures of unlabeled and BODIPY-labeled cholesteryl oleate. The positions of carbon atoms C3 and C17, which define the director of the molecule, are also shown.

2.2. Force Field and Simulation Parameters. We used the Berger force field for the lipids[38] together with the OPLS-AA force field for the proteins.[39] Combining the two force fields has been validated in an earlier study.[40] We applied the combination rules with the technique described by Neale and Pomes[41] to combine the two force fields. The force field parameters for the BODIPY probe were adapted from an earlier study.[31] For water, we used the SPC model.[42] We applied the Nosé−Hoover thermostat[43,44] and the Parrinello−Rahman barostat[45] to maintain a temperature of 310 K and a pressure of 1 bar. We used a time constant of 5 ps for temperature and pressure coupling, and a compressibility of 4.5×10^{-5} bar^{-1} for the coupling of pressure in the barostat.

DOI: 10.1021/acs.jpcb.5b10188
J. Phys. Chem. B 2015, 119, 15848−15856

Table 1. Summary of the simulations made in this study[a]

simulation	CE/BODIPY-CE counts	simulation type	pulled molecule	pull direction	reaction coordinate
1	15/1	REUS	BODIPY-CE	in	HDL COM – ring COM
2	13/3	REUS	BODIPY-CE	in	HDL COM – BODIPY-CE COM
3	13/4	REUS	BODIPY-CE	in	HDL COM – ring COM
4	13/3	REUS	BODIPY-CE	out	HDL COM – ring COM
5	13/3	REUS	CE	in	HDL COM – ring COM
6	14/3	REUS	CE	in	HDL COM – ring COM
7	13/3	REUS	CE	out	HDL COM – ring COM
8	13/3	unbiased	none	n/a	n/a
9	13/3	unbiased	none	n/a	n/a
10	15/1	unbiased	none	n/a	n/a
11	16/0	unbiased	none	n/a	n/a

[a]The details on preparing and running the simulations are described in sections 2.3 and 2.4. In the reaction coordinate, "ring COM" refers to the center of mass (COM) of the cholesterol rings in the pulled molecule, and "BODIPY-CE COM" refers to the center of mass of the whole pulled molecule. "REUS" stands for Replica Exchange Umbrella Sampling, "unbiased" stands for MD simulations without any biasing potential, and "n/a" stands for not available. The pull directions "in" and "out" correspond to motion that is directed towards the HDL center, and away fror it, in respective order.

We used a cubic simulation box with sides of 11.8 nm in length and applied periodic boundary conditions in all directions. The linear constraint solver (LINCS) algorithm[46] was used to constrain all bond lengths. The Lennard-Jones interaction cutoff was 1.4 nm. Electrostatic interactions were calculated by the particle mesh Ewald method[47] with a grid spacing of 0.12 nm and a Coulomb cutoff of 1.0 nm. A time step of 2 fs was used in the simulations.

2.3. Replica Exchange Umbrella Sampling. We calculated all free energy results with the REUS technique,[48] which has been shown to improve the quality of the resulting free energies compared to regular umbrella sampling.[36,37] We used the REUS simulations to calculate the free energy change of detaching CE and BODIPY-CE molecules from HDL. The REUS method combines umbrella sampling[49,50] with replica exchange of the umbrella potentials. In conventional replica exchange, exchanges take place between systems at different temperatures. In REUS the exchange is done between neighboring umbrella windows, which are all considered at the same temperature, and a replica exchange event then means exchanging the umbrella potentials of two neighboring umbrella windows. To carry out REUS simulations, we used a customized version of the GROMACS 4.6.5 molecular dynamics software package.[51] We used a force constant of 1000 kJ mol^{-1} nm^{-2} for the umbrella potentials and an exchange attempt interval of 2 ps for replica exchange. The free energy profiles were computed with the weighted histogram analysis method and the error estimation was done with bootstrap analysis with autocorrelation estimation.[52,53]

For the REUS simulations, we started with an initial configuration for HDL from a well-equilibrated system (simulated for ~650 ns without any umbrella potential). To generate the initial configurations for the umbrella windows, four different methods were used. For the two 13/3 CE/BODIPY-CE systems with the pull direction outward from HDL, we pulled a single CE or BODIPY-CE molecule out of the HDL particle into the water phase (for the simulated systems, see Table 1). For the two 13/3 systems with the pull direction inward, the system was first let to evolve for 100 ns with the pulled CE or BODIPY-CE molecule kept at a distance of 5.5 nm from HDL center, followed by pulling the molecule back to the inside of the HDL particle. For the 13/4 and 14/3 systems, a BODIPY-CE or CE molecule was added to the water phase and pulled into the HDL particle. Finally, for the 15/1 system, a single CE molecule was removed from the HDL particle and a BODIPY-CE molecule was added to the water phase, followed by pulling the BODIPY-CE molecule inside the HDL particle. Using the above procedures, we generated 54 umbrella windows for each system with a spacing of 0.1 nm between the windows. To get the free energy profiles, we ran the umbrella simulations for 200 ns per window for a total simulation time of 10.8 μs per system. The first 50 ns of each umbrella window were discarded as equilibration.

The reaction coordinate r was chosen as the distance between the center of mass (COM) of HDL and the COM of the cholesterol ring in the target CE or BODIPY-CE molecule, except in one test case where the COM of the whole pulled molecule was used instead of the COM of the cholesterol ring.

In the free energy profiles, we define ΔE_{min} as the minimum free energy with respect to the free energy in the water phase, $r(\Delta E_{min})$ as the corresponding value for the distance r, and ΔE_{core} as the free energy difference between the minimum free energy and the free energy at r = 0.2 nm.

The free energies discussed in the results section correspond to the two systems with CE/BODIPY-CE counts of 13/3 and 15/1. In the 13/3 system, we calculated the free energy profiles for both CE and BODIPY-CE. In the 15/1 system, we made the profile for BODIPY-CE only. To make sure that our main findings were not compromised by any of the practical choices made for the calculations in the studied systems, we performed additional REUS simulations where we varied the lipid counts, the pulling of the center of mass, and the pull direction. Full description of the additional simulations is given in the Supporting Information (SI).

2.4. Unbiased Simulations. To study the behavior of CE and BODIPY-CE molecules in HDL without any biasing potential, we made four separate simulations with no umbrella sampling (Table 1). The length of each of these unbiased simulations was 1 μs, and the CE/BODIPY-CE counts were 13/3, 13/3, 15/1, and 16/0. An energy minimization followed by a 100 ns equilibration run was done for each model system before starting production simulations. The unbiased simulations were made with the GROMACS 4.6.5 software.[51]

2.5. Radial Distribution Functions and Orientation Angles. We calculated the radial distribution function (RDF) from the four independent unbiased simulations listed in Table 1. The RDFs were computed atom-wise using volume and density normalization and using the COM of HDL as the reference point (r = 0).

To study the orientations of CE and BODIPY-CE in the umbrella sampling simulations, we defined the molecular director as the vector from the carbon atom C17 to C3 in the steroid moiety of the molecule (see Figure 1). Further, for this calculation the effective local normal of HDL was taken as the vector from the COM of HDL to the midpoint of the director. The orientation angle θ was then defined as the angle

DOI: 10.1021/acs.jpcb.5b10188
J. Phys. Chem. B 2015, 119, 15848−15856

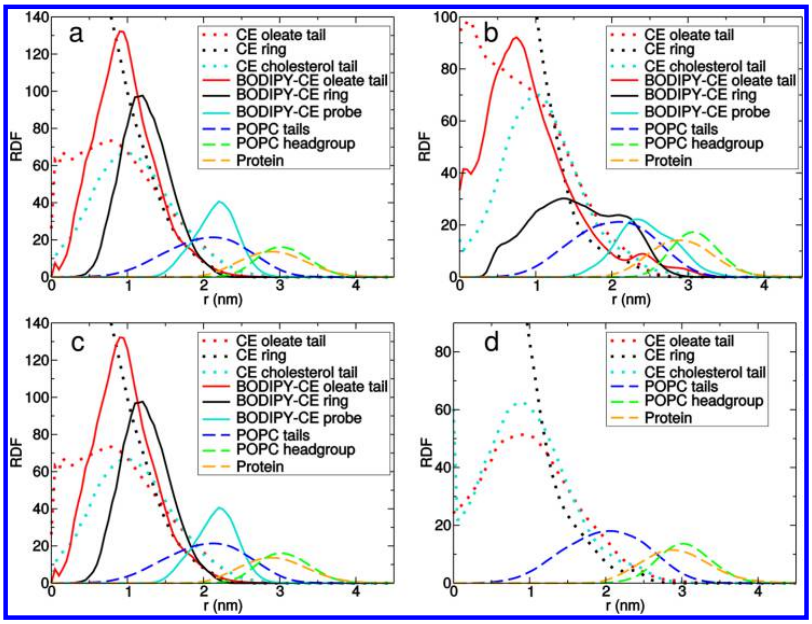

Figure 2. Radial distribution functions from four independent unbiased simulations of HDL. From a to d, the CE/BODIPY-CE counts are 13/3, 13/3, 15/1, and 16/0, in respective order. At small distances the RDF value of the CE ring extends to ∼250, but for clarity's sake we draw the plot only up to 140. In panel b, one of the BODIPY-CE molecules is oriented tangentially with respect to HDL, giving rise to a shoulder in the plot of the BODIPY-CE ring at r = 2.3 nm.

between the director and the effective normal. To plot the density map of orientations, we divided the distance r into 0.1 nm bins and calculated the angle distribution in each bin.

2.6. Diffusion. We used the method described by Vuorela[25] to compute the diffusion coefficients of CE and BODIPY-CE. In this approach, we calculated over a time interval Δt the displacement of the molecule whose motion was being followed. During the time interval Δt the molecule moved a relatively short distance inside the HDL particle. Then one finds the probability distribution function to find the molecule at a distance r from the origin after time Δt has elapsed:

$$P_{2D}(\Delta t, r) = \frac{r}{2D_{2D}\Delta t} \exp\left(-\frac{r^2}{4D_{2D}\Delta t}\right)$$

in two dimensions (2D) and

$$P_{3D}(\Delta t, r) = \frac{4\pi r^2}{(4\pi D_{3D}\Delta t)^{3/2}} \exp\left(-\frac{r^2}{4D_{3D}\Delta t}\right)$$

in three dimensions (3D). The displacement distribution function is then the probability distribution for the distance that the COM of the particle has traveled during the given time interval Δt. Importantly, as the above equations highlight, the distribution is different in 2D and 3D motion, which provides a means to clarify whether the molecule in question moves along the particle surface (approximately in a 2D manner) or uniformly in the hydrophobic core region (as in 3D motion).

To fix the value of Δt, we used the value of $D = 0.36 \times 10^{-7}$ cm^2 s^{-1} reported earlier for CE diffusion in HDL.[25] Then based on the expected 3D diffusion of CE, the average length migrated by the diffusing particle during a period Δt is $l_D = (6D\Delta t)^{1/2}$. To consider particle displacements smaller than the molecular size, we used an educated guess of about 1 nm for l_D, which is satisfied if Δt is 50 ns. During the analysis (see section 3.3), this choice turned out to be appropriate.

The displacements were calculated for the center of mass of the sterol rings in CE and BODIPY-CE. The data for the displacements were taken from the same 1 μs unbiased simulations that we used to calculate the radial distribution functions. For each molecule type in each of the four simulated systems, we calculated an averaged diffusion coefficient using the displacement data of all the identical molecules.

3. RESULTS AND DISCUSSION

3.1. Labeled Cholesteryl Ester Orients So that the BODIPY Moiety Touches the Headgroup Region at the Surface of HDL. The radial distribution functions are shown in Figure 2. One finds that in the unlabeled (pristine) HDL (without BODIPY-CE; Figure 2d) there are apoA-I proteins located at the surface region surrounding the lipid particle, which in turn has a surface region comprised of POPCs. The CE molecules are in the core, and based on their radial distribution they are randomly oriented as in a melt.

Comparison of the unlabeled HDL (Figure 2d) to the HDL systems with BODIPY-CE (Figures 2a–c) reveals that there is one major difference: the structure in the core of HDL where cholesteryl esters and BODIPY-CE molecules reside. The surface region comprised of apoA-I and POPC is largely similar, however, with minimal changes induced by the probe.

BODIPY-CE does not favor being in the center of the HDL particle. This is highlighted by the data in Figures 2a–c, which show that both the oleate tail and the ring part of BODIPY-CE avoid the particle center. This is due to the BODIPY moiety, which instead of the hydrophobic core of HDL favors being in the region between the acyl chains and the headgroups of the

DOI: 10.1021/acs.jpcb.5b10188
J. Phys. Chem. B 2015, 119, 15848–15856

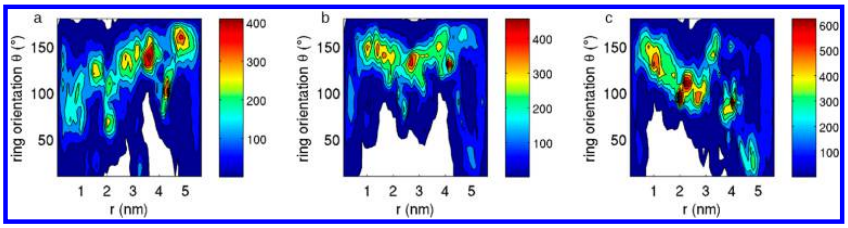

Figure 3. Orientation of the cholesterol ring during umbrella sampling for (a) 13/3 CE, (b) 13/3 BODIPY-CE, and (c) 15/1 BODIPY-CE. White regions correspond to no observations. Angles between 90 and 180° correspond to the BODIPY probe pointing "outward" away from the center of HDL and the oleate tail pointing "inward" toward the HDL center. At r < 1.5 nm, the density of angles in (a) is almost uniform. In contrast, there is a high density of angles between 110 and 160° in (b) and (c) at this distance.

phospholipids. As the BODIPY unit is tightly bound to this region, it also affects the radial distribution of the probe overall, which is quite evident when the radial distribution functions of CE and BODIPY-CE are compared in Figures 2a–c: the large-distance tails of the distributions of the ring and the oleate chains of BODIPY-CE are ∼0.5 nm closer to the HDL surface than in the corresponding distributions of CE.

The orientation angles of CE and BODIPY-CE are shown in Figure 3. The most important difference between CE and BODIPY-CE is found at the respective $r(\Delta E_{min})$ of each system, where the free energy is minimized (see Figure 4, section 3.2): at about 0.8 nm for 13/3 CE, and at ∼1.6 nm for 13/3 and 15/1 BODIPY-CE. For CE, the orientation of the cholesterol ring at r = 0.8 nm covers all possible values from 0 to 180° with a slight preference for angles between 50 and 140°. In contrast, in the 13/3 and 15/1 systems close to 1.6 nm, BODIPY-CE strongly favors angles from 110 to 150°, while the angles below 60° are completely absent. Thus, BODIPY-CE aims to orient itself in a manner where the fluorescent probe is pointing outward from the center of HDL. The same conclusion holds over the entire range of r for which the free energy is less than ΔE_{min} + 3 kcal mol^{-1} (c.f. section 3.2), regarding both CE and BODIPY-CE.

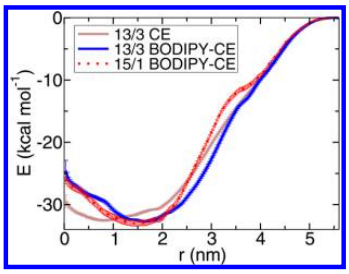

Figure 4. Free energy E as a function of distance r shown for CE and BODIPY-CE. The distance r is from the COM of HDL to the COM of the cholesterol ring in CE or BODIPY-CE. The free energy is set to zero at r = 5.5 nm. The presented data also show the error bars depicted by varying thickness of the curves.

The two BODIPY-CE simulations (Figures 3b,c) differ from each other in their angle distributions at 2 nm < r < 5 nm. This is due to the fact that in these two sets of umbrella sampling simulations, the BODIPY-CE molecule took different paths from the water phase into its minimum free energy position inside the HDL particle. For example, at r = 4 nm, the angle distributions show a "probe up" orientation for the 13/3 simulation and a sideways orientation for the 15/1 simulation. Despite these different ways to enter HDL, the free energy results are very similar in the two simulations, as discussed in the following section.

3.2. Free Energy Calculations Show Different Localization of Unlabeled and BODIPY-Labeled Cholesteryl Ester. The free energy profiles of CE and BODIPY-CE are shown in Figure 4. The values of free energy minimum positions as well as the corresponding free energies are listed in Table 2. For BODIPY-CE, there are results shown from two different simulations to illustrate the fact that independent simulations with slight differences in system preparation result in similar conclusions. This conclusion holds for all the seven different REUS simulations, but for the sake of conciseness, we focus here on the three simulations shown in Figure 4. For a full description of all the free energy profiles based on the REUS simulations, see SI.

Table 2. Free Energy Differences and the Positions of the Minima for the Systems Shown in Figure 4[a]

system	ΔE_{min} (kcal mol^{-1})	ΔE_{core} (kcal mol^{-1})	$r(\Delta E_{min})$ (nm)
13/3 CE	−32.6 ± 0.2	−1.6 ± 0.4	0.8
13/3 BODIPY-CE	−32.7 ± 0.2	−5.9 ± 0.4	1.7
15/1 BODIPY-CE	−33.0 ± 0.5	−5.7 ± 0.9	1.4

[a] ΔE_{min} is the minimum energy, $r(\Delta E_{min})$ is the corresponding value of distance r, and ΔE_{core} is the free energy difference between the minimum free energy and the free energy at r = 0.2 nm. The value of 0.2 nm is used here instead of r = 0, since the number of samples in the HDL center is very low, and the value of 0.2 nm was the limit very close to the origin where sampling was still considerable. The values of $r(\Delta E_{min})$ listed here are consistent with the RDF data from our unbiased simulations in Figure 2.

Based on the values for ΔE_{min}, it is very favorable for both labeled and unlabeled CE to enter the HDL particle from the water phase. The free energy minima of CE and BODIPY-CE are essentially identical with respect to the free energy in the water phase. The main difference is the position of the free energy minimum, $r(\Delta E_{min})$, which for BODIPY-CE is about 0.7–0.8 nm closer to the HDL surface than in the case of CE. In the minimum free energy position, the BODIPY probe is in contact with the HDL-water interface region composed of the apoA-I proteins and the phospholipid headgroups. This places the ring and the oleate tail of BODIPY-CE into the core of HDL, in contact with cholesteryl esters and POPC hydrocarbon tails. CE also has more freedom than BODIPY-CE to move in the HDL core. To express this quantitatively, the range of distance r for which the free energy is less than ΔE_{min} + 3 kcal mol^{-1} is 2.1 nm (between 0.04 and 2.12 nm) for CE

DOI: 10.1021/acs.jpcb.5b10188
J. Phys. Chem. B 2015, 119, 15848–15856

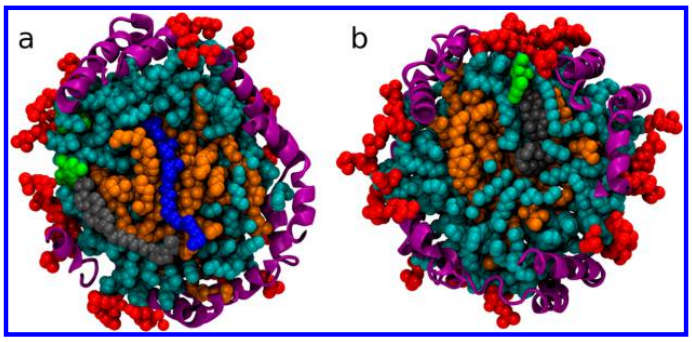

Figure 5. Cross sections of HDL taken from REUS simulations of (a) unlabeled CE and (b) BODIPY-CE. In (a), the CE molecule (shown in blue) is the subject of the umbrella potential and shown in its minimum free energy position $r(\Delta E_{min})$ = 0.8 nm. Likewise, in panel (b), the BODIPY-CE molecule (shown in green and gray) is the subject of the umbrella potential and shown here at $r(\Delta E_{min})$ = 1.4 nm. The CE snapshot is taken from the 13/3 simulation and the BODIPY-CE snapshot is based on the 15/1 simulation. Color code is as follows: umbrella sampled CE (blue); BODIPY probe attached to CE (green); CE attached to the BODIPY probe (gray); CE (orange); phospholipid tails (cyan); phospholipid headgroups (red); apolipoprotein A-I (purple).

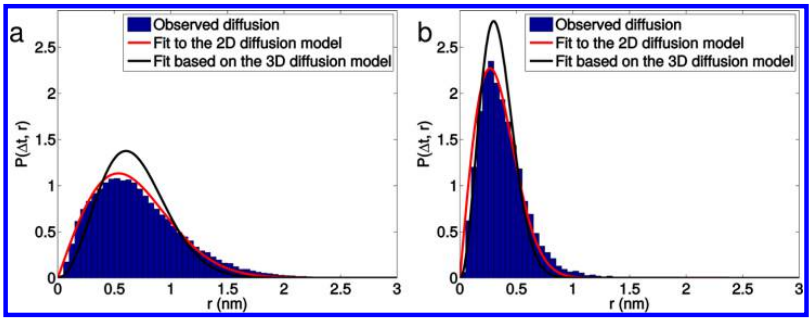

Figure 6. Particle displacement distributions (shown in blue) of (a) CE and (b) BODIPY-CE in HDL. The distributions are based on displacements over a period of 50 ns. Also shown are fits based on diffusion in 2D (red line), which was found to describe the data better than a fit in 3D (black line).

compared to 1.6 nm (between 0.86 and 2.41 nm in 13/3 and 0.75−2.25 nm in 15/1) for BODIPY-CE, see Figure 4.

The different values of ΔE_{core} for BODIPY-CE and CE bring out another important difference between the labeled and unlabeled molecules. For BODIPY-CE, the high free energy cost to approach the HDL center implies that the labeled molecule does not diffuse all the way to the core but remains in the region between the core and the hydrophilic surface of HDL. For CE, the free energy barrier is much smaller and of the order of thermal energy, thus in this case the unlabeled CE does readily migrate in the HDL center region, too. These results are consistent with the data in Figure 2.

Consideration of the contacts of each molecule in their respective free energy minimum energy positions (see SI) reveals that the ring of CE is surrounded mostly by other CE molecules as well as some POPC tails, while the ring of BODIPY-CE is mostly in contact with POPC tails rather than CE molecules. Therefore, CE and BODIPY-CE are in quite different local environments. The free energy minimum of BODIPY-CE correlates with the smallest value of r where the BODIPY moiety makes contact with the POPC headgroup and the protein regions. This indicates that BODIPY-CE is balancing between the tendency of the CE body to reside in the core and the anchoring of the fluorescent label to the headgroup region. This has implications for the ability of BODIPY-CE to diffuse and rotate, which is discussed in section 3.3.

Figure 5 depicts snapshots of HDL based on the REUS simulations, where the umbrella sampled molecules CE and BODIPY-CE are shown in their respective equilibrium positions at $r(\Delta E_{min})$. It is clearly visible that the fluorescent BODIPY moiety in BODIPY-CE associates with the headgroup region of HDL, while unlabeled CE resides in the HDL core. The snapshots are also consistent with the angle distributions shown in Figure 3 and the results for contacts discussed in SI.

It is worth pointing out that ΔE_{core} is negative also for unlabeled CE, while one could assume ΔE_{core} to be zero if the core were homogeneous. However, as Figures 2 and 5 show, it is not. Based on Figure 2 the size (diameter) of the core under the phospholipid tail region is about 2 nm, which implies that there is no space in the HDL core for the formation of a true bulk region. If the size of the lipoprotein were increased, such as to consider the low-density lipoprotein (LDL) instead of HDL, then the situation would likely change. Here, however, molecular features give rise to the minor free energy barrier close to the HDL center.

CE and BODIPY-CE have similar values for ΔE_{min}, which suggests that the two molecules will in a similar manner readily assemble into HDL upon contact. In the same spirit, the partitioning of CE and BODIPY-CE between HDL and the water phase is expected to be similar.

DOI: 10.1021/acs.jpcb.5b10188
J. Phys. Chem. B 2015, 119, 15848−15856

Comparison of the two BODIPY-CE profiles (15/1, 13/3) shows that both simulations yield essentially the same values of ΔE_{min} and ΔE_{core}. The location and the width of the free energy minima are almost the same as well. These results suggest that in the considered dilute limit the interactions between BODIPY-CE probes do not affect the results to a significant extent. Therefore, if in experiments several probes ended up in the same lipoprotein, the results would still correspond to those of the dilute limit in BODIPY concentration.

3.3. BODIPY Probe Slows Down the Diffusion of Cholesteryl Ester. We next studied the influence of the BODIPY probe on the rate and type of diffusion of CE within HDL. Figure 6 shows the distributions of particle displacements for CE and BODIPY-CE, together with a fit to the 2-dimensional (2D) diffusion model (both CE and BODIPY-CE undergo diffusion in 2D instead of 3D, see the discussion below). The diffusion coefficient D_{2D} resulting from the fit is $(0.29 \pm 0.02) \times 10^{-7}$ cm^2 s^{-1} for CE and $(0.07 \pm 0.02) \times 10^{-7}$ cm^2 s^{-1} for BODIPY-CE. In an earlier computational study using a coarse-grained model, a diffusion coefficient of 0.36×10^{-7} cm^2 s^{-1} was reported for CE in HDL,[25] in good agreement with the present result.

Because the CE and BODIPY-CE molecules occupy different radial positions in HDL, differences in their respective diffusion rates can be due to differences in the viscosities of local environments. In order to differentiate between the intrinsic properties of CE and BODIPY-CE and the effect of the local environment, we separately analyzed the diffusion coefficient of those CE molecules, which are located at the same distance from the HDL core as the BODIPY-CE molecules, allowing us to compare the diffusion of BODIPY-CE and CE on equal footing. The analysis showed that CE molecules in the BODIPY-CE region have a diffusion coefficient of $(0.14 \pm 0.04) \times 10^{-7}$ cm^2 s^{-1}. Comparing this value to the diffusion coefficient of all CE molecules in the system ($(0.29 \pm 0.02) \times 10^{-7}$ cm^2 s^{-1}) suggests that the viscosity in the core is higher than in the BODIPY-CE region that is close to the surface of HDL, and the difference between the calculated BODIPY-CE and CE diffusion coefficients is partly due to this difference in the local viscosities. Nevertheless, when the diffusion of CE and BODIPY-CE is compared in the same local environment, CE still diffuses twice as fast as BODIPY-CE.

Recently, Dergunov et al. reported experimentally measured values of $0.17–0.33 \times 10^{-7}$ cm^2 s^{-1} for the lateral diffusion coefficient for a cholesteryl 1-pyrenedecanoate (CPD) probe in reconstituted HDL particles.[35] This value is in agreement with our result for unlabeled CE. Also, there are some important similarities between our unlabeled CE and the CPD probe. In CPD, the pyrene moiety is located in the end of the decanoate tail and the short lipid tail in the cholesterol moiety is unchanged from regular cholesterol BODIPY. Furthermore, the pyrene moiety is hydrophobic, which makes the 1-pyrenedecanoate tail chemically similar to the unlabeled oleate tail, only somewhat bulkier. Although caution is advised when comparing our CE and BODIPY-CE calculations to the measurements done with CPD, the aforementioned similarities between CPD and unlabeled cholesteryl oleate may explain why the CPD probe would diffuse at the same rate as unlabeled CE, while BODIPY-labeled CE diffuses more slowly.

Several factors may contribute to the result that normal CE diffuses faster than BODIPY-CE. First, the BODIPY probe is much bulkier than the isobutyl group it replaces in the cholesterol tail of CE, which slows down the movement of BODIPY-CE. Second, our free energy calculations show that BODIPY-CE stays within a narrow distance range from the center of HDL, approximately between 1 and 2 nm in terms of distance between the COM of HDL and the COM of the cholesterol ring, while the equivalent range for CE is 0 to 2 nm. This limits the distance that BODIPY-CE can diffuse along the direction of the HDL normal. Third, the apoA-I protein chains hinder the tangential diffusion of BODIPY-CE close to the surface region, especially because BODIPY-CE cannot easily pivot under the protein because the fluorophore moiety resists entering the hydrophobic part of the HDL particle.

Interestingly, both types of molecules carry out diffusion in 2D rather than 3D (Figure 6). For normal CE, this suggests that movement along the inner boundary of the amphipathic surface region of HDL is the dominant type of diffusion. Despite this, we expect that the movement of CE within the hydrophobic core of HDL would follow diffusion in 3D over some time scale larger than the considered Δt = 50 ns. However, one has to keep in mind that the diffusion of CE takes place in a confined environment, thus consideration of diffusion over length scales larger than 6 nm (see Figure 2), and thus over time scales larger than ~3 μs is not relevant. In a LDL particle with a larger core, one could try to fit the overall diffusion of CE to a linear combination of the 2D and 3D models, where the contributions from 2D and 3D would reflect the numbers of CE molecules at the boundary of the hydrophilic–hydrophobic region and in the hydrophobic core. As for the diffusion of BODIPY-CE, we concluded from our free energy calculations that BODIPY-CE tends to stay at the boundary between the surface and the core regions, thus our finding that BODIPY-CE undergoes diffusion in 2D is consistent with this.

4. CONCLUSIONS

In summary, we have considered how well BODIPY-CE mimics the distribution of CE inside a HDL particle, and how its partitioning and dynamics deviate from the behavior of unlabeled CE molecules. The atomistic simulation results from our replica exchange umbrella sampling studies as well as our unbiased MD simulations showed that BODIPY-labeled cholesteryl ester localizes just below the phospholipid headgroup and the apolipoprotein regions in HDL particles, while unlabeled CE resides in the HDL core. Despite this, the free energy barriers for CE and BODIPY-CE desorption from HDL to the water phase were found to be essentially identical. Furthermore, BODIPY-CE was observed to diffuse more slowly than CE due to the double constraint of keeping the BODIPY probe in the surface region and the CE body away from it. We conclude that while BODIPY-CE is a useful marker to mimic CE behavior, the influence of BODIPY is strong enough to render the behavior of the BODIPY-labeled cholesteryl ester qualitatively differently from its unlabeled counterpart in a lipoprotein environment. Our results suggest that in order to fluorescently label cholesteryl ester molecules in spherical HDL without affecting the behavior of the molecules, one requires a probe with no affinity for the hydrophilic surface region.

■ ASSOCIATED CONTENT

Supporting Information

The Supporting Information is available free of charge on the ACS Publications website at DOI: 10.1021/acs.jpcb.5b10188.

DOI: 10.1021/acs.jpcb.5b10188
J. Phys. Chem. B 2015, 119, 15848–15856

The Journal of Physical Chemistry B Article

Results of additional free energy calculations for CE and BODIPY-CE and an analysis of the contacts between different components of the studied systems during REUS simulations. (PDF)

AUTHOR INFORMATION

Corresponding Author

*E-mail: ilpo.vattulainen@tut.fi.

Notes

The authors declare no competing financial interest.

ACKNOWLEDGMENTS

We thank the Academy of Finland (Center of Excellence in Biomembrane Research project) and the European Research Council (Advanced Grant CROWDED-PRO-LIPIDS) for financial support. T.K. thanks the Väisälä Foundation for the Ph.D. study grant. We also wish to thank CSC-IT Center for Science (Espoo, Finland) for providing us with ample computing resources.

REFERENCES

(1) Rudin, M. *Molecular Imaging*; Imperial College Press: London, 2013.
(2) Sahl, S. J.; Moerner, W. E. Super-Resolution Fluorescence Imaging with Single Molecules. *Curr. Opin. Struct. Biol.* **2013**, *23*, 778−787.
(3) Massoud, T. F.; Gambhir, S. S. Molecular Imaging in Living Subjects: Seeing Fundamental Biological Processes in a New Light. *Genes Dev.* **2003**, *17*, 545−580.
(4) Wüstner, D. Fluorescent Sterols as Tools in Membrane Biophysics and Cell Biology. *Chem. Phys. Lipids* **2007**, *146*, 1−25.
(5) Somerharju, P. Pyrene-Labeled Lipids as Tools In Membrane Biophysics and Cell Biology. *Chem. Phys. Lipids* **2002**, *116*, 57−74.
(6) Wysockia, L. M.; Lavis, L. D. Advances in the Chemistry of Small Molecule Fluorescent Probes. *Curr. Opin. Chem. Biol.* **2011**, *15*, 752−759.
(7) Róg, T.; Vattulainen, I. Cholesterol, Sphingolipids, and Glycolipids: What Do We Know About Their Role in Raft-Like Membranes? *Chem. Phys. Lipids* **2014**, *184*, 82−104.
(8) Vattulainen, I.; Róg, T. Lipid Simulations: A Perspective on Lipids in Action. *Cold Spring Harbor Perspect. Biol.* **2011**, *3*, a004655.
(9) Fraňová, M. D.; Vattulainen, I.; Ollila, O. H. S. Can Pyrene Probes Be Used to Measure Lateral Pressure Profiles of Lipid Membranes? Perspective Through Atomistic Simulations. *Biochim. Biophys. Acta, Biomembr.* **2014**, *1838*, 1406−1411.
(10) Repáková, J.; Holopainen, J. M.; Morrow, M. R.; McDonald, M. C.; Čapková, P.; Vattulainen, I. Influence of DPH on the Structure and Dynamics of a DPPC Bilayer. *Biophys. J.* **2005**, *88*, 3398−3410.
(11) Čurdová, J.; Čapková, P.; Plášek, J.; Repáková, J.; Vattulainen, I. Free Pyrene Probes in Gel and Fluid Membranes: Perspective Through Atomistic Simulations. *J. Phys. Chem. B* **2007**, *111*, 3640−3650.
(12) Neuvonen, M.; Manna, M.; Mokkila, S.; Javanainen, M.; Róg, T.; Liu, Z.; Bittman, R.; Vattulainen, I.; Ikonen, E. Enzymatic Oxidation of Cholesterol: Properties and Functional Effects of Cholestenone in Cell Membranes. *PLoS One* **2014**, *9*, e103743.
(13) Skaug, M. J.; Longo, M. L.; Faller, R. The Impact of Texas Red on Lipid Bilayer Properties. *J. Phys. Chem. B* **2011**, *115*, 8500−8505.
(14) Loura, L. M. S.; Ramalho, J. P. P. Recent Developments in Molecular Dynamics Simulations of Fluorescent Membrane Probes. *Molecules* **2011**, *16*, 5437−5452.
(15) Fraňová, M.; Repáková, J.; Čapková, P.; Holopainen, J. M.; Vattulainen, I. Effects of DPH on DPPC-Cholesterol Membranes With Varying Concentration of Cholesterol: From Local Perturbations to Limitations in Fluorescence Anisotropy Experiments. *J. Phys. Chem. B* **2010**, *114*, 2704−2711.
(16) Lund-Katz, S.; Phillips, M. C. High Density Lipoprotein Structure-Function and Role in Reverse Cholesterol Transport. *Subcell. Biochem.* **2010**, *51*, 183−227.
(17) Davidson, M. H.; Toth, P. P. High-Density Lipoprotein Metabolism: Potential Therapeutic Targets. *Am. J. Cardiol.* **2007**, *100*, 32N−40N.
(18) Duivenvoorden, R.; van Wijk, D.; Klimas, M.; Kastelein, J. J. P.; Stroes, E. S. G.; Nederveen, A. J. Detection of Liquid Phase Cholesteryl Ester in Carotid Atherosclerosis by 1H-MR Spectroscopy in Humans. *J. Am. Coll. Cardiol. Img.* **2013**, *6*, 1277−1284.
(19) Ruberg, F. L.; Viereck, J.; Phinikaridou, A.; Qiao, Y.; Loscalzo, J.; Hamilton, J. A. Identification of Cholesteryl Esters in Human Carotid Atherosclerosis by Ex Vivo Image-Guided Proton MRS. *J. Lipid Res.* **2005**, *47*, 310−317.
(20) Blanche, P. J.; Gong, E. L.; Forte, T. M.; Nichols, A. V. Characterization of Human High-Density Lipoproteins by Gradient Gel Electrophoresis. *Biochim. Biophys. Acta, Lipids Lipid Metab.* **1981**, *665*, 408−419.
(21) Duverger, N.; Rader, D.; Duchateau, P.; Fruchart, J. C.; Castro, G.; Brewer, H. B., Jr. Biochemical Characterization of the Three Major Subclasses of Lipoprotein A-I Preparatively Isolated from Human Plasma. *Biochemistry* **1993**, *32*, 12372−12379.
(22) Segrest, J. P.; Cheung, M. C.; Jones, M. K. Volumetric Determination of Apolipoprotein Stoichiometry of Circulating HDL Subspecies. *J. Lipid Res.* **2013**, *54*, 2733−2744.
(23) Yetukuri, L.; Söderlund, S.; Koivuniemi, A.; Seppänen-Laakso, T.; Niemelä, P. S.; Hyvönen, M.; Taskinen, M.-R.; Vattulainen, I.; Jauhiainen, M.; Orešič, M. Composition and Lipid Spatial Distribution of HDL Particles in Subjects with Low and High HDL Cholesterol. *J. Lipid Res.* **2010**, *51*, 2341−2351.
(24) Huang, R.; Silva, R. A.; Jerome, W. G.; Kontush, A.; Chapman, M. J.; Curtiss, L. K.; Hodges, T. J.; Davidson, W. S. Apolipoprotein A-I Structural Organization in High-Density Lipoproteins Isolated from Human Plasma. *Nat. Struct. Mol. Biol.* **2011**, *18*, 416−422.
(25) Vuorela, T.; Catte, A.; Niemelä, P. S.; Hall, A.; Hyvönen, M. T.; Marrink, S.-J.; Karttunen, M.; Vattulainen, I. Role of Lipids in Spheroidal High Density Lipoproteins. *PLoS Comput. Biol.* **2010**, *6*, e1000964.
(26) Koivuniemi, A.; Vattulainen, I. Revealing Structural and Dynamical Properties of High Density Lipoproteins Through Molecular Simulations. *Soft Matter* **2012**, *8*, 1262−1267.
(27) Äijänen, T.; Koivuniemi, A.; Javanainen, M.; Rissanen, S.; Rog, T.; Vattulainen, I. How Anacetrapib Inhibits the Activity of the Cholesteryl Ester Transfer Protein? Perspective through Atomistic Simulations. *PLoS Comput. Biol.* **2014**, *10*, e1003987.
(28) Catte, A.; Patterson, J. C.; Bashtovyy, D.; Jones, M. K.; Gu, F.; Li, L.; Rampioni, A.; Sengupta, D.; Vuorela, T.; Niemelä, P.; et al. Structure of Spheroidal HDL Particles Revealed by Combined Atomistic and Coarse Grained Simulation. *Biophys. J.* **2008**, *94*, 2306−2319.
(29) Wu, Z.; Gogonea, V.; Lee, X.; May, R. P.; Pipich, V.; Wagner, M. A.; Undurti, A.; Tallant, T. C.; Baleanu-Gogonea, C.; Charlton, F.; et al. The Low Resolution Structure of ApoA1 in Spherical High Density Lipoprotein Revealed by Small Angle Neutron Scattering. *J. Biol. Chem.* **2011**, *286*, 12495−12508.
(30) Loudet, A.; Burgess, K. BODIPY Dyes and Their Derivatives: Syntheses and Spectroscopic Properties. *Chem. Rev.* **2007**, *107*, 4891−4932.
(31) Hölttä-Vuori, M.; Uronen, R.-L.; Repakova, J.; Salonen, E.; Vattulainen, I.; Panula, P.; Li, Z.; Bittman, R.; Ikonen, E. BODIPY-Cholesterol: a New Tool to Visualize Sterol Trafficking in Living Cells and Organisms. *Traffic* **2008**, *9*, 1839−1849.
(32) Li, Z.; Mintzer, E.; Bittman, R. First Synthesis of Free Cholesterol - BODIPY Conjugates. *J. Org. Chem.* **2006**, *71*, 1718−1721.
(33) Ariola, F. S.; Li, Z.; Cornejo, C.; Bittman, R.; Heikal, A. A. Membrane Fluidity and Lipid Order in Ternary Giant Unilamellar Vesicles Using a New Bodipy-Cholesterol Derivative. *Biophys. J.* **2009**, *96*, 2696−2708.

DOI: 10.1021/acs.jpcb.5b10188
J. Phys. Chem. B 2015, 119, 15848−15856

(34) Shaw, J. E.; Epand, R. F.; Epand, R. M.; Li, Z.; Bittman, R.; Yip, C. M. Correlated Fluorescence-Atomic Force Microscopy of Membrane Domains: Structure of Fluorescence Probes Determines Lipid Localization. *Biophys. J.* **2006**, *90*, 2170−2178.
(35) Dergunov, A. D.; Shabrova, E. V.; Dobretsov, G. E. Cholesteryl Ester Diffusion, Location and Self-Association Constraints Determine CETP Activity With Discoidal HDL: Excimer Probe Study. *Arch. Biochem. Biophys.* **2014**, *S64*, 211−218.
(36) Neale, C.; Madill, C.; Rauscher, S.; Pomès, R. Accelerating Convergence in Molecular Dynamics Simulations of Solutes in Lipid Membranes by Conducting a Random Walk along the Bilayer Normal. *J. Chem. Theory Comput.* **2013**, *9*, 3686−3703.
(37) Karilainen, T.; Timr, S.; Vattulainen, I.; Jungwirth, P. Oxidation of Cholesterol Does Not Alter Significantly Its Uptake into High-Density Lipoprotein Particles. *J. Phys. Chem. B* **2015**, *119*, 4594−4600.
(38) Berger, O.; Edholm, O.; Jähnig, F. Molecular Dynamics Simulations of a Fluid Bilayer of Dipalmitoylphosphatidylcholine at Full Hydration, Constant Pressure, and Constant Temperature. *Biophys. J.* **1997**, *72*, 2002−2013.
(39) Jorgensen, W. L.; Maxwell, D. S.; Tirado-Rives, J. Development and Testing of the OPLS All-Atom Force Field on Conformational Energetics and Properties of Organic Liquids. *J. Am. Chem. Soc.* **1996**, *118*, 11225−11236.
(40) Tieleman, D. P.; MacCallum, J. L.; Ash, W. L.; Kandt, C.; Xu, Z.; Monticelli, L. Membrane Protein Simulations with a United-Atom Lipid and All-Atom Protein Model: Lipid−Protein Interactions, Side Chain Transfer Free Energies and Model Proteins. *J. Phys.: Condens. Matter* **2006**, *18*, S1221−S1234.
(41) Neale, C.; Pomès, R. Pomès Lab. http://www.pomeslab.com/files/lipidCombinationRules.pdf (accessed September 14, 2015).
(42) Berendsen, H. J. C.; Postma, J. P. M.; Van Gunsteren, W. F.; Hermans, J. Interaction Models for Water in Relation to Protein Hydration. In *Intermolecular Forces*; Pullman, B., Ed.; Springer: Netherlands, 1981; Vol. *14*, pp 331−342.
(43) Nosé, S. A Unified Formulation of the Constant Temperature Molecular Dynamics Methods. *J. Chem. Phys.* **1984**, *81*, 511−519.
(44) Hoover, W. G. Canonical Dynamics: Equilibrium Phase-Space Distributions. *Phys. Rev. A: At., Mol., Opt. Phys.* **1985**, *31*, 1695−1697.
(45) Parrinello, M.; Rahman, A. Polymorphic Transitions in Single Crystals: a New Molecular Dynamics Method. *J. Appl. Phys.* **1981**, *52*, 7182−7190.
(46) Hess, B.; Bekker, H.; Berendsen, H. J. C.; Fraaije, J. G. E. M. LINCS: a Linear Constraint Solver for Molecular Simulations. *J. Comput. Chem.* **1997**, *18*, 1463−1472.
(47) Essmann, U.; Perera, L.; Berkowitz, M. L.; Darden, T.; Lee, H.; Pedersen, L. G. A Smooth Particle Mesh Ewald Method. *J. Chem. Phys.* **1995**, *103*, 8577−8592.
(48) Sugita, Y.; Kitao, A.; Okamoto, Y. Multidimensional Replica-Exchange Method for Free-Energy Calculations. *J. Chem. Phys.* **2000**, *113*, 6042−6051.
(49) Roux, B. The Calculation of the Potential of Mean Force Using Computer Simulations. *Comput. Phys. Commun.* **1995**, *91*, 275−282.
(50) Torrie, G.; Valleau, J. Nonphysical Sampling Distributions in Monte Carlo Free-Energy Estimation: Umbrella Sampling. *J. Comput. Phys.* **1977**, *23*, 187−199.
(51) Hess, B.; Kutzner, C.; van der Spoel, D.; Lindahl, E. GROMACS 4: Algorithms for Highly Efficient, Load-Balanced, and Scalable Molecular Simulation. *J. Chem. Theory Comput.* **2008**, *4*, 435−447.
(52) Kumar, S.; Rosenberg, J. M.; Bouzida, D.; Swendsen, R. H.; Kollman, P. A. The Weighted Histogram Analysis Method for Free-Energy Calculations on Biomolecules. I. The Method. *J. Comput. Chem.* **1992**, *13*, 1011−1021.
(53) Hub, J. S.; de Groot, B. L.; van der Spoel, D. g_wham — A Free Weighted Histogram Analysis Implementation Including Robust Error and Autocorrelation Estimates. *J. Chem. Theory Comput.* **2010**, *6*, 3713−3720.

DOI: 10.1021/acs.jpcb.5b10188
J. Phys. Chem. B 2015, 119, 15848−15856

Tampereen teknillinen yliopisto
PL 527
33101 Tampere

Tampere University of Technology
P.O.B. 527
FI-33101 Tampere, Finland

ISBN 978-952-15-4115-5
ISSN 1459-2045